UNIVERSITA' DEGLI STUDI DI GENOVA

DOCTORATE SCHOOL IN SCIENCES AND TECHNOLOGIES OF CHEMISTRY AND MATERIALS

Curriculum in pharmaceutical, food and cosmetic sciences

XXXII cycle

PhD Thesis

"Synthesis and biological evaluation of pyrazolo[3,4-*d*]pyrimidine derivatives active as SGK1, Fyn and Src kinases inhibitors"

Chiara Greco

Advisor: Prof. Silvia Schenone

Defense date:

Tables of contents

SUMMARY

Protein kinases are enzymes that regulate the biological activity of target proteins by phosphorylation of specific amino acids with ATP as the source of phosphate, thereby inducing a conformational change from an inactive to an active form of the target protein. Depending on the substrate, protein kinases can be classified into serine-threonine kinases and tyrosine kinases. According to their cellular location, both classes can be further divided into receptor kinases (located in the cell membrane) or cytoplasmic kinases (located within the cell). Protein kinases are key regulators of cell functions. They direct the activity, localization and other functions of many proteins, and serve to orchestrate the activity of almost all cellular processes. Overexpression and dysregulation of protein kinases frequently characterize the pathogenesis of many cancers and other diseases. As a result, increasing attention has been directed towards the identification of novel kinase inhibitors for cancer therapy.

The research group where I worked synthesized a wide library of pyrazolo[3,4-*d*]pyrimidines which represent a promising class of compounds capable of inhibiting several oncogenic kinases.

The work here performed focuses on the synthesis and biological evaluation of a series of pyrazolo[3,4-*d*]pyrimidine derivatives as inhibitors of the serine-threonine kinase SGK1, and the tyrosine kinases Fyn and Src.

SGKs are implicated in a huge variety of cellular processes, such as cell stress, survival, proliferation and transport of ions, nutrients and amino acids. Among these kinases, SGK1 has demonstrated to be involved in cancer development and resistance, and in the metabolic syndrome, a pathological state mainly characterized by hypertension, obesity and diabetes. In this context, an in silico screening of our pyrazolo[3,4-*d*]pyrimidines has been performed with the aim to find new SGK1 inhibitors. One of these compounds, SI113, has been widely investigated and several biological studies have further demonstrated its promising activity on different type of tumors.

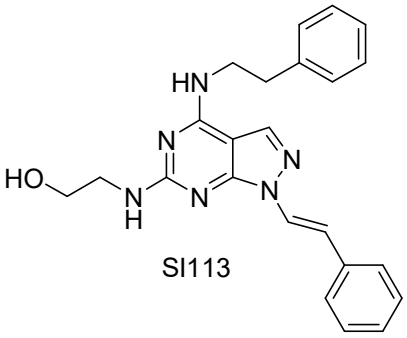

SI113

The main project which I carried out during my PhD study is based on the synthesis of a library of SI113 analogues. This new pyrazolo[3,4-*d*]pyrimidines potential SGK1 inhibitors are characterized by different anilino- and amino- groups in C4 and are decorated in C6 with polar chains, i.e. ethanolamine, diethanolamine, ethylene glycol and ethylenediamine. (**Chapter 5**).

The Src family kinases are non-receptor tyrosine kinases and regulate cell growth, differentiation, migration, adhesion and apoptosis.

Fyn belongs to the Src family kinases and it is physiologically involved in several transduction pathways in the brain and in the peripheral immune system. To date, the implication of Fyn in cancers has become more evident and its abnormal activity has been shown to be related into severe central nervous system pathologies such as Alzheimer's and Parkinson's diseases.

In this context the structures of the second set of compounds, which I synthesized during my PhD, are related to the in-house Fyn inhibitor SI308. From previously published studies on the first generation of Fyn inhibitors, SI308 was reported as the most potent compound, demonstrating both antiproliferative activity on cancer cell lines and the ability to inhibit protein Tau phosphorylation in a cellular model of Alzheimer's disease.

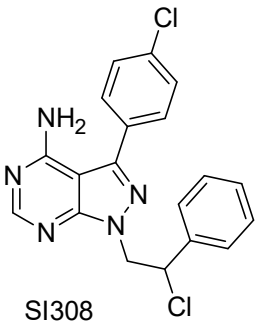

SI308

The new generation of SI308 related compounds present a methyl group in C6 and a (substituted) phenyl ring in C3. (**Chapter 6**).

Preliminary screening, using enzymatic assays, demonstrates that some of the novel compounds are active and therefore suitable for further *in vitro* studies. Subsequent *in vitro* data will aid in the design of future compounds.

The hyperactivation of c-Src, the prototype member of Src family kinases, has been proved to be closely connected with the development and progression of several tumor types.

Furthermore, previous data on another in-house compound SI306, which is a Src inhibitor, reported promising results on an *in vivo* xenograft model of neuroblastoma.

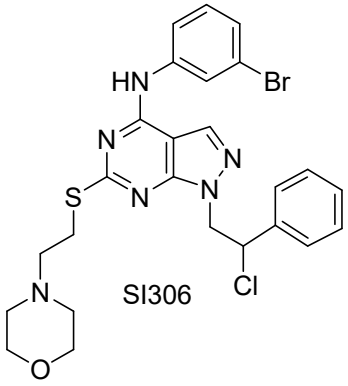

SI306

To further study its biological activity, SI306 was re-synthesized and additional experiments were performed on *in vitro* models. Testing of this compound on on three neuroblastoma cell lines characterized by a different MYCN status, (HTLA-230 and SK-N-BE-2C with MYCN amplification and SH-SY-5Y without MYCN amplification), further confirmed the activity of SI306, providing increased support for the inhibition of Src as a valid approach for neuroblastoma treatment. (**Chapter 7**).

I performed additional *in vitro* studies, on the three previously cited in-house pyrazolo[3,4-*d*]pyrimidines, SI113, SI308 and SI306, using patient derived glioblastoma multiforme (GBM) cell lines. This substantial work was undertaken during a research fellowship period performed in collaboration with the School of Pharmacy at the University of Nottingham (United Kingdom). Kinase inhibitor activity has been evaluated on series of patient derived GBM cell lines isolated from both the central tumor core (GCE28) and from the invasive margin of the tumor (GIN28 and GIN8). The use of such phenotypically relevant *in vitro* models represents an important step for GBM drug development and screening. The results gathered using these relevant cell models further demonstrate the anti-cancer activity of the pyrazolo[3,4-*d*]pyrimidine compounds. Moreover, the investigation of different combinations of our

inhibitors reveals that synergy can be achieved, and this finding has additional implications for potentially overcoming GBM drug resistance. Additionally, to overcome the low water solubility of our lead compound (SI306), polymers formulations of SI306 were prepared using a miniaturized screening process based on inkjet printing technology. The observed activity of our compounds *in vitro,* together with the application of a successful formulation, highlight that our kinase inhibitors are attractive candidates for the treatment of GBM. (**Chapter 8**).

Finally, during my research period in Nottingham, I also had the opportunity to test a set of our pyrazolo[3,4-*d*]pyrimidines on bacteria. This project is supported by many studies, highlighting prokaryotic protein kinases as potential targets for truly novel antibiotics. Additionally, in literature a number of pyrazolo[3,4-*d*]pyrimidine derivatives showing interesting activity against bacterial proliferation are reported.

For these reasons a representative number of pyrazolo[3,4-*d*]pyrimidines, presenting different substituents in position N1, C4 and C6 has been chosen to be tested on the Gram positive bacteria *S. aureus*, and the Gram negative bacteria *E. coli* in order to obtain the widest information about the structure-activity relationship (SAR). The combination of pyrazolo[3,4-*d*]pyrimidines with the antibiotics β-lactam ampicillin and the aminoglycoside kanamycin has been included in the assays in order to hypothesize a possible mechanism of action.

The results obtained represents a first step in the exploration of a potential dual activity of pyrazolo[3,4-*d*]pyrimidines in the context of bacterial infections in oncologic patients. (**Chapter 9**).

CHAPTER 1

Protein kinases family

The large family of protein kinases catalyzes the transfer of the γ-phosphate group of ATP onto substrate residues. This enzymatic phosphorylation produces a signal transduction which terminally leads to a biological response. Protein kinases regulate signalling pathways and cellular processes that mediate metabolism, transcription, cell-cycle progression, differentiation, cytoskeleton arrangement, cell movement, apoptosis, intercellular communication, neuronal and immunological functions[1].

Approximately 2% of all human genes correspond to protein kinase genes (total 518) which are responsible for carrying out these numerous biochemical processes (**Fig.1**)[2].

Protein kinases require ATP, the substrate protein and an essential bivalent metal ion (Mg^{2+} or Mn^{2+}) to catalyze the following reaction:

$$\mathbf{MgATP^{1-} + protein - OH \rightarrow protein - OPO_3^{2-} + MgADP + H^+}$$

The phosphate group is transferred on tyrosine, serine or threonine residues present on protein substrates. Many studies demonstrated that this reaction possesses an extraordinary catalytic power. In fact, it is reasonable to think that the alkoxide of serine or threonine or the phenolate of tyrosine, formed by the metal ion interaction, are more potent nucleophiles than the corresponding alcoholic or phenolic forms and, thus, may enhance phosphoryl group transfer.

The eukaryotic protein kinases are a large superfamily of homologous proteins. Depending on their ability to phosphorylate serine, threonine, or tyrosine residues, the superfamily members are subdivided in two main groups:

- Serine-threonine protein kinases (STKs).
- Tyrosine kinases (TKs).

The catalytic domain (**Fig.2**), a conserved region of approximately 200-250 amino acids, structurally consists of two lobes, the N-terminal lobe and the C-terminal lobe.

The first is composed of a β-sheet and a single α-helix (the "C-helix") which interacts with the ATP phosphate groups. The C-terminal lobe comprises the substrate-binding sites for ATP and peptides[3].

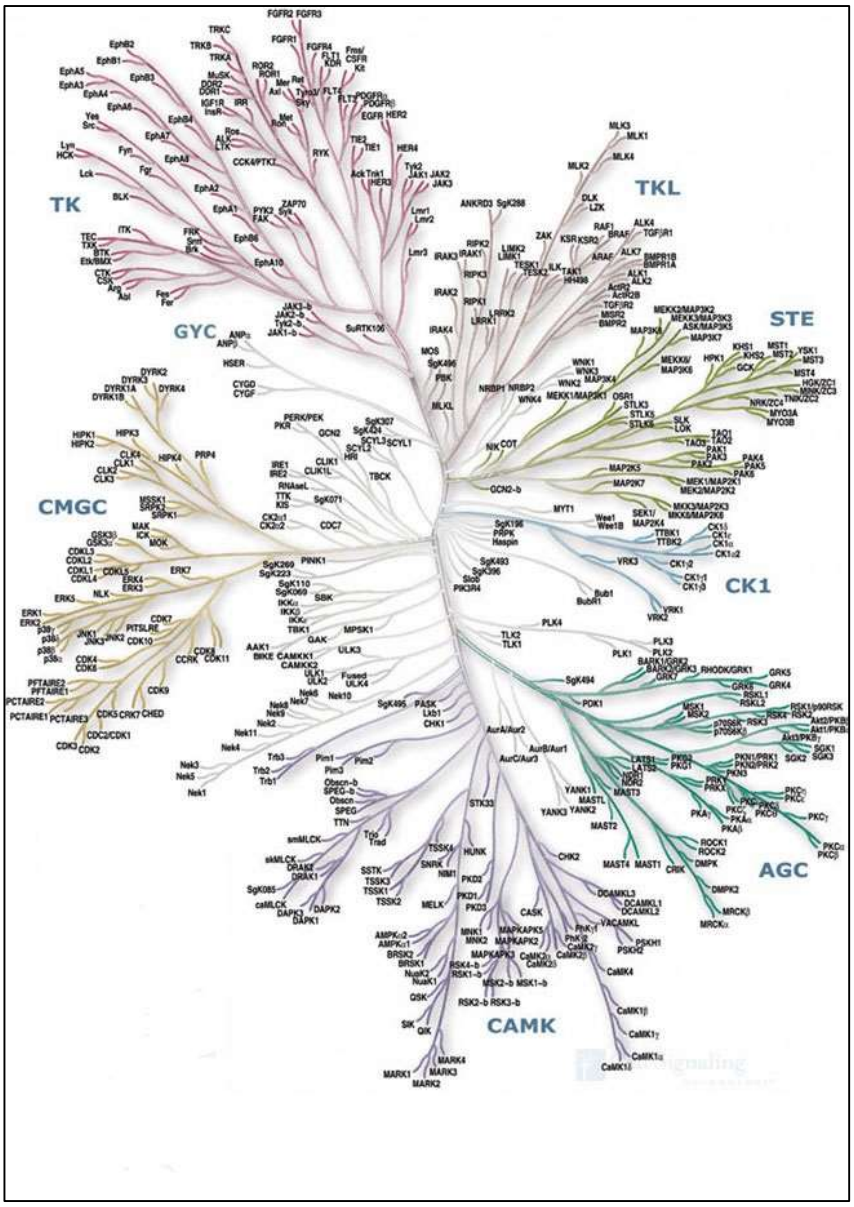

Fig.1. Human protein kinases. (From Cell Signaling Technology®).

It is predominantly α-helical and includes the activation loop (A-loop), a segment typically containing tyrosine, serine or threonine residues that can be phosphorylated.

The A-loop non-phosphorylated state prevents the substrate binding. On the contrary, the phosphorylation of the A-loop increases the enzymatic activity.

In the catalytic domain there are key residues extremely important for the interaction with ATP. Asp184, a strictly conserved residue, interacts with the essential Mg^{2+} ion, which chelates the β and γ phosphates of ATP. The chelation of this metal may position the terminal phosphate for

the direct transfer to the hydroxyl acceptor. Another key residue is Lys72, which interacts with α and β phosphates of ATP, giving additional stabilization and facilitating the phosphoryl group transfer without influencing ATP binding[4].

In addition to the catalytic domain, the structure of protein kinases includes other well characterized domains such as Src homology 2 (SH2) and 3 (SH3) domains in cytoplasmic TKs. Typically, these domains mediate inter- and intramolecular interactions among protein kinases, thus playing an important role in their functional regulation[1].

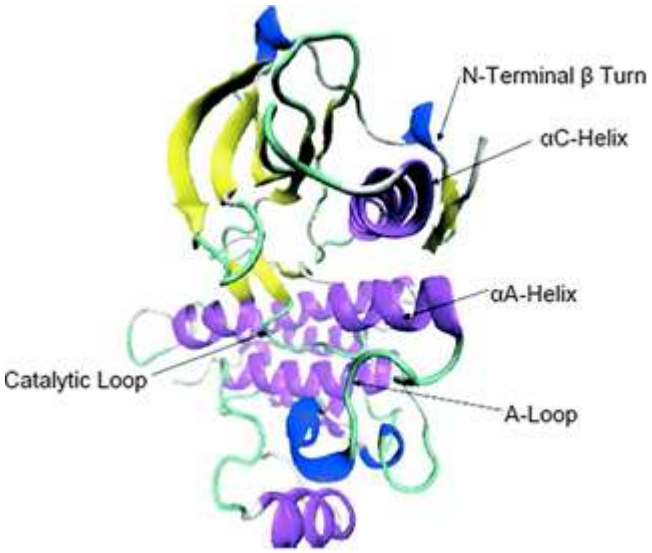

Fig.2. Protein kinases catalytic domain.

Since overexpression, dysregulation and mutations of protein kinases play essential roles in the pathogenesis of many diseases, including autoimmune, cardiovascular, inflammatory, and nervous system disorders, as well as cancer, this family of enzymes has become one of the most important drug targets.

To date, 49 small molecule protein kinase inhibitors have been approved by Food and Drug Administration (FDA)[5] and 212 are currently in clinical trials worldwide[6].

Most of the currently approved protein kinase inhibitors are directed toward the treatment of cancer and represent a valid alternative from conventional chemotherapy[7].

In conclusion, kinase inhibitor research is swiftly expanding, and the scientific progress in preclinical target validation, medicinal chemistry and computational technologies means this field appears likely to continue along this rapid growth trajectory.

1.1 Serine-threonine kinases

STKs play a pivotal role in cellular homeostasis and signaling through their ability to regulate the activation of transcription factors, cell cycle regulators, and a wide array of cytoplasmic and nuclear effectors[8].

STKs can be classified into six large groups:

- AGC (cAMP-dependent protein kinase/protein kinase G/protein kinase C extended family). This group includes more than 60 protein kinases in the human genome, classified into 14 families. They are cytoplasmic kinases that are regulated by secondary messengers such as cyclic-AMP or lipids. This group includes PKA, Akt and SGK (Serum- and glucocorticoid-regulated kinase)[9].
- CaMK (Ca^{2+}/calmodulin-dependent protein kinases). This group is mainly characterized by Ca^{2+}/calmodulin activity modulation. Most of the members of this group exhibit activation by the binding of Ca^{2+} or calmodulin to a small domain C-terminal to the catalytic domain[10].
- CMGC (CDK, MAP kinase, glycogen synthase kinase, and CDK-like). This group includes mitogen-activated protein kinases (MAPKs)[11].
- STE (homologues of STE11 and STE20).
- CK1 (casein kinase-1).
- TKL (tyrosine kinase like). This group includes the receptor STKs and is one of the most recently discovered kinase group.

STKs can also be divided depending on their cell location in receptor STKs and cytoplasmic STKs.

Receptor STKs group includes the transforming growth factor-β (TGFβ) receptors and activin receptors. TGFβ receptors exist as heterodimers of type I and type II receptors and the ligand binding domain is located in the type II receptor. Upon ligand-receptor binding, the type I receptors are recruited to the complex and are phosphorylated by the type II receptor. Phosphorylation allows receptor I to propagate the signal to downstream substrates. This process of ligand dependent type I receptor activation and substrate phosphorylation is regulated at different levels (**Fig.3**)[12].

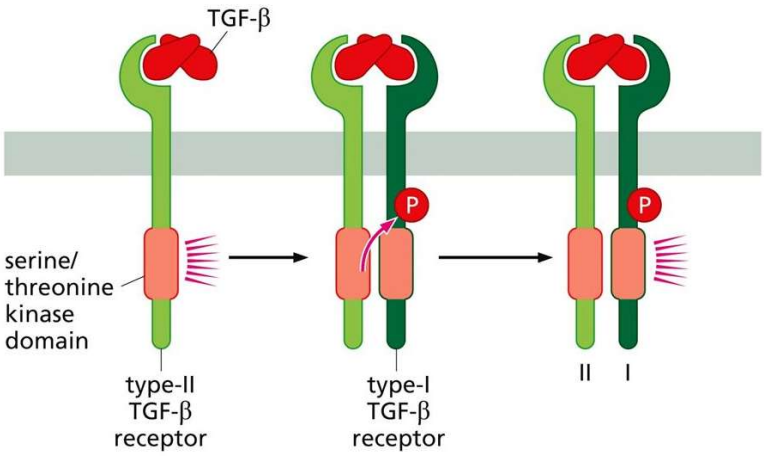

Fig. 3. Receptor STKs.

Cytoplasmic STKs are the largest and more studied class of STKs. They comprise many members including Raf, MEK and MAPK which are involved in the Ras-MAPK signalling cascade, a signal transduction pathway very important for the regulation of cell life. The activation element of this pathway is the binding of the extracellular mitogen to the membrane ligand. This leads to Ras (a GTPase) activation and the subsequent activation of Raf, MEK, MAPK and other downstream substrates. The cross-talk of all these pathways creates a wide and intricate network of communications in the cell, allowing the fine regulation of physiological functions.

STKs have been implicated in human cancer[13]. Moreover, many high-throughput strategies have been exploited to evaluate the involvement of STKs in the initiation and progression of cancer either by searching for activating mutations or by identifying misregulated expression in gene profiling experiments[14].

1.2 Tyrosine kinases

TKs are a subclass of protein kinases which selectively phosphorylate the OH group on tyrosine residues in target proteins. Upon activation, TKs regulate many key processes in cell, such as growth, survival, organ morphogenesis, neovascularization, and tissue repair and regeneration[15].

Similarly to STKs, TKs can be subdivided in two main classes:

- Transmembrane receptor TKs (RTKs).
- Cytoplasmic or non-receptor TKs.

The family members of RTKs are subdivided in 20 subclasses (Alk, Axl, Ddr, EGFR, Eph, FGFR, Insr, Met, Musk, PDGFR, Ptk7, Ret, Ror, Ros1, Ryk, Tie, Trk, VEGFR, AATYK) and are constituted by an extracellular portion that works as a receptor and an intracellular portion endowed with catalytic activity. The activation of RTKs requires the non-covalent association between two monomers to form a dimer[16]. This dimerization is triggered by the binding of extra-cellular factors to the extracellular portion of the kinase and in turn is responsible for the enhancement of intrinsic catalytic activity- accomplished by autophosphorylation on tyrosine residues- and the creation of binding sites to recruit downstream signaling proteins (**Fig.4**).

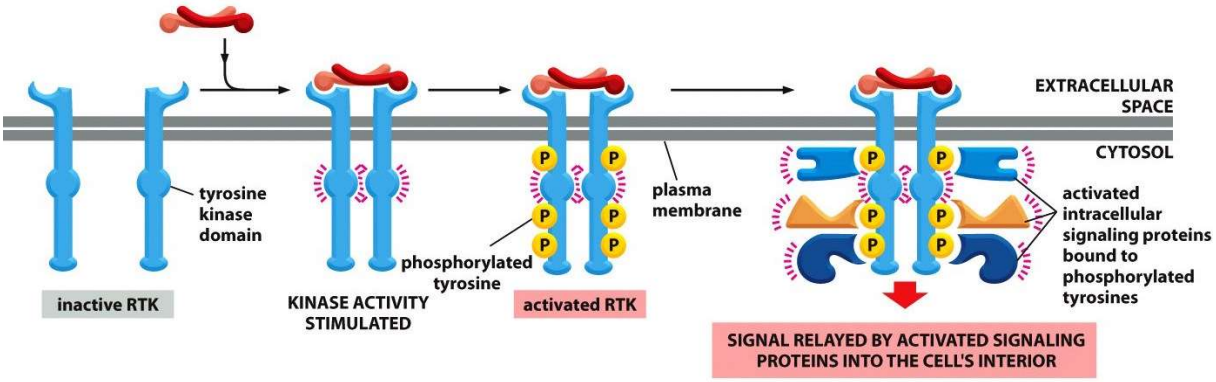

Fig.4. Transmembrane receptor TKs.

The ligands, for example the growth factors, by binding to the extracellular domain, lead to conformational changes that induce and stabilize receptor dimerization and lead to an increased kinase activity and autophosphorylation of tyrosine residues.

One way to effectively block signaling from RTK is the inhibition of its catalytic activity using small-molecule inhibitors. Examples of approved RTK inhibitors include imatinib, originally born as Bcr-Abl inhibitor, but also active on the RTK c-Kit, for the treatment of gastrointestinal stromal tumors with mutant c-Kit, gefitinib and erlotinib, for treatment of non-small cell lung cancers with mutant epidermal growth factor receptor (EGFR), pazopanib, targeting vascular endothelial growth factor receptor 2 (VEGFR2) /platelet-derived growth factor (PDGFR) /c-kit, and crizotinib, targeting Alk/Met[17].

The family of cytoplasmic TKs include 10 subfamilies (Abl, Ack, Csk, Fak, Fes, Frk, Jak, Src, Tec, Syn), indirectly regulated by extra-cellular signals (**Fig.5**). Some cytoplasmic TKs are anchored to the cell membrane through amino-terminal modifications, such as myristoylation or palmitoylation. Besides the catalytic domain, they possess domains that mediate protein-protein, protein-lipid, and protein-DNA interactions. The most commonly found protein-protein interaction domains in cytoplasmic TKs are SH2 and SH3 domains. The structures of TKs in the active state are all very similar, despite the fact that they have different substrate specificities and different mechanisms of control. Structural biology has revealed several different mechanisms of self-regulation. In most cases, the position of C-helix and/or the A-loop is involved, and very often regions outside the kinase domain fold back to block the binding sites or cause conformational changes in order to inactivate the kinase. Many of these mechanisms are shared by kinases from distinct TKs subgroups and also with non-tyrosine kinases[18].

In general, phosphorylation of tyrosine residues in the A-loop of cytoplasmatic TKs leads to an increase the in enzymatic activity. A-loop phosphorylation occurs via trans-autophosphorylation or phosphorylation by a different cytoplasmic TK. On the other hand, phosphorylation of tyrosine residues outside of the A-loop can negatively regulate kinase activity[15].

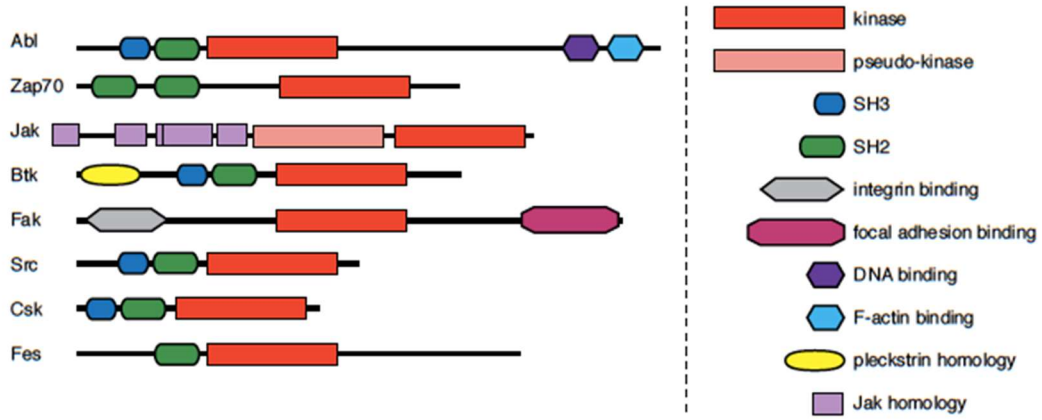

Fig.5. Cytoplasmatic TKs.

Medicinal chemistry research has led to the development of many TK inhibitors (TKI).

In 2001, the first TKI drug imatinib was rapidly approved by the FDA and opened up new research opportunities for cancer treatment. Until 2018 a total of more than 20 kinds of TKI

have been approved by the FDA[19] and by European Medicines Agency (EMA). These drugs have high selectivity, high efficacy, low side effects, are easy to prepare, and have many advantages in the treatment of different cancers (including chronic myeloid leukemia, non-small cell lung cancer, renal cell carcinoma) than the traditional cytotoxic antineoplastic agents[20]. Some TKIs have become the first-line drug for the treatment of specific malignancies.

CHAPTER 2

SGK1

2.1 SGK family kinases

The SGK family consists of three separate but highly homologous isoforms (SGK1, SGK2, and SGK3) encoded by three different genes[21]. SGKs are cytoplasmatic STKs belonging to the AGC family. Accordingly, they display structural and functional similarities with others AGC family members such as Akt, PKC and S6K1–3 (Ribosomal S6 Kinase). Structurally, SGKs consist of three domains: an N-terminal variable region, a catalytic domain, and the C-terminal tail[22]. For each SGK isoforms, several variants have been identified. All SGK isoforms have at least two key regulatory sites, a serine in the C-terminal hydrophobic domain and a threonine in the A-loop of the catalytic domain, both of which require phosphorylation for the complete activation. Each SGKs is able to produce multiple splice variants. SGK1 has four distinct variants which all differ in the N-terminal region, two of which contain an ER motif and are rapidly degraded via the 26S proteasome. Both SGK2 and SGK3 produce two variants, with SGK3 containing a PX domain in the N-terminal region[23] (**Fig.6**).

To become functional, SGK family members require activation by phosphorylation, which is accomplished through a signaling cascade involving the 3-phosphoinositide kinase (PI3K) pathway. Once activated, SGKs becomes potent regulators of metabolism, transport, transcription, and activity of different enzymes and thus participate in the regulation of diverse functions such as epithelial transport, excitability, cell proliferation, and apoptosis[24]. The most studied isoform is SGK1 for its implication in cancer and in the metabolic syndrome[25,26], a very common pathologic state characterized by hypertension, obesity and diabetes.

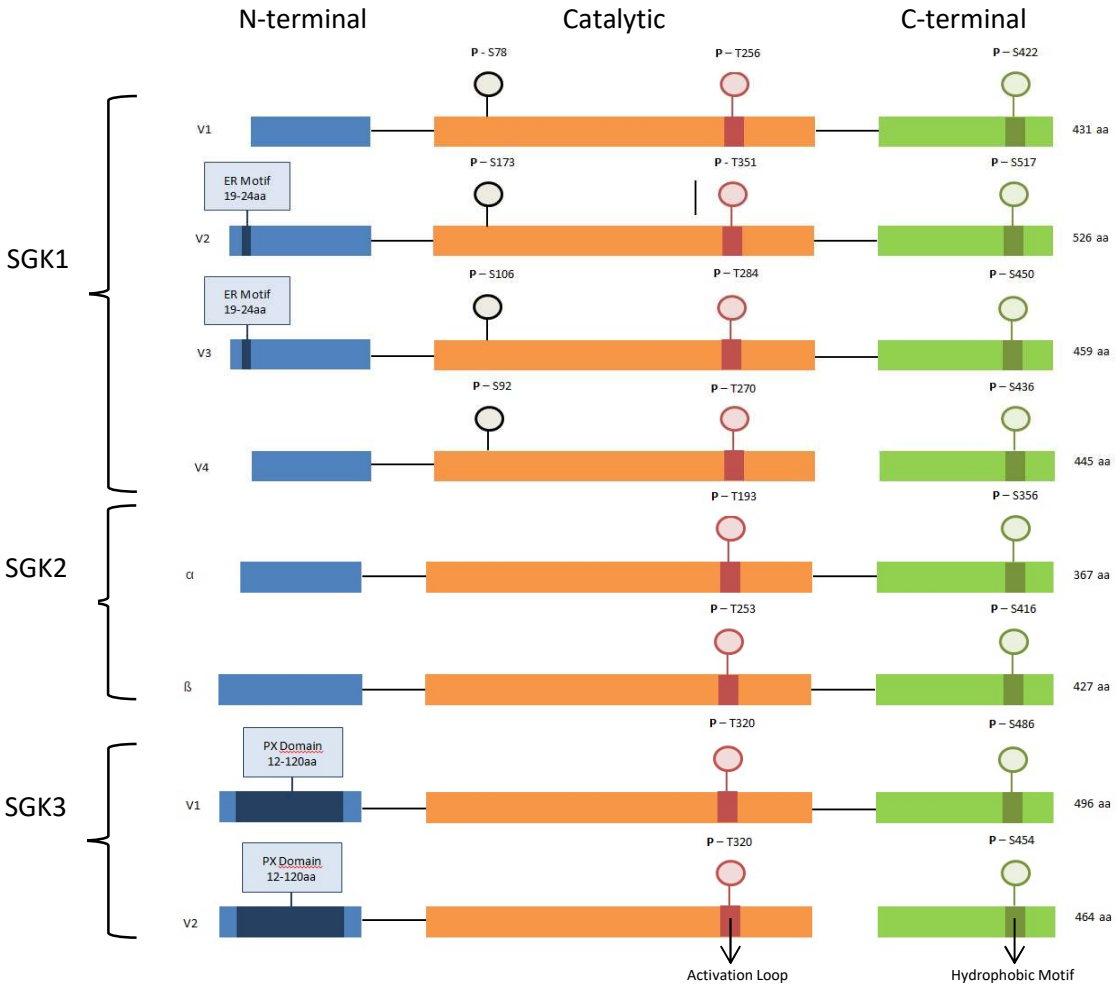

Fig.6. SGK isoforms and variants.

2.2 SGK1 structure and functions

In 1993, the ubiquitously expressed[27] SGK1 has been discovered in rat mammary tumor cells, as a gene transcriptionally responsive to serum and glucocorticoids[28]. Later the human SGK1 has been identified as a gene up-regulated by cell shrinkage[29]. SGK1 regulates diverse effects of extracellular agonists by phosphorylating regulatory proteins that control cellular processes such as ion transport and growth[27].

Within its catalytic domain, SGK1 is 54% homologous to Akt, and both kinases share the same phosphorylation consensus motif (RXRXXS/T)[25].

The X-ray crystallographic structure of inactive SGK1 (pdb entry:2R5T), reported by Zhao and coworkers[30], reveals that SGK1 is composed of two lobes, a N-terminal lobe featuring mainly anti-parallel β-strands and a C-terminal lobe comprising α-helices and loops (**Fig.7**). The A-loop containing the catalytic element DFG motif is present in the C-lobe. The DFG motif is responsible for positioning the molecule of ATP for the phosphorylation. In Akt and generally in AGC kinases, the A-loop is connected to the N-lobe through the C-helix[31]. However, in SGK1 the C-helix is not present, which makes SGK1 different from other AGC family members.

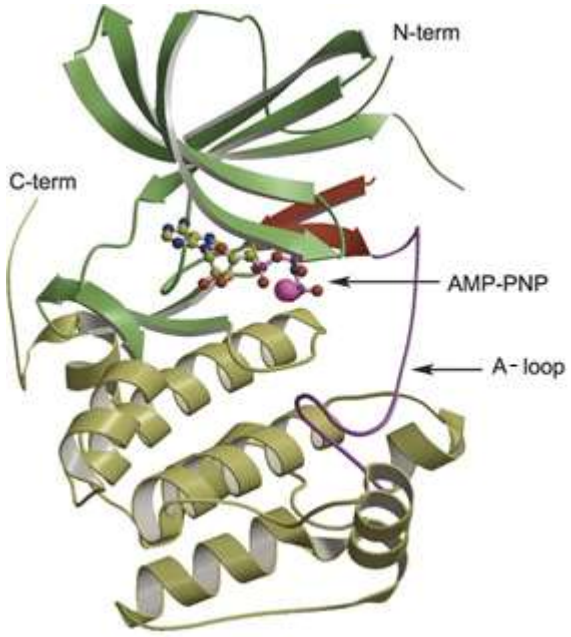

Fig.7. SGK1 kinase domain in complex with AMP–PNP and Mg^{2+}.

2.3 SGK1 regulation and activation

SGK1 transcription is up-regulated by a multitude of different stimuli**,** growth factors, the p53 tumour suppressor protein, and various cellular stressors such as ischemic injury, heat shock and ultraviolet stress[27]. Once expressed, SGK1 can be activated by insulin, insulin-like growth factor 1 (IGF1), hepatic growth factor (HGF), follicle stimulating hormone (FSH), thrombin and corticosterone[32]. SGK1 activators also include PI3K and 3-phosphoinositide-dependent kinase (PDK1). PI3K induce mammalian target of rapamycin mTOR complex-2 (mTORC2) to

phosphorylate SGK1 hydrophobic motif (H-motif) on Ser422. Then PDK1 binds to the H-motif of SGK1, at the level of phospho-Ser422, and further phosphorylates the protein at Thr256 [33] (**Fig.8**). SGK1 is regulated by multiple protein kinases including also the cyclic AMP-dependent protein kinase (PKA)[34] and interleukin-2 (IL-2) a cytokine essential for lymphocytic survival and function[35]. Moreover SGK1 is considered a convergence point in peptide and steroid hormone regulation of epithelial Na^+ channel (ENaC) mediated Na+ transport[36].

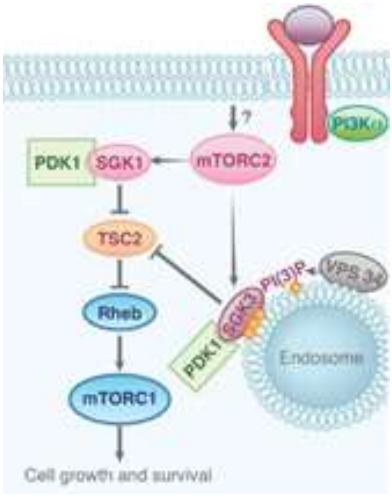

Fig.8. SGK1 regulation and activation by mTORC2 and PDK1 phosphorylation.

2.4 SGK1 targets

Specific SGK1 targets are N-myc down-regulated genes (NDRG) 1 and 2. Other SGK1 targets are shared by other kinases including SGK and Akt isoforms[27]. SGK1 influences a variety of enzymes including ubiquitin ligase NEDD4-2, inducible nitric oxide synthase (iNOS), the STKs WNK4 and MAPK1, mitogen-activated protein kinase/ERK kinase kinase 3 (MEKK3), stress-activated kinase (SEK1), B-Raf kinase, glycogen synthase kinase 3 (GSK3), p53-ubiquitinating mouse double minutes 2 (MDM2)[37]. SGK1 up-regulates transcription factors such as CREB, AP-1 and Nuclear factor κB (NF-κB). On the other hand, SGK1 phosphorylates and thus activates NDRG1, which in turn down-regulates NF-κB signaling[38]. SGK1 is a powerful regulator of several ion channels including ENaC, voltage-gated Na^+ channel SCN5A, renal outer medullary K^+ channel ROMK1 and voltage-gated K^+ channels[39].

2.5 SGK1 and cancer

Over time, growing and impressive evidence has been accumulated, linking SGK1 to the cell survival, de-differentiation, cell cycle control, regulation of caspases, response to chemical, mechanical and oxidative injury in cancer models as well as to the control of mitotic stability. Much evidence shows that SGK1 is over-expressed and/or activated in a variety of tumors such as breast[25], ovarian[40], prostate[41], non-small cell lung cancer[42] and glioblastoma multiforme (GBM)[43]. Recently, SGK1 expression has been described as related to events of invasiveness and metastasization[44,45]. Moreover, many contributions to the literature demonstrate that SGK1 can mediate chemo-and radio-resistance during the treatment of various human tumors, both *in vitro* and *in vivo*[46].

Taken together, all the evidence points to SGK1 as a key element in the development and/or progression of human cancer (**Fig.9**).

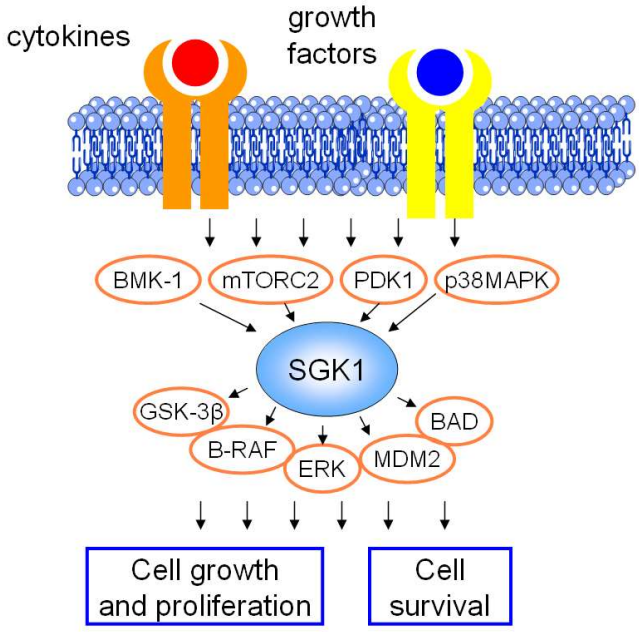

Fig.9. SGK1 involvement in cancer.

2.5.1 SGK1 and prostate cancer

The majority of prostate cancers express the androgen receptor (AR) and rely on androgens for growth and survival. For this reason, patients with prostate cancers generally undergo androgen deprivation therapy with chemical and/or surgical castration as a primary intervention. In this

context, Sherk *et al*. demonstrated that the SGK1 gene is an androgen-regulated target gene in cellular models of prostate cancer. Importantly, RNAi mediated knockdown of SGK1 expression attenuates androgen-mediated growth of the prostate cancer cell line LNCaP[47].

Szmulewitz *et al.*, investigating in SGK1 and glucocorticoid receptor (GR) implication in prostate cancer, reported that SGK1 expression is high in most untreated prostate cancers and declines with androgen deprivation. Moreover, GR expression increased with androgen deprivation, potentially providing a mechanism for the maintenance of androgen pathway signalling in these tumors[48].

Unfortunately, due to acquired resistance to AR-directed therapy the prognosis of patients presenting castrate-resistant prostate cancer (CRPC) remains very poor. GR and AR share several transcriptional targets, including the anti-apoptotic genes SGK1. Because GR expression increases in a subset of primary prostate cancer cells (PCa) following androgen deprivation therapy, Isikbay *et al*. decided to investigate the GR activation contribution to AR-directed therapy resistance. Increased GR-regulated SGK1 expression appears, at least in part, to mediate enhanced PCa cell survival. Therefore, GR and/or SGK1 inhibition may be useful adjuncts to AR blockade for treating CRPC[49]. Recently, Liu *et al.* investigated the effects of the competitive SGK1 inhibitor GSK650394 on PCa cell lines and on PC3 xenografts models demonstrating that SGK1 inhibition exhibits significant antitumour effects *in vitro* and *in vivo*[50].

2.5.2 SGK1 and colon cancer

In 2009 published work demonstrate that SGK1 deficiency counteracts the development of colonic tumors, an effect at least in part due to up-regulation of proapoptotic transcription factor FOXO3a which in turn stimulates transcription of the Bcl2-interacting mediator BIM[51].

By RNA silencing of SGK1 on RKO human colon carcinoma cell line, Amato *et al.* demonstrated that SGK1 affects mitotic stability through regulation of Ran-specific binding protein 1(RANBP1) expression and enhances taxol sensitivity in RKO cell lines[52]. In 2015, the same research group, decided to test the pyrazolo[3,4-*d*]pyrimidine SI113 which previously demonstrated specificity for SGK1 in enzymatic assays. The compound possesses antiproliferative activity on colon cancer cells and potentiate cell sensitivity to paclitaxel[53].

Liang *et al.* developed a novel analog of GSK650394 (previously reported in the field of prostate cancer), called QGY-5-114-A, and further evaluated its effects on colorectal cancer (CRC) cells and tumor growth both *in vitro* and *in vivo*. QGY-5-114-A showed a lower IC_{50}

value compared to its analogue. Moreover, QGY-5-114-A inhibits CRC cell proliferation and migration in *vitro* and decreases colonic tumor growth *in vivo*[54].

Recently another work demonstrated strong SGK1 implication in CRC. In particular, knockdown of long non-coding RNA XIST inhibited doxorubicin resistance in CRC cells by upregulation of miR-124 and downregulation of SGK1[55].

2.5.3 SGK1 and endometrial, cervical and ovarian cancer

Endometrial cancer is often characterized by PI3K/Akt pathway deregulation, implicating a possible SGK1 involvement in the pathogenesis. In this context, Conza *et al.* successfully demonstrated that SGK1 expression is increased in tissue specimens from neoplastic endometrium. Moreover, the previously cited SGK1 inhibitor SI113[53] induced autophagy, apoptosis, and endoplasmic reticulum stress in endometrial cancer cells[56].

Furthermore, D'Antona *et al.* reported *in vitro* data obtained in ovarian carcinoma cell lines and *in vivo* data from ovarian carcinoma xenografts in nude mice. Their results indicated that SI113 inhibits cancer cell proliferation, potentiates the effects of paclitaxel-based chemotherapy, counteracts the development of paclitaxel resistance, and restores sensitivity to paclitaxel in paclitaxel-resistant A2780 ovarian cancer cells[40].

A recent study reported by Wang *et al*. highlights the role of SGK1 in promoting cervical cancer cell survival by an anti-ROS mechanism. Mechanistically, SGK1 activation exerts antioxidant effect through induction of c-JUN-dependent nuclear factor E2-related factor 2 (Nrf2) expression and activity. Importantly, they find out that inhibition of SGK1 confers vulnerability to melatonin as a pro-oxidant, resulting in ROS over-accumulation and consequently enhanced cell cytotoxicity. They further demonstrate that the combined use of the previously reported SGK1 inhibitor GSK650394 and melatonin yields substantial regression of cervical tumors *in vivo*[57].

2.5.4 SGK1 and breast cancer

Increased SGK1 expression represents one mechanism which cause Akt inhibitor resistance in breast cancer. For this reason, SGK1 inhibitors or dual Akt/SGK1 inhibitors could be useful for treating Akt-resistant cancer cells possessing elevated SGK1[58].

Salis *et al.*, investigating in the cytotoxic effect of fluvastatin on MCF-7 breast cancer cells, suggested that the drug antiproliferative activity may be related to the decreased levels of SGK1 and caveolin-1 (CAV1)[59].

Later, another research group, demonstrated that in breast cancer cells resistant to PI3Kα inhibitors, targeting SGK1 restores the antitumoral effects of PI3Kα inhibition[60].

Recently, an integrated siRNA screen, performed by Ma *et al.*, identified SGK1 as essential for Src-induced transformation of mammary epithelial cells. Accordingly, they find that Src positively regulates SGK1 expression in triple negative breast cancer cells, which exhibit a prominent signalling network governed by Src family kinases. Promising results demonstrated that the combined inhibition of Src and SGK1 reduces colony formation and xenograft growth more effectively than either treatment alone[61].

2.5.5 SGK1 and hepatocellular carcinoma

Analysis of gene expression in human hepatocellular carcinoma (HCC) cells demonstrates that SGK1 and Akt are equally overexpressed when compared with normal human hepatocytes, suggesting that both kinases might have roles in hepatocellular dysregulation[62].

In 2016, Salis *et al.* correlated the activity of fluvastatin in reducing human hepatocellular carcinoma (Hep3B) cell migration with the expression of some genes, including SGK1[63].

Talarico *et al.* demonstrated that SI113, previously cited for its activity in inducing cell death in colon carcinoma and endometrial cancer cells[53,56], also inhibits tumour growth in HCC models *in vitro* and *in vivo*. In details, proteome-wide biochemical studies confirmed that SI113 down-regulates the abundance of proteins downstream of SGK1 with established roles in neoplastic transformation. Consistent with knock-down and over-expressing cellular models for SGK1, SI113 potentiated and synergized with radiotherapy in tumor killing. Furthermore no short-term toxicity induced by SI113 was observed in treated animals during *in vivo* experiments[64]. In conclusion, SGK1 inhibition can be effective in hepatic cancer therapy, either alone or in combination with radiotherapy.

2.5.6 SGK1 and glioblastoma multiforme

Talarico *et al.* found that SGK1 expression is correlated with high-grade glial tumors in a cohort of GBM patients. Accordingly, they decided to expand the analysis of SI113 efficacy in GBM cellular models demonstrating that SI113 produces a dramatic decrease in cell viability by

inducing apoptosis in GBM cell lines. They demonstrated that the SGK1 inhibitor enhances the effects of ionizing radiations in the induction of cell death and distortion of cell cycle progression. Indeed, SI113 synergizes with oxidative stress, the primary mechanism of the radio-dependent tumor killing, and modulates the autophagic response and the reticulum stress[43].

Additionally, the same research group investigated on the combined effects of $^{64}CuCl_2$ (association between copper levels and cancer deregulation has been established in the last few years) and SI113 on human GBM cell lines with variable p53 expression. They demonstrate that $^{64}CuCl_2$ is able to induce a time and dose dependent modulation of cell viability in highly malignant gliomas and the co-treatment with SI113 leads to an additive/synergistic effects in terms of cell death[65].

GBM-stem-like cells (GBM-SCs) are known to be enriched in hypoxic niches which probably contribute to drugs resistance. Kulkarni *et al.* identified new genetic targets for GBM-SC using an unbiased pooled shRNA screening approach. SGK1, in addition to other potential targets, was validated as key essential protein in multiple GBM-SCs[66].

Very recently, Matteoni and colleagues employed GBM cell lines, either established or primary (neurospheres), and used a Reverse-Phase Protein Arrays (RPPA) platform to assess the effect of SI113 in this aggressive brain tumor. They demonstrated that SI113 strongly affected the PI3K/mTOR pathway, evoking a pro-survival autophagic response in neurospheres. For this reason, the association of SI113 with an autophagy inhibitor has been further investigate. Data showed that the combination of SI113 with the antimalarial drug quinacrine, induced a strong synergistic effect in inhibiting GBM growth in all the tested cells. RPPA clearly identified the molecular pathways influenced by SI113 in GBM cells, highlighting their vulnerability when the drug was administered in association with autophagy inhibitors[67].

2.6 SGK1 and the metabolic syndrome

Metabolic syndrome is a pathological state mainly characterized by hypertension, obesity and diabetes. SGK1 plays a key role in the hypertensive effects induced by glucocorticoids[39].

In humans a specific variant of SGK1 gene is associated with moderately enhanced blood pressure and with insulin-sensitivity of blood pressure increase[68]. Additionally, the same SGK1 gene variant is correlate to an increased body mass index. Accordingly, the SGK1 gene variant

is more prevalent in patients with type II diabetes than in individuals without family history of diabetes[69]. These evidences implicate the involvement of SGK1 in metabolic syndrome pathophysiology (**Fig.10**).

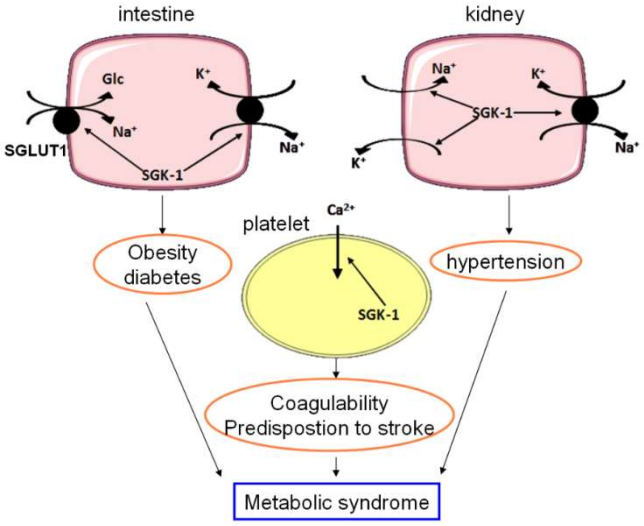

Fig.10. SGK1 in metabolic syndrome.

2.6.1 SGK1 and blood pressure

SGK1 plays a key role in blood pressure control due to its influence on renal salt excretion and salt intake[70]. Accordingly, induction of hyperinsulinemia in mice by pretreatment with a high-fructose diet sensitizes arterial blood pressure to high-salt intake in wild type (wt) but not SGK1 deficient mice. Thus SGK1 mediates the salt-sensitizing effect of hyperinsulinism on blood pressure[24]. Moreover, the activity of SGK family members is essential for ENaC-mediated Na+ transport. It has been confirmed that expression of normal SGK over endogenous levels results in a potentiated natriferic response to ADH, suggesting that the enzyme is a rate-limiting step for the hormone response[36].

2.6.2 SGK1 in obesity and diabetes

SGK1 is involved in obesity development[71] which leads to insulin resistance and ultimately impair insulin release causing type II diabetes. The mechanisms which causes insulin resistance in obese individuals include intracellular lipid-induced inhibition of insulin-stimulated insulin-receptor substrate (IRS)-1 tyrosine phosphorylation, resulting in reduced IRS-1-associated PI3K activity and subsequent decrease of insulin-stimulated glucose transporter type 4

(GLUT4) activity[72]. SGK1 promotes the development of obesity at least partially by stimulation of the Na^+ coupled glucose transporter (SGLT1), which accelerates the intestinal uptake of glucose. As a consequence, an excessive amount of insulin is released causing an enhancement of fat deposition, with subsequent decrease of plasma glucose concentration, which triggers repeated glucose uptake and thus obesity. Conversely, obesity could be counteracted by inhibitors of SGLT1. In diabetes mellitus, the excessive plasma glucose concentrations could, at least in part, upregulate intestinal SGK1 expression and the enhanced SGK1-dependent stimulation of SGLT1 could contribute to the maintenance of obesity[73].

CHAPTER 3

Src family kinases

Src family kinases (SFKs) counts eleven members: Src, Fyn, Yes, Fgr, Blk, Hck, Lck, Lyn, Frk, Srm and Brk. They regulate multiple signal transduction pathways involved in growth, proliferation, differentiation, migration, metabolism, and apoptosis by interaction with a diverse array of molecules, including growth factor receptors, cell-cell adhesion receptors, integrins and steroid hormone[74].

The prototypical member of this family is c-Src, the first discovered oncogene. In the early 1900s, Rous described a transforming factor present in tissue of sarcoma bearing chickens that drove the formation of tumors in normal chickens. Injection of a tissue homogenate made from tumor-bearing chickens allowed for transmission of this factor. This tissue factor was later known as the Rous Sarcoma Virus (containing v-Src). In 1979, J. Michael Bishop and Harold Varmus discovered that normal cellular Src (c-Src) had the potential to be altered in a manner that allowed it to drive a cancerous phenotype. Their work in elucidating the mechanism of malignant transformation won them the Nobel Prize in medicine in 1989 and opened the field of oncogenesis[75]. Subsequent proteomic studies led to the identification of other members of the entire family of these proteins including Fyn, Src, Yes, Fgf, Lyn, Hck, Blk, Lck, and Yrk[76]. Among them, Src, Yes, Fyn, and Yrk are ubiquitously expressed in mammals, while the expression pattern of the other members is restricted to specific tissues[77].

Since they have been discovered, many studies have correlates SFKs as cellular oncogenes. Furthermore, evidence suggests that SFKs play roles in cancer cell invasion and metastasis.

3.1 c-Src kinase

Human c-Src is a 535 amino acids protein and has a structure that shares common features with the other SFK members. Indeed all SFKs present a conserved domain organization that includes a N-terminal SH4 domain, followed by a “unique” region, SH2, SH3, a poly-proline type II (PPII) domain, a catalytic domain (called SH1) and finally a short C-terminal tail (**Fig.11**).

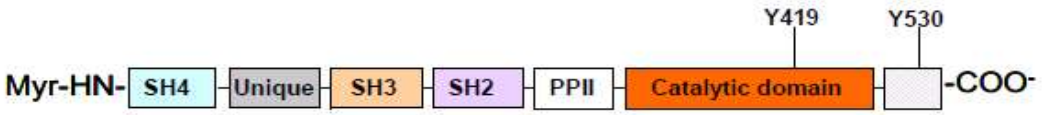

Fig.11. Schematic presentation of c-Src structure.

The SH4 domain which is always myristoylated and sometimes palmitoylated[78], is the membrane-targeting region that allows the association between the protein and the inner surface of the cell membrane. The "unique" region, comprising about 70 amino acids, is the most divergent domain among SFK members providing functional specificity.

The two highly conserved domain SH2 and SH3 regulate Src activity. SH2 presents a central three-stranded β-sheet with a single helix packed against each side; this structure leads to the formation of two recognition pockets. SH3 domain, instead, consists of five antiparallel β-strands and two loops that bind the PPII domain. The PPII domain is characterized by proline-rich sequences that adopt a helical conformation in complex with the SH3 domain, binding with aromatic amino acid side chains on the SH3 surface. The catalytic domain SH1, responsible for the kinase activity, presents a bilobal structure (a small N-terminal lobe and a large C-terminal lobe) which forms the ATP and substrate binding site at the interlobe cleft. In the C-terminal lobe is located the positive regulatory site A-loop, where the Tyr419 is the key residue. A flexible chain, called the "hinge region", connects N- and C- lobes.

Src exists in two forms: a closed, inactive conformation and an open and active one. There are two key elements that regulate the Src conformation: the amino acids Tyr419 and Tyr530. When Tyr419 is phosphorylated and Tyr530 dephosphorylated, Src is in the active state, while, when Tyr419 is dephosphorylated and Tyr530 phosphorylated, the kinase is in the inactive state. The inactive enzyme is forced in a closed conformation by intramolecular contacts among the SH2 and SH3 domains and the catalytic site.

The activation of Src occurs displacing regulatory subunit SH3 and SH2 domains from the kinase domain. This permits Tyr419 autophosphorylation. In particular, several extracellular molecules can activate Src binding receptors, such as growth factor receptors, integrins and other adhesion receptors, guanosine phosphate binding-coupled receptors (GPCRs), cytokine receptors and ion channels. Src, in response to these extracellular signals, becomes activated

and phosphorylates various downstream targets, regulating multiple signal transduction pathways, including Ras/Raf, RhoGAP, PI3K/Akt pathways and many others (**Fig.12**).

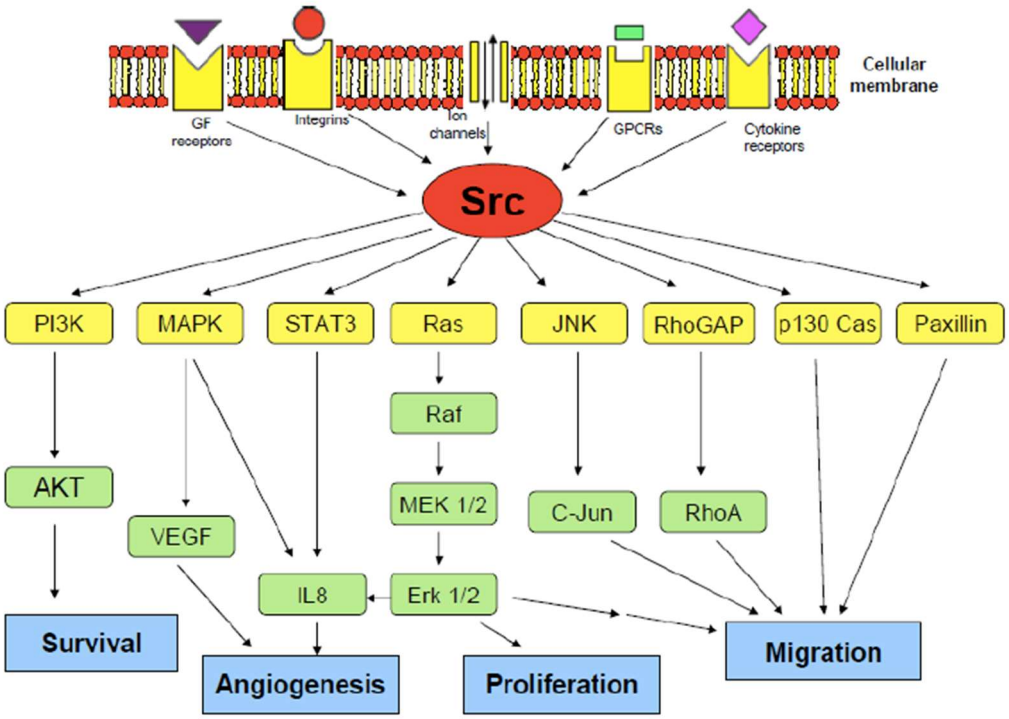

Fig.12. Schematic representation of Src signalling pathway.

3.1.1. Src and cancer

Src is the most studied member of the Src family kinases (SFKs), both in cancer and in other pathologies. An increased Src activity is found transiently in almost every aspect of a normal cell life in response to different physiological conditions, including mitogenesis, proliferation, survival, adhesion and motility, all of them deregulated during cancer progression[79].

High expression of Src have been detected in several cancers and are generally correlated to a poor prognosis with respect to overall survival. Moreover, recent studies suggest that Src could be associated with the development of acquired drug resistance[80,81].

3.1.1.1 Src and brain cancer

Src is a key downstream intermediate of growth factor receptors frequently overexpressed in brain tumors, including EGFR and PDGFR, involved, in association with focal adhesion kinase (Fak), in cytoskeletal-linked cell survival and migration[82].

Initial studies have found elevated Src activity in GBM compared with normal brain samples, and have revealed its oncogenic properties for brain tumors[83]. In preclinical models of GBM, genetic and pharmacologic blockade of Src resulted effective in inhibiting cell proliferation and invasion[84,85].

More specifically a pyrazolo[3,4-*d*]pyrimidine derivative, called SI306, selected for its favorable activity against Src, was tested *in vitro* and *in vivo* on GBM cell lines. *In vivo*, combination treatment with SI306 and radiotherapy was strongly active in reducing U-87 xenograft growth with respect to control and single treatments[86].

Moreover a recent study highlights the capability of SI306 to increase the intracellular accumulation of Rho123, and to enhance the efficacy of paclitaxel in P-glycoprotein (P-gp) overexpressing GBM cells[87].

It has been reported that c-Src also plays a key role in the differentiation, adhesion, and survival of neuroblastoma (NB) cells, due to its hyperactivation rather than overexpression[88]. Src was also hypothesized to have an oncogenic role in the progression of aggressive NB forms[89]. Inhibiting its catalytic activity with small molecule inhibitors has been recently reported as a potential approach to the treatment of NB[90]. In particular, some pyrazolo[3,4-*d]*pyrimidine derivatives, including the previously reported SI306, resulted also active in the inhibition of neuroblastoma cell proliferation showing *in vivo* activity in xenograft model using SH-SY-5Y cells[91,92].

Sikkema *et al*. identified a panel of tyrosine kinase associated with pediatric brain tumors such as medulloblastoma, astrocytoma, and ependymoma. The researchers found high SFK activity in these tumors, as established by high levels of phosphorylation, in comparison with normal tissues. This observation suggests that Src could have a key role in the development of medulloblastoma. It has been reported that some pyrazolo[3,4-*d*]pyrimidines reduced the growth rate of medulloblastoma cells by inhibiting Src in a mouse model[93].

Recently a proteomic and phosphoproteomic analyses identify aberrant ERBB4-Src signaling as a specific hallmark in group 4 medulloblastoma (the most prevalent biological subtype, comprising approximately 40% of all medulloblastoma patients with 80% of 5-year survival when treated with standard therapy)[94].

3.2 Fyn kinase

Fyn is a member of the SFKs originally identified in 1986 as Syn or Slk, in normal and polyoma virus transformed cells[95]. Fyn is localized to the inner layer of the cell membrane to which it is attached in its myristoilated or palmitoilated form[96].

There are three isoforms of Fyn (1, 2 and 3, also called FynT, FynB and FynΔ7, respectively) which are encoded by the Fyn gene, located on chromosome 6q21. The first 2 variants are known to have biological activity, while for the third, although it has been shown to have functional mRNA in an expression system, no biological effect has been reported[97].

FynT is expressed in cells of hematopoietic origin, while FynB shows more ubiquitous expression with higher levels observed in the brain. These 2 variants differ exclusively within a sequence of about 50 amino acids located at the end of the SH2 domain and the beginning of the SH1 domains, and this difference may account for their distinct biochemical activities, which may dictate functional differences of Fyn variants in normal cells[98].

3.2.1 Fyn structure

Fyn is a 59 KDa non-receptor TK that, similar to other SFKs, consists of SH domains that include an N-terminal SH4 domain followed by the domains SH3 and SH2 and a C-terminal SH1 kinase domain (**Fig.13**). The three first SH domains are shared between the SFKs[76], whiles SH4 is a 14-carbon myristoyl sequence on the N-terminal end of the molecule unique to individual members of the SFKs[99] and it is this domain that associates the molecule with cell membranes. Myristoylation that occurs on glycine residue 2 and palmitoylation at cysteine residues 3 and 6 allow Fyn to attach to plasma membrane and lipid rafts[96].

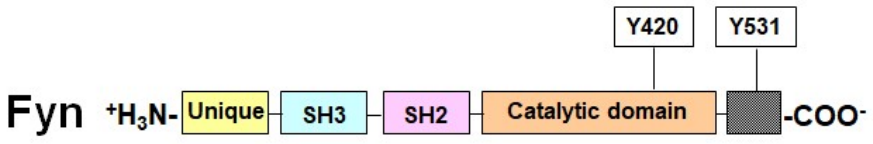

Fig.13. Schematic representation of Fyn structure.

Fyn is characterized also by a common regulatory mechanism with the other SFKs. Indeed, the activation or inhibition of kinase activity depends on intramolecular interactions between SH2 and SH3 with the kinase domain and on phosphorylation/dephosphorylation of two critical tyrosine residues (Tyr420 situated in the A-loop and Tyr531 situated in the C-terminal region).

3.2.2 Fyn functions

Fyn has different molecular functions, including regulation of cell growth, survival, adhesion, cytoskeletal remodeling and motility (**Fig.14**)[100].

In the central nervous system (CNS), Fyn exerts an important role in brain development. In fact, Fyn is involved in axon-glial signal transduction, oligodendrocyte maturation and myelination[101]; it also stimulates the synthesis of abundant myelin associated oligodendrocytic basic protein, thus influencing oligodendroglial morphology, and it is implicated in synapse formation and post-synaptic excitatory transmission[102]. Moreover, Fyn was found to be implied in T-cell development, homoeostasis, activation and to have a critical role in thymocyte development together with Lck kinase, which is another member of the SFKs[103].

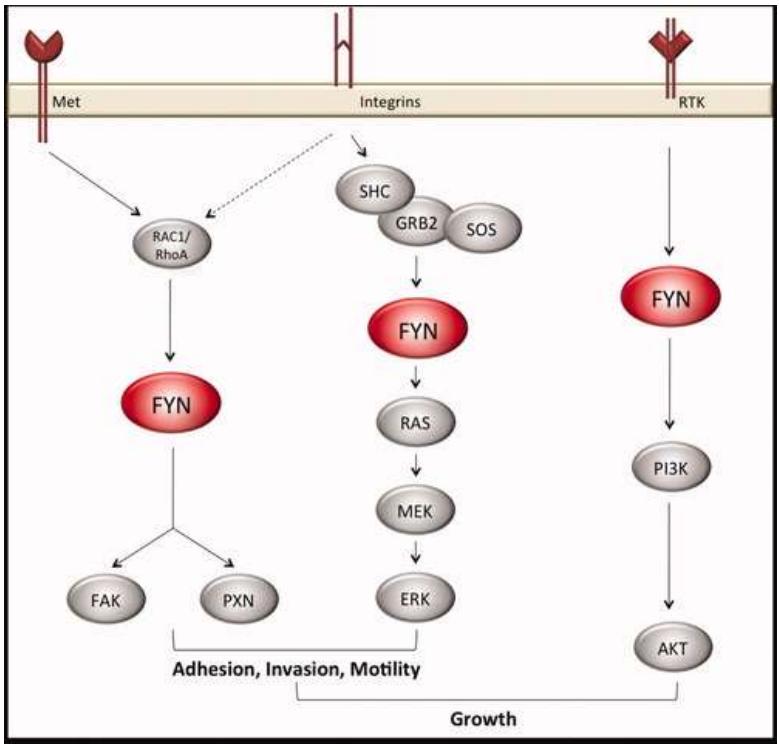

Fig.14. Fyn mediates signals from cell surface receptors to several critical growth and motility pathways.

Due to its many physiological roles, an aberrant expression of Fyn kinase or a dysregulation of its activity is involved in the development and progression of different pathological conditions.

3.2.3 Fyn and cancer

Similar to most SFKs, Fyn signaling affects multiple tumor-related properties in a number of cancer types. Fyn overexpression results in the promotion of antiapoptotic activity of Akt[100].

Firstly, in 1988, Kawakami and colleagues demonstrated that Fyn overexpression induces morphologic transformation and anchorage-independent growth in NIH 3T3 cells. Furthermore, even if a relatively low frequency, Fyn acquires properties of a dominant-acting oncogene capable of inducing a complete tumorigenic phenotype[104].

Fyn, through phosphorylation of Cas, is involved in matrix rigidity, which is important in cell motility and spreading, matrix remodelling and anchorage independency. All these processes, if altered, promote cancer and metastasis formation (**Fig.15**).

In fact, an increased matrix rigidity leads to tissue disorganization and malignant transformation[105].

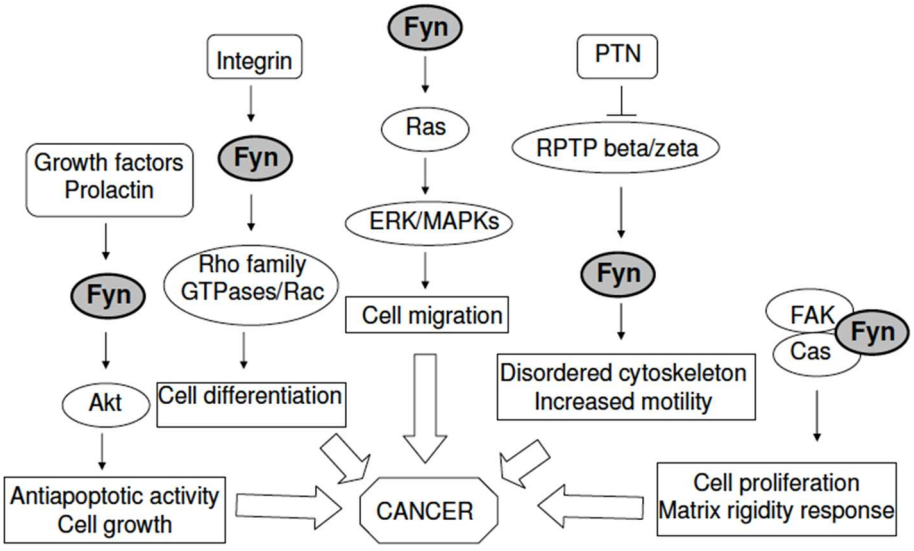

Fig.15. Fyn involvement in cancer.

Enhanced expression and/or activation of Fyn has been observed in various cancers, in particular melanoma, glioblastoma, prostate and breast cancers[106, 100].

Several studies on different cancers have recently demonstrated the importance of Fyn in promoting resistance to anti-cancer agents[107,98,108,109]. Further evidence to support the involvement of Fyn in anti-cancer drug resistance comes from a study on myelogenous leukemia in which increased expression of Fyn was shown to be associated with tumor growth and resistance to imatinib in K562 cell lines[110]. These studies show that Fyn plays a critical role in the development, progression and resistance to anti-cancer drugs in solid and hematologic tumors.

3.2.3.1 Fyn and breast cancer

It has been demonstrated that some breast cancer cell lines express elevated levels of Fyn. Enhanced metastasis formation promoted by Fyn is facilitates by a cell transformation program, known as epithelial to mesenchymal transition (EMT), characterized by loss of cell adhesion, repression of E-cadherin expression, and increased cell mobility.

Moreover it has been reported that Fyn expression in breast cancer cells is associated with poor survival of patients and increased neoangiogenesis, correlated with c-Met and Fak kinases upregulation[111].

Elias *et al.* showed that Fyn is upregulated in tamoxifen-resistant breast cancer cell lines and plays a critical role in the resistance mechanism. Further, the cellular localization of Fyn within cancer cells of primary estrogen receptor positive (ER+) breast tumor tissue may serve as a prognostic marker[98].

Recently, it has been demonstrated a pivotal role of Fyn through signal transducer and activator of transcription 5 (STAT5)/ NOTCH2 signaling node in maintaining the features of basal type (the most aggressive and highly metastatic) breast cancer[112]. Besides, Mi *et al.* demonstrated that miR-381 overexpression increased doxorubicin sensitivity and enhanced doxorubicin-induced apoptosis in breast cancer cells by targeting Fyn gene. Therefore, miR-381/Fyn/MAPK pathway may be applied as a novel target to overcome doxorubicin resistance in breast cancer patients[113].

3.2.3.2 Fyn and prostate cancer

Fyn activity in prostate cancer is perhaps more relevant than that of other SFKs. Accordingly, Posadas *et al*. demonstrated that overexpressed Fyn in prostate cancer interacts with Fak and paxillin (PXN), that are regulators of cell morphology and motility. In addition, data highlight a greater Fyn expression, and not of others SFKs, in prostate cancer compared to normal tissue[114].

Few years later, the same research group demonstrated that Fyn is strongly up-regulated also in human neuroendocrine prostate cancer (NEPC) tissues and xenografts, as well as cells derived from a NEPC transgenic mouse model[115].

Furthermore, performing *in vitro* and *in vivo* experiments, Jensen and colleagues showed that Fyn is an important molecule in the HGF/Met signaling pathway that contributes to prostate cancer metastases. Consistently, reduced Fyn expression results in impaired cancer cell growth and motility, key events in the metastatic process[116].

3.2.3.3 Fyn and melanoma

Huang and colleagues reported that Fyn, is selectively activated among SFKs, in a murine melanoma cell line characterized by a high metastatic potential. Significant tyrosine phosphorylation of cortactin (a cytoplasmatic protein promoting polymerization and rearrangement of the actin cytoskeleton and involved in cell migration) induces complex formation between activated Fyn and cortactin in cell membranes. The authors demonstrated that cortactin is a specific substrate of Fyn in integrin-mediated signalling processes regulating metastatic potential[117]. Recently, Fyn has been identified as a melanoma biomarker which contributes to the tumor development[118].

3.2.3.4 Fyn and brain tumors

Regarding brain tumors, Fyn gene, together with other genes involved in brain development and neural differentiation, is strongly enriched in astrocytoma, a common and lethal human malignancy.

In 2010, Lu *et al.* demonstrated that the pan-SFK inhibitor dasatinib inhibits invasion, promotes tumor regression, and induces apoptosis *in vivo*, significantly prolonging mice survival in an orthotopic GBM model. This study elucidates a mechanism linking EGFR signalling with Fyn

and Src activation to promote tumor progression and invasion and provides the rationale for combined anti-EGFR and anti-SFK targeted therapies[119].

Lewis-Tuffin and colleagues observed that Fyn knockdown reduced the growth and migration of glioma cell lines and was associated with reduced phosphorylation of cell motility-associated molecules such as catenin or Cas[120].

In a glioblastoma cell line model, Zhang *et al.* demonstrated that Fyn plays an important role in oncogenic activities of AMP-activated protein kinase (AMPK) signaling by antagonizing the tumor suppressor function of AMPK through the activation of PIKE-A, a molecule that impairs the functions of AMPK[121].

Recently, Comba *et al*. confirmed that Fyn expression positively correlates with GBM cell aggressiveness. The histopathological evaluation of gliomas indicates that the loss of Fyn reduced malignant features such as pseudopalisades, necrosis, and hypervascularization. This study indicates an important role for Fyn in modulating many glioma cellular processes and its relevance as a novel regulator of GBM behaviour and therapy response[122].

3.2.4 Fyn and Alzheimer's disease

Alzheimer's disease (AD) is a progressive form of dementia that interferes with memory, thinking, and behavior. It is characterized by a gradual loss of neurons, particularly in the cortex and hippocampus. Pathologically, AD is characterized by the presence of extracellular neuritic plaques containing the β-amyloid peptide (Aβ) and neurofibrillary tangles (NFTs) composed of hyperphosphorylated Tau protein in the brain[123].

Fyn plays a key role in the development and progression of AD, being involved in the synaptic toxicity and cognitive impairments produced by Aβ oligomers and promoting the formation of neurofibrillary tangles by phosphorylating Tau protein[124]. In fact, Fyn kinase, Aβ and Tau protein have been even referred to as the "toxic triad" of AD.

Recently, deeper understanding of Aβ physiology has led to the recognition of distinct neuronal signaling pathways linking Aβ to synaptotoxicity and neurodegeneration. Preclinical studies demonstrated that soluble assemblies of Aβ, termed Aβ oligomers (Aβo), bind the receptor Cellular Prion Protein (PrPC) on the neuronal cell surface with high affinity, initiating a pathologic cascade converging on Fyn. This mechanism leads to acute changes in *N*-methyl-D-aspartate receptor (NMDA) receptor trafficking, and persistent activation of Pyk2 and eEF2. Therefore, targeting specific signaling pathways involving Aβ, including Fyn, rather than

directly target Aβ, represents an innovative strategy to explore[125] (**Fig.16**). In conclusion Fyn is an attractive target for AD therapeutics, not only based on its activation by Aβ via PrPC, but also due to its interaction with tau, uniquely linking the two key pathologies in AD.

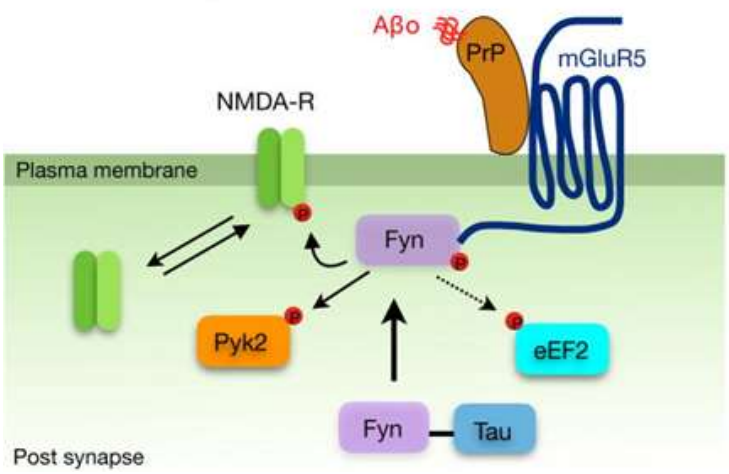

Fig.16. Aβo bind PrPC to activate Fyn kinase.

3.2.5 Fyn and Parkinson's disease

Parkinson's disease (PD) is a neurodegenerative movement disorder characterized by the death of dopaminergic neurons within the nigrostriatal tract. Intracytoplasmic inclusions rich in misfolded α-synuclein (αSyn) are the major histopathological characteristic of PD. Various studies implicate chronic, microglia-mediated sterile neuroinflammation as a crucial contributing factor in the progression of PD[126].

In 2001 two different research groups simultaneously reported that Fyn phosphorylates αSyn. Consistently, phosphorylation by Fyn on αSyn Tyr125 was inhibited by the SFK inhibitor PP2[127,128].

Additionally, Fyn activation plays an upstream regulatory role in evoking proinflammatory signalling following both acute and chronic states of microglia stimulation. Fyn serves as a major upstream regulator of proinflammatory signalling involving PKC, MAPK, and NFκB[126]. For these reasons, Fyn could be exploited as a target in the development of novel antineuroinflammatory drug candidates for treating PD[129].

Therapy with levodopa is the first treatment of choice for PD. However, its long-term use causes levodopa-induced dyskinesia (LID). Recently, Sanz-Blasco *et al.* found that mice lacking Fyn displayed reduced LID compared to wt control mice. Administration of saracatinib, an inhibitor of Fyn activity, also significantly reduced LID in dyskinetic wt mice. These results support that Fyn has a pivoltal role in the molecular pathways affected during the development of LID and identify Fyn as a novel potential therapeutic target for the control of LID in PD[130].

CHAPTER 4

Protein kinases inhibitors

Overexpression, dysregulation and mutations of protein kinases play essential roles in the pathogenesis of many diseases. As a result, increasing attention has been directed towards the identification of novel kinase inhibitors as treatment of various types of human diseases.

The interest in protein kinase inhibitors started to increase since the approval of imatinib (Gleevec®) in 2001 for the treatment of Philadelphia-chromosome-positive (Ph+) chronic myeloid leukemia (CML)[131].

Categorized by binding modes, kinase inhibitors can be grouped into two classes: irreversible and reversible. The latter can be further classified on the basis of the protein region they interact with in:

- kinase domain inhibitors. This group includes the majority of inhibitors and are defined as ATP-competitive inhibitors. They can be further classified on type I and type II (**Fig.17**). Type I inhibitors target the ATP-binding site in the active open conformation. Type II inhibitors target the ATP-binding site of the enzyme in the inactive closed conformation and also occupy the adjacent hydrophobic pocket I (sometimes defined as allosteric pocket) that is only accessible when the kinase is in an inactivated form[132];
- allosteric inhibitors. They can be classified as type III which bind the allosteric pocket near the catalytic site or as type IV which interact with a different allosteric pocket far from the catalytic site (**Fig.17**). They act by inducing conformational changes to modulate the enzymatic activity. This type of inhibitors could be useful to overcome clinically acquired resistance mutations to the first generation of ATP-competitive kinase inhibitors[5];
- bisubstrate and bivalent inhibitors, defined as type V, exhibit more than one of the binding modes described above[133].

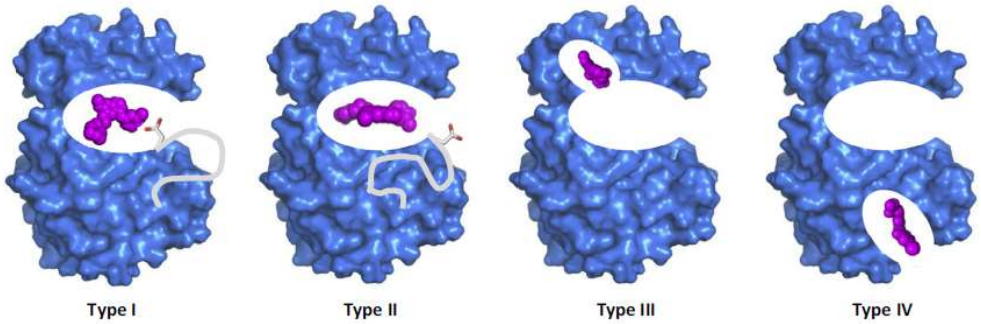

Fig.17. Kinase structure and different types of kinase inhibitors binding modes.

The dominant dogma that the kinase domain was too conserved to enable selective inhibition by small molecules was challenged in the late 1980s when the first examples of selective kinase inhibitors against the EGFR were reported[134]. Since then, a large number of kinase inhibitors of various structural features and inhibition profiles have been identified.

I will discuss below the few SGK1 inhibitors reported in the literature and some examples of the large class of SFKs inhibitors focusing on their activity toward the kinases Src and Fyn.

4.1 SGK1 inhibitors

Despite SGK1 validated role and significance, only a few selective and potent SGK1 inhibitors have been described so far.

In 2008, Sherk *et al.* reported the first selective SGK1 inhibitor, developed by GlaxoSmithKline, the pyrrolo-pyridine GSK650394 **1**[47]. Initially, this compound demonstrated to be able to stop cell growth in different prostate cancer cell lines. Successively, compound **1** showed a synergic effect with cisplatin in the treatment of head and neck tumors in *in vivo* assays[135].

Very recently, Wang *et al.* demonstrated that the combined use of GSK650394 **1** and melatonin yields substantial regression of cervical tumors *in vivo*[57]. However, GSK650394 is equally active on SGK1 and SGK2, moreover, is only about 30 times more selective for SGK1 than for other targets such as Akt, Rho-associated protein kinase, and Janus kinase isoforms (Jak1, Jak3)[46].

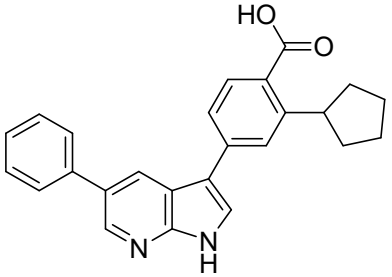

1 GSK650394

The second oldest SGK1 inhibitor reported in the literature is the benzohydrazide derivative **2**, named EMD638683, by Ackermann *et al.*[136] Originally described as an inhibitor of the SGK1-dependent metabolic effects, it has been further evaluated in experimental models of colon cancer. The compound showed to induce apoptosis and modulate radiation-dependent effects, at least at very low dose-rate (3Gy). Also, EMD63868 was able to prevent the chemically-induced colon carcinogenesis *in vivo*, in accordance with the murine knock-out model for SGK1[137].

Recently, Schmid *et al.* demonstrated that compound **2** decreases the viability of rhabdomyosarcoma cells, and enhances the effects of the cytotoxic drug doxorubicin leading to reduced migration and decreased cell proliferation[138]. However, **2** shows poor cell permeability, and it also has an inhibitory effect on PKA, mitogen- and stress-activated protein kinase 1 (MSK1), protein kinase C-related kinase (PRK2), and other SGK isoforms[137].

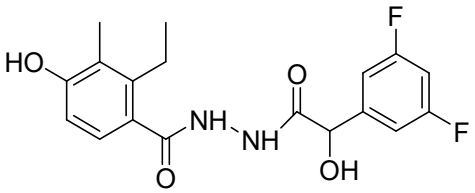

2 EMD638683

Besides, Sanofi has patented several sulphonamide derivatives of pyrazolo-pyrazines which showed an inhibitory activity on SGK1. In particular, compound **3** has shown an IC_{50} value of 1 nM in enzymatic assays on SGK1[139].

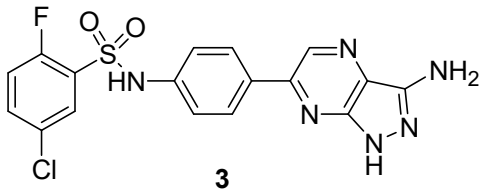

3

Furthermore, Bezzerides *et al.* identified a novel class of SGK1 inhibitors among which 5377051 **4** has been identified as the lead compound. Compound **4** selectively inhibits SGK1 in cultured cardiomyocytes and inhibits phosphorylation of a-SGK1-specific target as well as proliferation in the prostate cancer cell line LNCaP. Finally, 5377051 can reverse SGK1's effects on Nav1.5 (predominant cardiac voltage-dependent sodium channel subtype) and shorten the action potential duration in induced pluripotent stem cell (iPSC)-derived cardiomyocytes from a patient with a gain-of-function mutation in Nav1.5 (long QT3 syndrome). This data suggest that SGK1 inhibitors warrant further investigation in the treatment of cardiac arrhythmias[140].

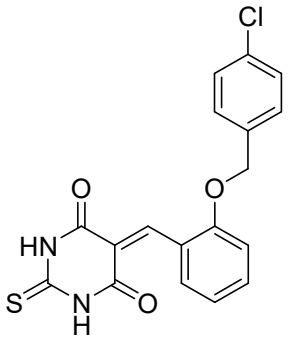

4 5377051

Schenone *et al*. synthesized the pyrazolo[3,4-*d*]pyrimidine SI113 **5** presenting high selectivity, in comparison with Akt1, for inhibiting SGK1 kinase activity by competing with ATP for the binding domain. In detail, a dose dependent curve of SI113-dependent SGK1 and Akt1 inhibition showed that the inhibition of the SGK1 activity occurred with an IC_{50} value of 600 nM, with a 100-fold selectivity compared to Akt1[141]. Similarly, the molecule was significantly less effective in the inhibition of other SI113-targeted substrates, toward which the molecules was originally developed e.g. Abl and Src[53].

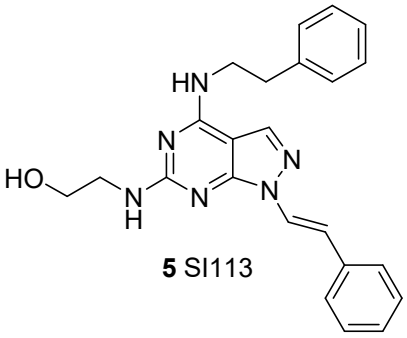

5 SI113

Subsequently, several biological studies have demonstrated a promising activity of SI113 on different type of tumors. In fact, this compound is able to generate cell cycle delay in cancer cells, with G0–G1 accumulation, thus hindering growth capabilities in several human cancer cell lines, *in vitro* and *in vivo*[53,43,64], also strengthening the effects of radiotherapy and oxidative stress, by inducing autophagic cell death[56,43]. SI113 is also able to influence the expression of stemness genes and synergize with mitotic spindle poisons in restraining GBM cell growth *in vitro* and *in vivo*[142]. In addition, a more in-depth analysis of the effect of SI113 on human GBM cells reveals that this compound induces, mainly in primary GBM cells growing as neurospheres, downregulation of mTOR activity and upregulation of AMPKα and acetyl-CoA carboxylase alpha phosphorylation, all markers that indicate the stimulation of an autophagic cellular response that can be either cytotoxic or cytoprotective[67]. Moreover a recent work presenting *in vitro* data obtained in ovarian carcinoma cell lines and *in vivo* data from ovarian carcinoma xenografts in nude mice indicates that SI113 inhibits cancer cell proliferation, potentiates the effects of paclitaxel-based chemotherapy, counteracts the development of paclitaxel resistance, and restores sensitivity to paclitaxel in paclitaxel-resistant A2780 ovarian cancer cells[40].

Very recently, an inhibitory effect of SI113 on cell migration, invading, and EMT has been highlighted by Abbruzzese *et al.* In fact, GBM, hepatocarcinoma and colorectal carcinoma cell lines, when exposed to SI113, showed a remarkable subversion of the cytoskeletal architecture characterized by F-actin destabilization, phospho-Fak delocalization, and tubulin depolimerization. These results were definitely concordant in attributing to SI113 a key role in hindering cancer cell malignancy and, due to its negligible *in vivo* toxicity, can sustain performing a phase I clinical trial to employ this drug in associative cancer therapy[143].

Very recent studies conducted on the natural compound *trans*-resveratrol **6** (RSV) demonstrate, by a series of molecular docking experiments, that this compound directly interacts with SGK1

showing an increased affinity for the phosphorylated forms, compared with the un-phosphorylated kinase. It has been confirmed that RSV inhibits SGK1 kinase activity in a dose-dependent manner, showing a K_i value of 50 μM in an enzymatic assay. In addition, the compound was able to inhibit the SGK1 associated kinase activity in a cell free *in vitro* systems as well as in intact cells using as substrates both specific target peptides and endogenous proteins like MDM2[144].

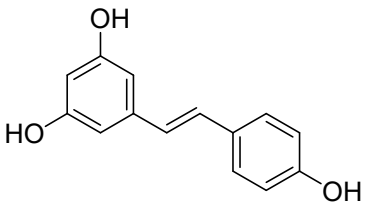

6 *trans* resveratrol

Summarizing, SGK1 inhibition could be a potential therapeutic approach, either alone or combined with traditional strategies, not only for cancer, but also for arrythmia and metabolic syndrome. However further pharmacological investigations are needed to advance clinical trials of SGK1-targeted therapies.

4.2 SFKs inhibitors

Due to the huge number of physiological and pathological processes in which SFKs are implied, the search for small molecules targeting these kinases constitutes a growing field of study. SFKs inhibitors endowed with selectivity toward a specific member of this family would be useful for their therapeutic potential in the treatment of tumors, brain diseases and infections. Moreover, a selective inhibition of these kinase family members would allow a better comprehension of all the different biological roles in which such enzymes are involved and which have not yet been fully understood. In any case, due to the high level of similarity among SFKs, most of the inhibitors show activity toward multiple members of the family and usually also toward other kinases.

The pyrazolo[3,4- *d*]pyrimidine based compounds PP1 **7** and PP2 **8** are two of the oldest and most famous SFKs ligands[145]. Reported by Pfizer in 1996, they can be considered the

representative compounds of a large class of derivatives; PP1 inhibits Lck, Fyn, c-Src and Hck and was later found to be also active on EGFR, c-Kit and Abl, thus resulting the first reported c-Src/Abl dual kinase-inhibitor[146]. Even if they have not been developed as therapeutic agents because of their poor biopharmaceutical property, these compounds remain the references for the synthesis of new compounds targeting SFKs. On the other hand, their activities on cancers are still investigated as demonstrated by many articles. For example, Kong *et al.* showed that compound **8** efficiently reduced cervical cancer cell proliferation trough the inhibition of Src and EGFR activity[147].

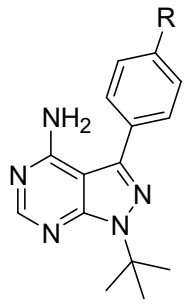

7 PP1, R = CH_3
8 PP2, R = Cl

The potent SFKs inhibitor Dasatinib **9**, (BMS-354825, Sprycel™), a thiazole-carboxamide derivative synthesized by Bristol-Myers Squibb, is the first dual Src/Abl inhibitor used for CML therapy, also useful to overcome several imatinib-resistances, with the exception of the T315I mutation. At the moment is studied in clinical trials for the treatment of non-Hodgkin′s lymphoma, metastatic breast cancer, prostate cancer, and other tumors[148].

Dasatinib is a type I inhibitor and shows IC_{50} values in the subnanomolar range for SFK members in particular of 0.5 and 1 nM for Src and Abl, respectively[149]. However, when Li *et al.* performed an enzymatic and phosphoproteomic characterization of dasatinib action in non-small-cell lung carcinoma (NSCLC), they identified nearly 40 different kinase targets of dasatinib. These include SFK members (Lyn, Src, Fyn, Lck and Yes), other non-receptor TKs and RTKs[150]. Furthermore, using drug-resistant gatekeeper mutants, they showed that particularly Src and Fyn, as well as EGFR, are relevant targets for dasatinib action, getting additional insight both in dasatinib action and in Fyn involvement in this particular malignancy[150,101].

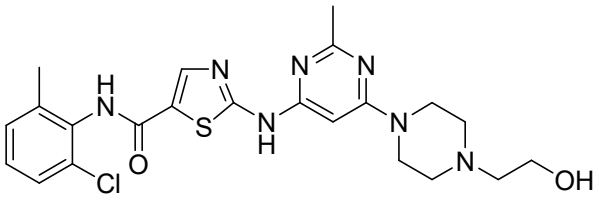

9 dasatinib

Another well-known pan-SFKs inhibitor endowed with anticancer activity is the anilino-quinazoline saracatinib (AZD0530) **10** which is active on c-Src, Lck, Yes, Lyn, Fyn, Fgr, Blk and Abl in the low nanomolar range[151]. Originally developed by AstraZeneca for various types of cancer, the compound showed promising data, inhibiting tumor growth in different xenografts models. Moreover **10** resulted orally available, displaying excellent pharmacokinetic parameters in animals, with good aqueous solubility and moderate binding to plasma proteins[151,152]. Unfortunately, several clinical trials on this compound as anticancer agent stopped on Phase 2 for lack of efficacy.

Interestingly, due to its activity on Fyn (IC_{50} value of 410 nM), saracatinib is currently studied in clinical trials for the treatment of Alzheimer and Parkinson diseases[125,130].

(https://clinicaltrials.gov/ct2/results?cond=&term=saracatinib&cntry=&state=&city=&dist=)

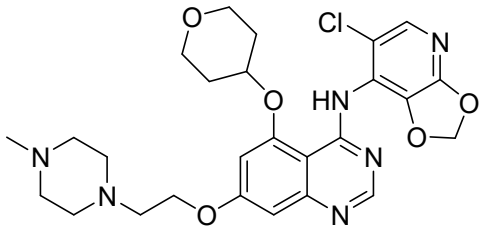

10 saracatinib

The 7-alkoxy-3-quinolinecarbonitrile derivative Bosutinib **11**, called also SKI-606, is an orally potent SFKs and Abl inhibitor reported by Boschelli *et al.* in Wyeth Pharmaceuticals[153].

Bosutinib showed an IC_{50} of 1.2 nM in an enzymatic assay and an IC_{50} of 100 nM on Src cell proliferation. Regarding Fyn, bosutinib showed an IC_{50} value of 410 nM[153].

The clinical efficacy of bosutinib in CML has been supported by several clinical trials and finally, the compound has been approved by FDA and EMA for the treatment of CML patients resistant to prior therapies. Bosutinib is also investigated for its application in solid tumors,

such as breast, prostatic, pancreatic, lung and cervical cancers. Phase I data showed that bosutinib is generally well tolerated with predominantly gastrointestinal adverse effects (NCT00195260)[154].

Luo *et al*., through the use of bosutinib, explored the function of Fyn kinase in signaling events during sperm–egg interactions, sperm incorporation, and meiosis II. They demonstrate that suppression of Fyn signaling prior to fertilization caused disruption of the functional polarity of the oocyte[155].

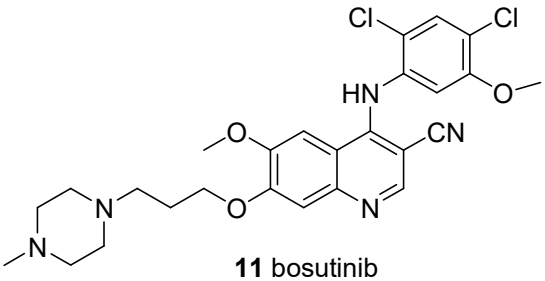

11 bosutinib

4.2.1 Src inhibitors

PH006 **12** is an ATP-competitive Src inhibitor, which selectively inhibits c-Src with an IC_{50} of 0.38 μM among a panel of 14 TKs. Compound **12** potently reduces Src activity, resulting in inhibition of cell proliferation, migration, and invasion in human breast cancer cells and in animal models[156].

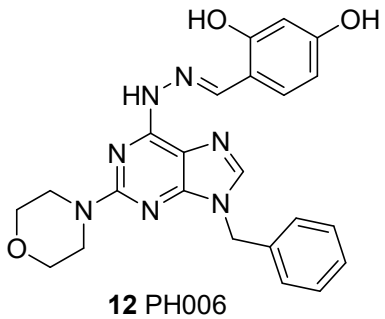

12 PH006

Huang *et al*. reported some purine derivatives, with potent and selective inhibitory activity against c-Src. These inhibitors were discovered by adopting a strategy that integrated focused combinatorial library design, virtual screening, chemical synthesis, and bioassays. Thirty-two compounds were synthesized and showed inhibitory activity against c-Src with IC_{50} values

ranging from 3.14 to 0.02 μM. Among these, compound **13** was identified as the most potent and selective agent (IC_{50} of 20 nM). Interestingly, it is 100-fold and 300-fold less potent against Kit and c-Abl, respectively and possesses weak inhibitory effect on many other kinases, with IC_{50} values of above 10 μM[157].

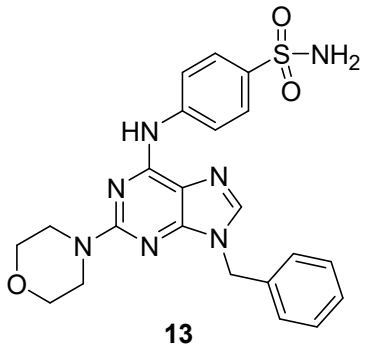

13

KXO1 **14** (tirbanibulin or KX2-391), synthesized by Kinex Pharmaceuticals is one of the few examples of type III inhibitors. It is a highly selective non-ATP Src inhibitor with an IC_{50} value of 20 nM[158].

Compound **14** inhibits Src, catalyzes trans-phosphorylation of Fak, Shc, PXN as well as Src kinase autophosphorylation, while it does not have any effect on PDGFR, EGFR, Jak1, Jak2 and Lck. However, it also showes effects on non-Src driving cells, suggesting that it may have other molecular targets[159]. Photoaffinity labeling of KXO1 identified tubulin as another target of KXO1, and further study showed that KXO1 could inhibit tubulin polymerization in a low nanomolar range. KX01 has shown activity against various types of cancers, including TNBC (triple negative breast cancer), ER+ breast cancer, and mucinous ovarian cancer, both *in vitro* and *in vivo*[160]. Studies have demonstrated the effectiveness of **14** in various solid and hematological tumor types, as well as its low toxicity with good bioavability[161]. It is currently being tested in several clinical trials for different tumors and for actinic keratosis. (https://clinicaltrials.gov/ct2/results?cond=&term=KX2391&cntry1=&state1=&recrs=)

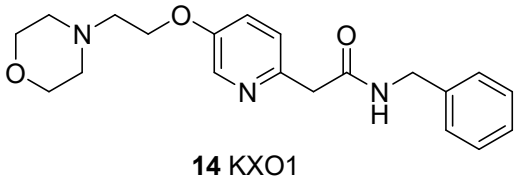

14 KXO1

Moroco and coworkers discovered a new c-Src inhibitor using a screening on a kinase-biased library with the aim of finding selective inhibitors of the Src/Fak complex versus c-Src alone. This approach led to the identification the aminopyrimidinyl carbamate compound **15**, WH-4-124-2, with nanomolar activity for c-Src. Molecular docking studies indicate that WH-4-124-2 may preferentially inhibits the DFG-out conformation of the kinase catalytic site[162].

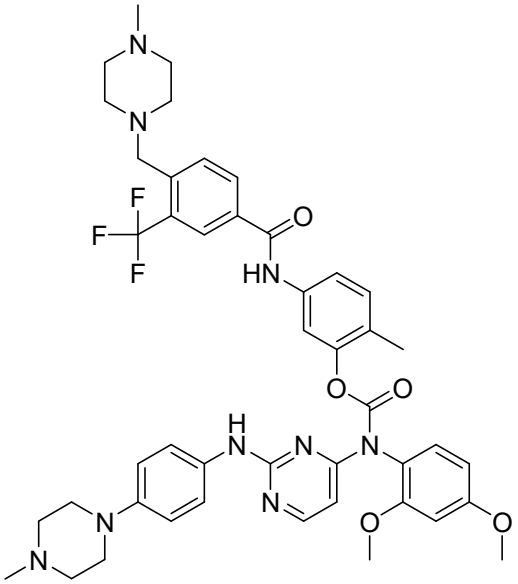

15 WH-4-124-2

Bisubstrate or bivalent inhibitor are, as reported above, molecules which interact both with the ATP and protein substrate-binding sites. This different kind of inhibition may represent a promising strategy for the identification of kinase inhibitors with increased potency and selectivity. However, in the literature there are few examples where the potency and selectivity advantages are completely realized[163]. In this context, Brandvold *et al.* have developed a modular approach to bisubstrate inhibition of TKs. Their strategy utilizes a promiscuous ATP-competitive inhibitor that is then linked to a peptide derived from known substrates for the target kinase. They applied the methodology to c-Src and identified a highly selective bisubstrate inhibitor for this target, compound **16**, which showed a K_d value of 0.28 nM. In addition, they developed a novel screening methodology to identify non-ATP-competitive inhibitors of c-Src and discovered one of the most potent non-ATP-competitive inhibitor reported to date, compound **17**[164].

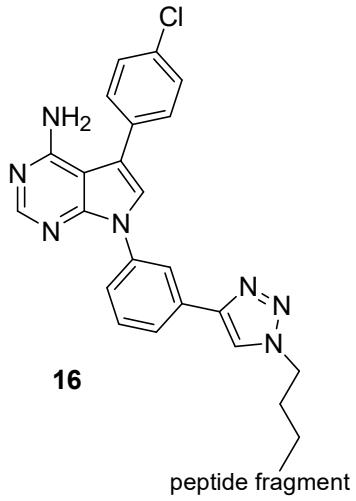

16

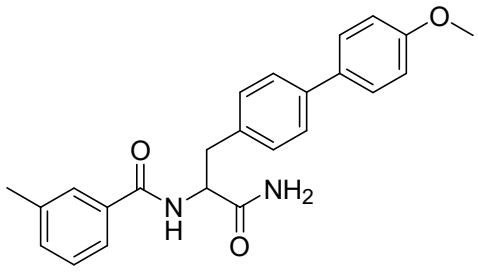

17

4.2.2 Fyn inhibitors

Many different kinase inhibitors, such as the previously reported PP1, PP2, dasatinib, saracatinib and bosutinb, have been identified for Fyn. Unfortunately, due to the strict similarity of SFK members in their catalytic domains, these inhibitors are not selective for this kinase. Some other interesting examples of compound endowed with Fyn inhibitory activity are reported below.

Derivative **18**, AP23464 is a purine compound developed by Ariad, which targets c-Src with picomolar affinity (450 pM). The compound showed also notable activity against Abl, Fyn, Yes, Lck, Lyn, EGFR, FGFR, PDGFR, C-Kit, b-Raf, all kinases characterized by a small gatekeeper residue[165,132].

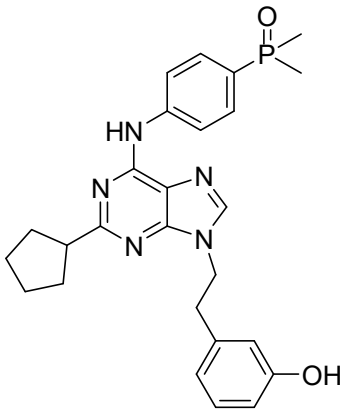

18 AP23464

Moy *et al.* synthesized compound **19**, classified as type II inhibitor, which exhibits nanomolar inhibitory activity against multiple kinases. The compound bears a pyrazolo[1,5-*a*]pyrimidine core linked to a tetramethylpiperidine-1-oxyl radical that, possessing a very slow electronic relaxation time and prolonged radical stability, is able to be used in the NMR spectroscopy of the complex with the enzyme. This derivative is particularly active on VEGFR2 (IC_{50} = 3.3 nM), Abl (IC_{50} = 5 nM) and on SFKs, including Fyn (5 nM). Since the compound is very active and endowed with paramagnetic properties, it could represent a useful tool in a screen for non-ATP site binders[166].

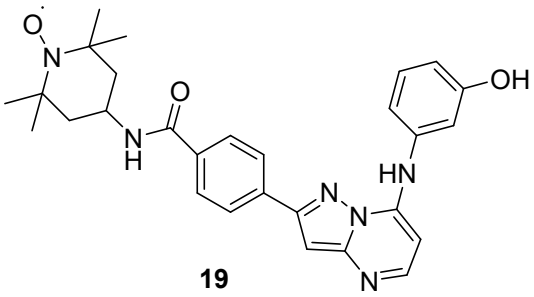

19

Bamborough *et al.* at GlaxoSmithKline tested more than 500 compounds against a panel of over 200 protein kinases chosen to represent the kinase inhibitor space. This important study has led to the identification of hits against new kinases and to the expansion of the inhibition profiles of several literature compounds. A detailed analysis of the data through the use of affinity fingerprints gave interesting indications for biological target selection, the choice of tool compounds for target validation, lead discovery and optimization. These results show how broad cross-profiling can provide important insights to assist kinase drug discovery. Regarding Fyn inhibitors, they found that the bis-anilinopyrimidine **20** potently inhibits also Fyn with an IC_{50} value of 0.4 nM[167].

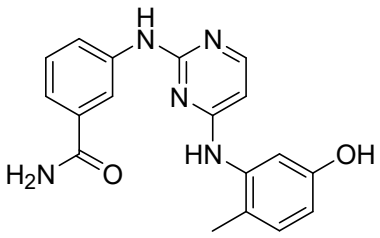

20

Wyeth researchers synthesized a series of 2-alkenyl thieno[2,3-*b*]pyridine carbonitriles, bearing a thieno-pyridine core isoster to the quinolinic one of bosutinib, as potent inhibitors of PKCθ, a STK espressed in lymphocytes and mast cells and involved in the inflammatory response. In the screening to assess compounds selectivity, they found that the most active derivatives also inhibited SFKs. Interestingly, compound **21** possessed an IC_{50} value of 25 nM for Fyn and comparable inhibition also versus Hck and Lck, while the IC_{50} value for c-Src was significantly higher (330 nM)[168].

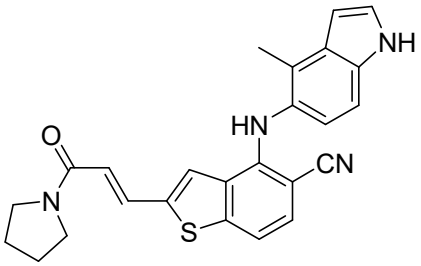

21

A thiazole derivatives family of compounds structurally related to dasatinib **9**, bearing 2-aminoheteroaryl groups has been reported as potent and orally active SFK inhibitors. Among these, compound **22** resulted one of the most interesting derivatives, possessing IC_{50} values of 1-2 nM for all SFKs, including Fyn, and excellent selectivity against receptor TKs and SFKs[169].

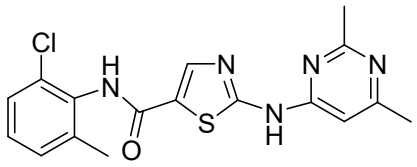

22

Several phenolic compounds are Fyn inhibitors. An example is rosmarinic acid (RosA) **23**, the ester of caffeic acid with 3,4-dihydroxyphenyl lactic acid. It is a natural polyphenol antioxidant carboxylic acid found in many Lamiaceae herbs, including Salvia officinalis and Rosmarinus officinalis and is responsible for antiinfective, antiinflammatory and antioxidative effects of these plants. Jelic *et al*., using immunochemical and in silico methods, discovered that RosA is a Fyn inhibitor (IC_{50} value of 1.3 μM)[170]. Recently, this compound has been studied for its potential use in the treatment of AD. The researchers strongly supported the hypothesis that

RosA attenuates Aβ-induced excess production of ROS (Reactive Oxygen Species) by inhibiting nuclear exclusion of Nrf2 in the Akt/GSK-3β/Fyn pathway. These results suggest that RosA can be a promising candidate for neuroprotective treatment of AD[171].

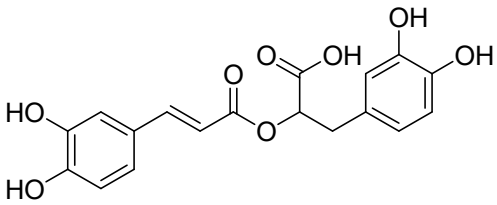

23 rosmarinic acid

In 2015 Tintori *et al.* synthesized a new library of pyrazolo[3,4-*d*]pyrimidines derivatives among which compound **24** demonstrated a K_i value of 70 nM on Fyn. Furthermore **24** was found able to inhibit the phosphorylation of the Tau protein in an Alzheimer's model cell line and showed antiproliferative activities against different cancer cell lines[124]. Recently compound **24**, called SI308, has been studied in the context of lymphoid malignancies development and showed inhibition values in the sub-micromolar range also for the related kinases Lyn and Blk[172].

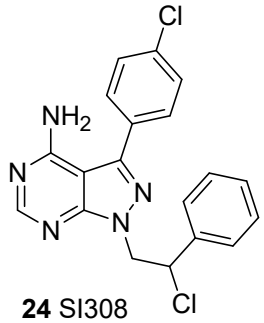

24 SI308

CHAPTER 5

Synthesis of pyrazolo[3,4-d]pyrimidines as potential SGK1 inhibitors

5.1 Background

My research group synthesized a large library of 4-amino substituted pyrazolo[3,4-*d*]pyrimidines **25**, bearing an alkylphenyl chain in N1, which resulted active as ATP-competitive Src and/or Abl inhibitors, with IC_{50} values in the nanomolar range in enzymatic assays and a potent antiproliferative and proapoptotic activity toward different cancer cell lines[173,174].

As previously reported, SGK1 is emerging as an essential and non-redundant target in medicinal chemistry. For this reason, an in silico screening was recently conducted in collaboration with the University of Magna Graecia of Catanzaro, to assess if some members of the in-house library were also active on SGK1 and Akt through an ATP competitive mechanism. This study allowed us to identify different pyrazolo[3,4-*d*]pyrimidines endowed with a good activity toward SGK1. In particular, the compound called SI113, **5**, already reported in chapter 4, is effective in inhibiting SGK1 with an IC_{50} value of 600 nM, while being much less effective on Akt1, Abl and Src.

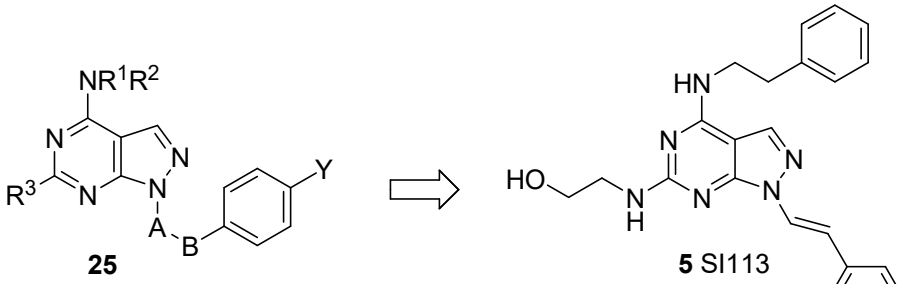

A-B = $CH_2CH(Cl)$, $CH_2CH(Br)$, CH_2CH_2, CH=CH
Y = H, F, Cl, Br
R^1R^2 = alkyl and aryl groups
R^3 = H, alkyl, S-alkyl, amino groups

Surprisingly, Akt1, which has been previously cited because of its high homology whit SGK1, was inhibited by SI113 with an IC_{50} value of 50 μM, which implies a selectivity on SGK1 with respect to Akt1 of almost 100 folds. Docking studies explain that this selectivity is probably due to a better fitting of SI113 into the larger lipophilic area of the ATP binding domain present in SGK1, which leads the molecule to a planar conformation. This conformation is not allowed in the Akt1 catalytic site[141] (**Fig.18**).

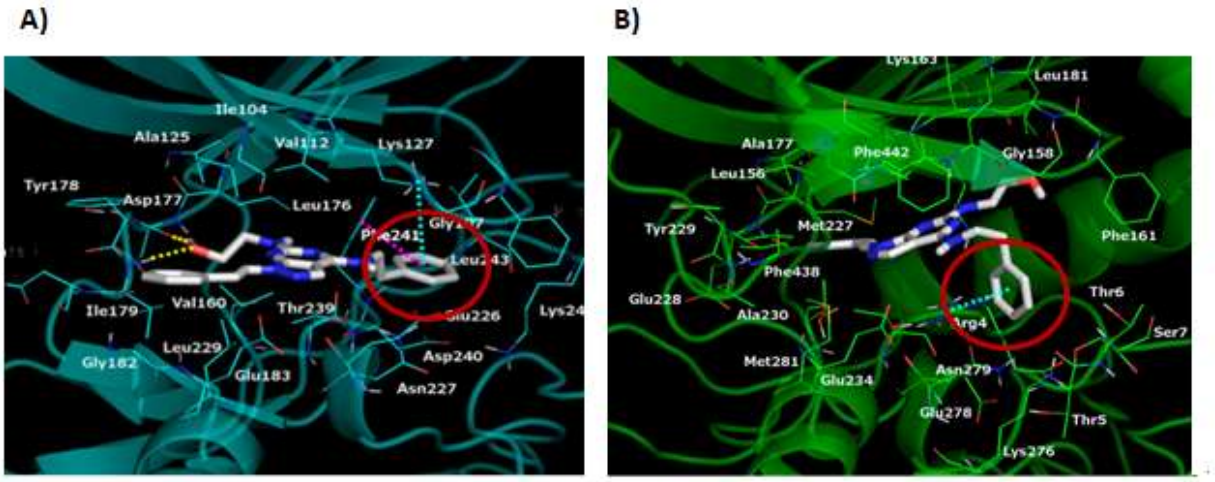

Fig.18. Binding mode of SI113 into SGK1 (A) and Akt1 (B). The SGK1 binding conformation of SI113 is flat, whereas in Akt1 the flat conformation of SI113 is not allowed due to the restricted lipophilic area present in Akt1.

5.1.1 SI113 anticancer activity

As it was previously reported, in the last five years, many *in vitro* and *in vivo* biological studies have been performed on SI113 demonstrating its strong anticancer activity.

Initially, our group reported that SI113 induces cell death in various malignant cell lines, including MCF-7 breast carcinoma, A-172 malignant glioma and RKO colon carcinoma and synergizes with paclitaxel in induction of apoptosis[53]. Further studies highlighted the capability of this SGK1 inhibitor to induce autophagy, apoptosis, and endoplasmic reticulum stress in endometrial cancer cells[43]. Very recently, using GBM, HCC and colorectal carcinoma cell lines, an inhibitory effect of SI113 on cell migration, invading, and EMT has been recognized. In addition, cancer cells, when exposed to this compound, showed a remarkable subversion of the cytoskeletal architecture, characterized by F-actin destabilization, phospho-Fak delocalization,

and tubulin depolimerization. Therefore, the results confirm a key role for SI113 in hindering cancer cell malignancy[143].

5.1.1.1 SI113 activity on HCC

Regarding HCC, *in vitro* data obtained in HepG2 and HuH-7 cell lines, as well as *in vivo* data from HCC xenografts in NOD/SCID mice, indicated that SI113 inhibits liver cancer cell proliferation, induces apoptosis and necrosis and potentiates the effects of radiotherapy, mimicking some of the effects of SGK1 knock-down. More specifically, the analysis of tumor volume and weight in the *in vivo* assays demonstrates that SI113 arrests tumor growth. Histology demonstrates high levels of necrosis in tumors from treated animals (**Fig.19**). Interestingly, no signs of toxicity were observed by histological examination of the livers from S113-treated mice, nor did the mice show signs of generally adverse side effects[64].

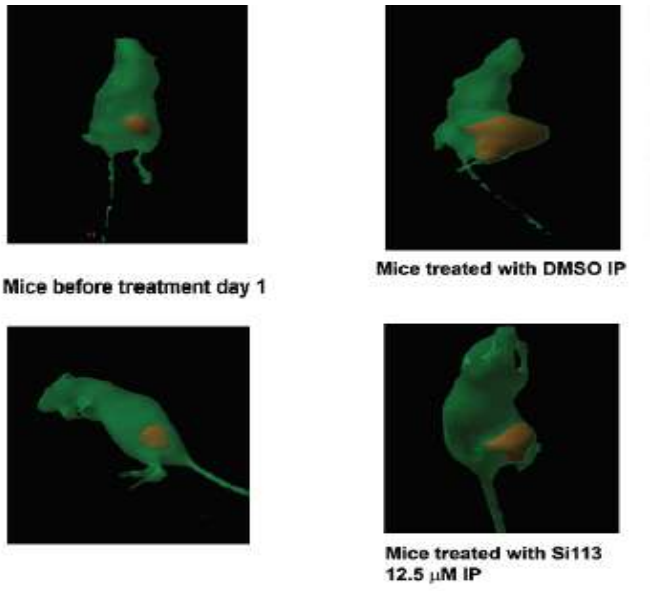

Fig.19. SI113 tumor suppressive activity in HCC xenograft models.

5.1.1.2 SI113 activity on GBM

This compound also showed very interesting results on GBM. In fact, an initial work on GBM cell lines, presented evidences that SGK1 plays an important role in GBM cell survival response to radiation and oxidative stress. SI113-dependent SGK1 inhibition demonstrated to counteract the activation of survival mechanisms and to enhance the cell death in response to radiation and

oxidative stress. Besides that, SI113 was also able to enhance cytotoxic autophagy which leads the cells exposed to radiation to an irreversible death fate[43]. Subsequently, SI113 demonstrated to promote theranostic effects induced by $^{64}CuCl_2$ in GBM cells[65]. Later it has been found that the association between SI113 and selected spindle poisons such as microtubule-destabilizing agent vincristine (VCR) and the microtubule-stabilizing agents epothilone A (EPO-A), generated a synergistic cytotoxic effect in GBM cells, drastically reducing their viability and clonogenic capabilities *in vitro* as well as inhibiting tumor growth *in vivo.* In particular, SI113 and VCR cooperate in restraining the growth of ADF glioblastoma cells xenografts in immunocompromised mice[142]. Recently, with the aim to explore in depth the pharmacological ability of SI113 in interfering with major signal transduction pathways in either established or primary (neurospheres) GBM cells, a RPPA platform has been performed upon 114 protein factors whose post-translational modifications are associated with activation or repression of specific signal transduction cascades. Data demonstrated that SI113 strongly affected the PI3K/mTOR pathway, evoking a pro-survival autophagic response in neurospheres. Therefore, the use of SI113 coupled with autophagy inhibitors is strongly recommended for a maximum efficiency. Indeed, the association of SI113 with quinacrine, an autophagy inhibitor, induced a remarkable synergistic effect in inhibiting GBM growth properties in all the cells tested, including neurospheres (**Fig.20**).

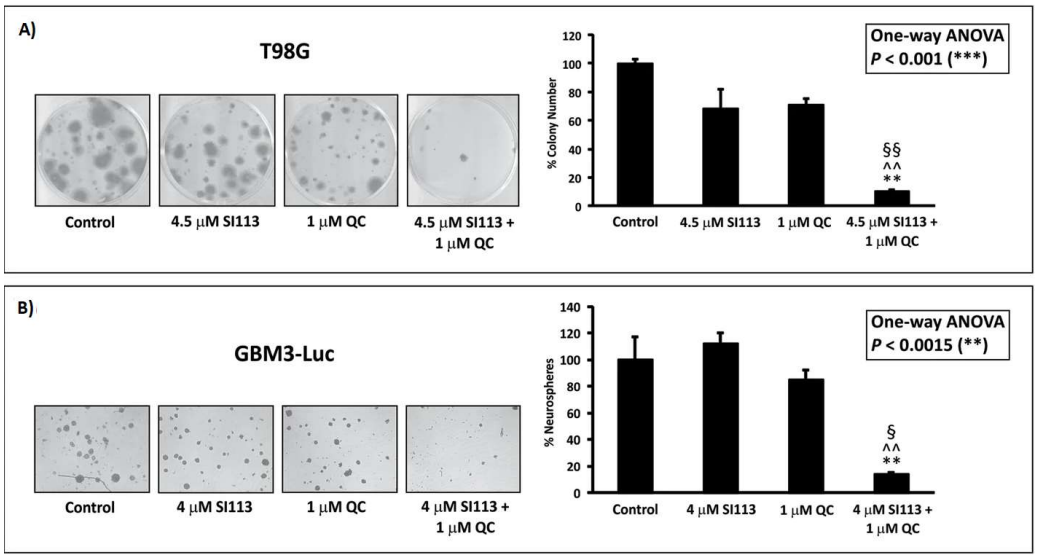

Fig.20. Clonogenic Assay. A) T98G GBM cell line. B) GBM3-Luc anchorage-independent neurospheres.

5.1.1.3 SI113 activity on ovarian cancer

Very recently, a study carried by D'Antona and colleagues demonstrated that SI113 can be helpful in inhibiting the development of paclitaxel resistance in human ovarian cancer cells and can restore paclitaxel sensitivity in cells that are resistant to this drug.

In more details, *in vitro* data obtained using ovarian carcinoma cell lines indicate that the SGK1 inhibitor SI113 inhibits cancer cell proliferation, potentiates the effects of paclitaxel-based chemotherapy, counteracts the development of paclitaxel resistance, and restores paclitaxel sensitivity in paclitaxel-resistant A2780 ovarian cancer cells. The *in vitro* results have been corroborated by preclinical studies of xenografts generated in nude mice through the implantation of paclitaxel-resistant human ovarian cancer cells. The compound SI113 synergizes with paclitaxel in the treatment of tumors derived from xenografted ovarian cancer cells[40].

5.2 Project

On the basis of these interesting results, we decided to expand the synthesis of a new generation of SI113 derivatives and start a lead optimization study with the aim to find new SGK1 inhibitors. Initially, Prof. Alcaro's group at the University Magna Graecia of Catanzaro, performed an in silico study on a virtual library of compounds of feasible synthesis. Then the compounds which showed the best docking scores have been selected for the synthesis.

In this new set of SGK1 inhibitors, the N1 phenylvinyl group has been maintained and the effects of substitutions on the N1 side chain phenyl ring and on C4 and C6 positions have been explored.

5.3 Results and discussion

During my PhD I mainly worked on the design and subsequent synthesis of a new library of potential SGK1 inhibitors **26a-t** (**Table 1**) and **27a-h** (**Table 2**). All compounds **26a-t** (**Table 1**) present the double bond in the N1 side chain, since this feature seems essential for the activity of compounds toward SGK1.

Table 1. Structure of potential SGK1 inhibitors synthesized.

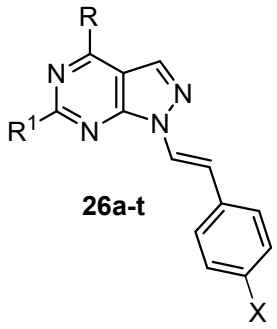

cpd	R	R^1	X
26a	$NHCH_2CH_2C_6H_5$	$N(CH_2CH_2OH)_2$	H
26b	$NHCH_2CH_2C_6H_5$	$NHCH_2CH_2NH_2$	H
26c	$NHCH_2CH_2C_6H_5$	OCH_2CH_2OH	H
26d	$NHCH_2C_6H_5$	4-morpholinyl	H
26e	$NHCH_2C_6H_4$-4F	4-morpholinyl	H
26f	$NHCH_2C_6H_4$-4Cl	$NHCH_2CH_2OH$	H
26g	$NHCH_2C_6H_4$-4Cl	$N(CH_2CH_2OH)_2$	H
26h	NHC_6H_4-4Cl	OC_4H_9	H
26i	NHC_6H_4-4Cl	$NHCH_2CH_2OH$	H
26j	NHC_6H_4-4Cl	$N(CH_2CH_2OH)_2$	H
26k	$NHCH_2C_6H_4$-3F	$NHCH_2CH_2OH$	F
26l	$NHCH_2C_6H_4$-3F	$N(CH_2CH_2OH)_2$	F
26m	NHC_6H_5	$N(CH_2CH_2OH)_2$	F
26n	NHC_6H_4-3Cl	$NHCH_2CH_2OH$	Cl
26o	NHC_6H_4-3Cl	$N(CH_2CH_2OH)_2$	Cl
26p	NHC_6H_4-3Cl	$NHCH_2CH_2OH$	Br
26q	4-morpholinyl	$NHCH_2CH_2OH$	H
26r	4-morpholinyl	$N(CH_2CH_2OH)_2$	H
26s	4-morpholinyl	$NHCH_2CH_2NH_2$	H
26t	4-morpholinyl	OCH_2CH_2OH	H

Furthermore, all compounds, with the exception of **26h**, are decorated in C6 with different polar groups to obtain a second generation of compounds endowed with an improved solubility compared to SI113. Besides, the butyl-ether derivate **26h** is an unexpected by-product, obtained in the last step of route 1 (reported below), which has been characterized and included into the set sent for biological assays, in order to extend structure-activity relationship (SAR) evaluations. Different amino substituents have been introduced in C4. Indeed, besides the phenylethylamino chain, already present in SI113, we introduced differently substituted anilines and benzylamines. Furthermore, a small set of morpholino derivatives **26q-t** has been synthesized.

Due to the presence of the double bound on N1 side chain, also intermediates **27a-h** (**Table 2**) have been included into the set of final compounds to be tested in the enzymatic assay.

Table 2. Structure of intermediates **27a-h.**

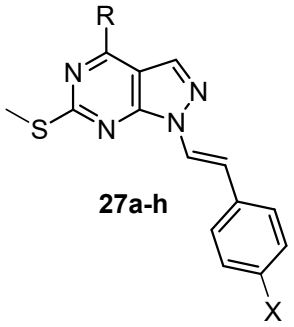

27a-h

Cpd	R	X
27a	NHC_6H_4-4Cl	H
27b	$NHCH_2C_6H_4$-4Cl	H
27c	$NHCH_2CH_2C_6H_5$	H
27d	$NHCH_2C_6H_4$-3F	F
27e	NHC_6H_5	F
27f	NHC_6H_4-3Cl	Cl
27g	NHC_6H_4-3Cl	Br
27h	4-morpholinyl	H

Finally, the scale-up synthesis of SI113 has been performed to obtain a large amount (about 3 grams) of compound for further biological assays.

5.3.1 Chemistry

The synthesis has been performed through a multi-step approach, which has as key intermediates compounds **33 a-d**. Then two different routes have been followed to obtain the desired compounds **26a-c**, **26f-t** and SI113 **5** (route 1) or **26d**,**e** (route 2).

The first step is the reaction between hydrazine monohydrate and styrene oxide or *para*-substitued styrene oxides **28a-d** which afforded intermediates **29a-d**. The treatment of intermediates **29a-d** with ethyl(ethoxymethylene)cyanoacetate at 80 °C in anhydrous toluene for 8 h gave **30a-d** in excellent yields. Compounds **30a-d** were reacted with benzoyl isothiocyanate in anhydrous THF, leading to the formation of **31a-d**. Then, **31a-d** were cyclized by treatment with sodium hydroxide (2M) and precipitated with glacial acetic acid, to give derivatives **32a-d**. These compounds were methylated on the C6 sulphur atom with methyl iodide at reflux for 12 h in anhydrous THF, leading to derivates **33a-d** (**Scheme 1**).

Scheme 1: Preparation of intermediates **33a-d.**

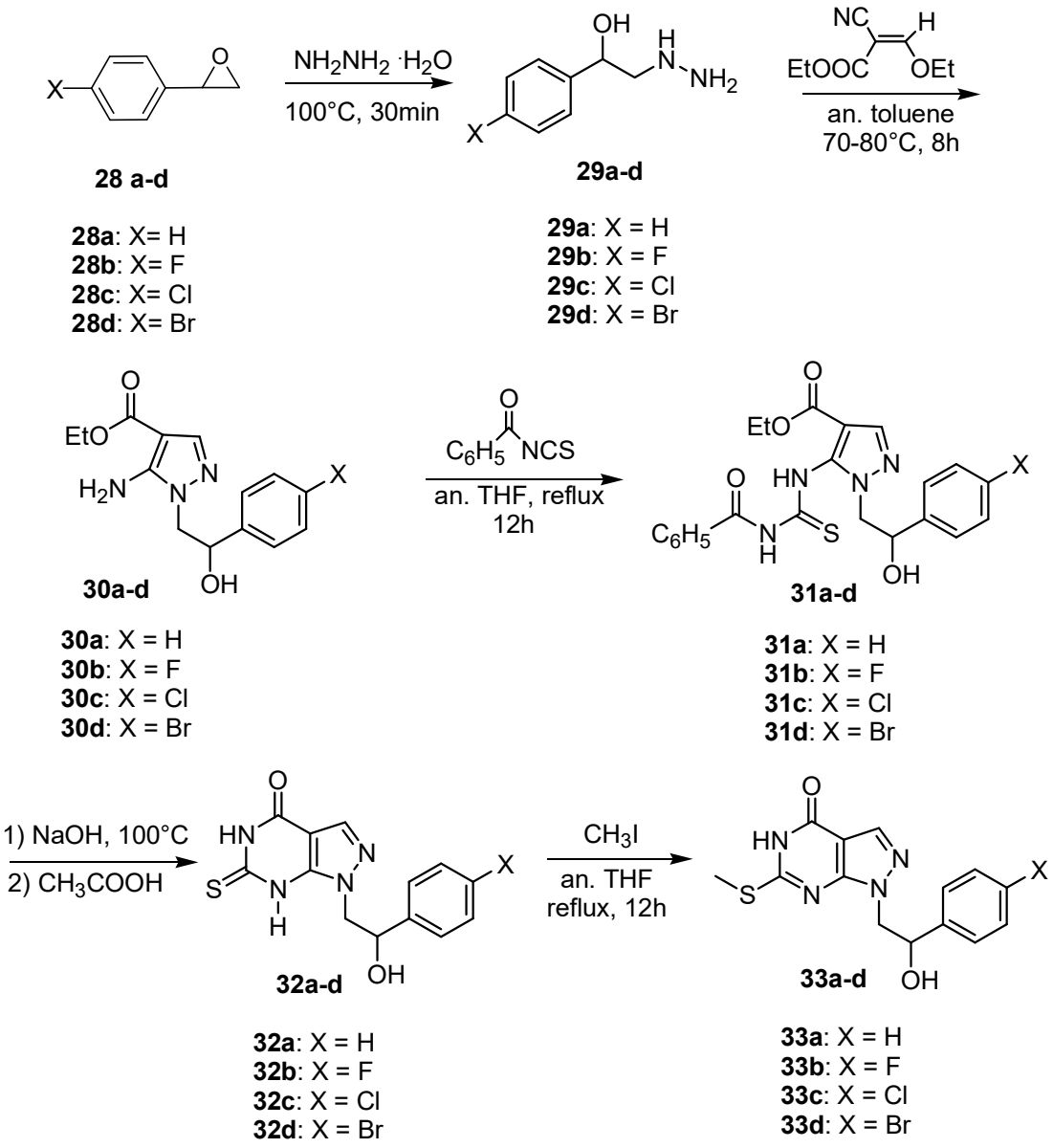

For the synthesis of compounds **27a-h,** intermediates **33a-d** were reacted with the Vilsmeier complex ($POCl_3$/DMF, 1:1) at reflux for 8 h in anhydrous chloroform, in order to obtain **34a-d**. The latter were reacted with different amines in opportune conditions, giving derivatives **35a-h**. Compounds **35a-h** were dehydrohalogenated by refluxing with aqueous NaOH (3.3 M) to give the corresponding N1-unsaturated derivatives **27a-h** (**Scheme 2**).

Scheme 2: Preparation of intermediates **27a-h.**

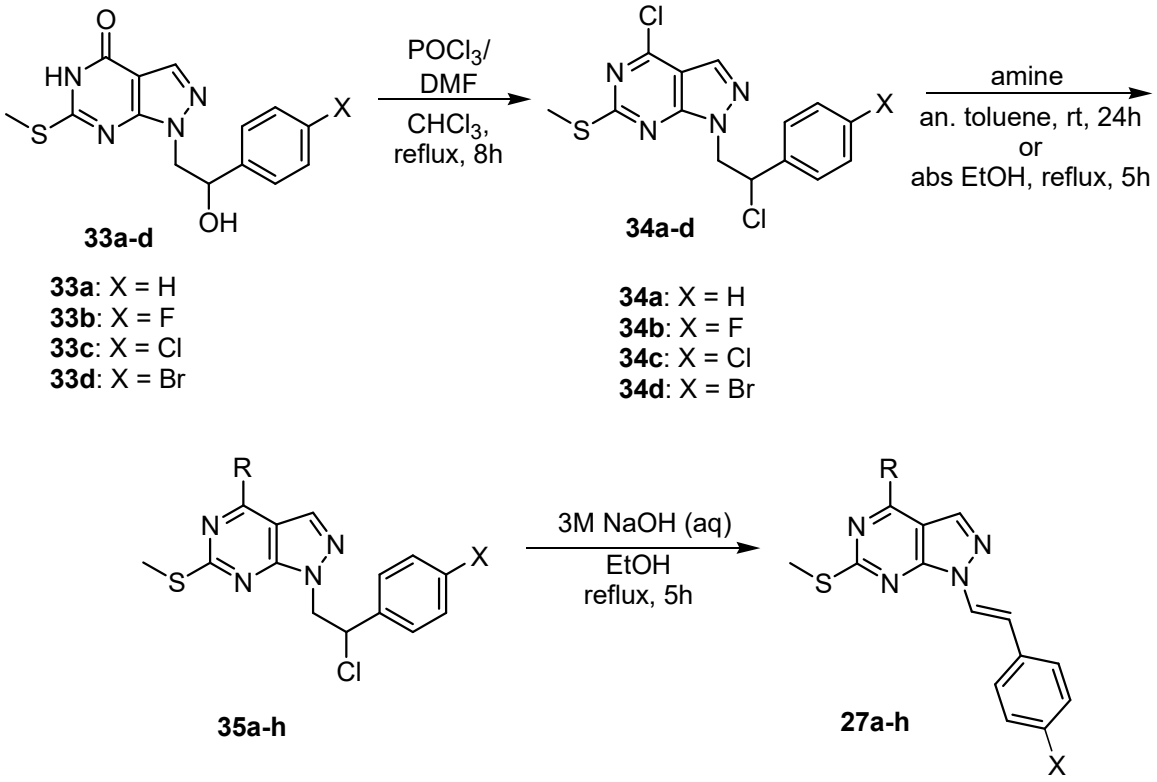

33a: X = H
33b: X = F
33c: X = Cl
33d: X = Br

34a: X = H
34b: X = F
34c: X = Cl
34d: X = Br

35a: X = H, R = $NHCH_2CH_2C_6H_5$
35b: X = H, R = $NHCH_2C_6H_4$-4Cl
35c: X = H, R = NHC_6H_4-4Cl
35d: X = F, R = $NHCH_2C_6H_4$-3F
35e: X = F, R = NHC_6H_6
35f: X = Cl, R = NHC_6H_4-3Cl
35g: X = Br, R = NHC_6H_4-3Cl
35h: X = H, R = 4-morpholinyl

27a: X = H, R = $NHCH_2CH_2C_6H_5$
27b: X = H, R = $NHCH_2C_6H_4$-4Cl
27c: X = H, R = NHC_6H_4-4Cl
27d: X = F, R = $NHCH_2C_6H_4$-3F
27e: X = F, R = NHC_6H_6
27f: X = Cl, R = NHC_6H_4-3Cl
27g: X = Br, R = NHC_6H_4-3Cl
27h: X = H, R = 4-morpholinyl

Then, all compounds **27a-h** were oxidized by reaction with *meta*-chloroperoxybenzoic acid (*m*CPBA) in chloroform at room temperature for 6h, giving compounds **36a-h**. Finally, the sulfone group was displaced by reaction with ethanolamine or diethanolamine, affording the final compounds **26a-c**, **26f, g, 26i-t** and SI113 **5** (**Scheme 3**).

Scheme 3: Preparation of final compounds **26a-c, 26f, g, 26i-t** and SI113

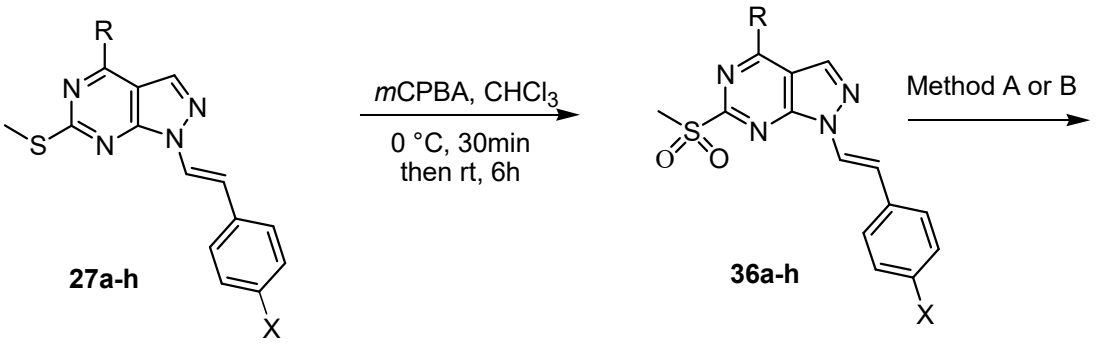

27a-h

27a: X = H, R = $NHCH_2CH_2C_6H_5$
27b: X = H, R = $NHCH_2C_6H_4$-4Cl
27c: X = H, R = NHC_6H_4-4Cl
27d: X = F, R = $NHCH_2C_6H_4$-3F
27e: X = F, R = NHC_6H_6
27f: X = Cl, R = NHC_6H_4-3Cl
27g: X = Br, R = NHC_6H_4-3Cl
27h: X = H, R = 4-morpholinyl

36a-h

36a: X = H, R = $NHCH_2CH_2C_6H_5$
36b: X = H, R = $NHCH_2C_6H_4$-4Cl
36c: X = H, R = NHC_6H_4-4Cl
36d: X = F, R = $NHCH_2C_6H_4$-3F
36e: X = F, R = NHC_6H_6
36f: X = Cl, R = NHC_6H_4-3Cl
36g: X = Br, R = NHC_6H_4-3Cl
36h: X = H, R = 4-morpholinyl

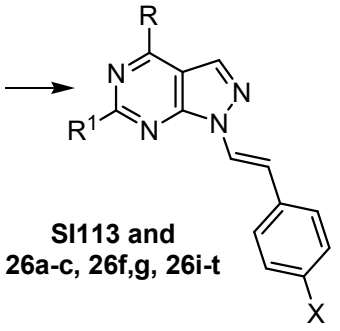

SI113 and 26a-c, 26f,g, 26i-t

SI113: X = H, R = $NHCH_2CH_2C_6H_5$, R^1 = $NHCH_2CH_2OH$

26a: X = H, R = $NHCH_2CH_2C_6H_5$, R^1 = $N(CH_2CH_2OH)_2$
26b: X = H, R = $NHCH_2CH_2C_6H_5$, R^1 = $NHCH_2CH_2NH_2$
26c: X = H, R = $NHCH_2CH_2C_6H_5$, R^1 = OCH_2CH_2OH
26f: X = H, R = $NHCH_2C_6H_4$-4Cl, R^1 = $NHCH_2CH_2OH$
26g: X = H, R = $NHCH_2C_6H_4$-4Cl, R^1 = $N(CH_2CH_2OH)_2$
26i: X = H, R = NHC_6H_4-4Cl, R^1 = $NHCH_2CH_2OH$
26j: X = H, R = NHC_6H_4-4Cl, R^1 = $N(CH_2CH_2OH)_2$
26k: X = F, R = $NHCH_2C_6H_4$-3F, R^1 = $NHCH_2CH_2OH$
26l: X = F, R = $NHCH_2C_6H_4$-3F, R^1 = $N(CH_2CH_2OH)_2$
26m: X = F, R = NHC_6H_5, R^1 = $N(CH_2CH_2OH)_2$
26n: X = Cl, R = NHC_6H_4-3Cl, R^1 = $NHCH_2CH_2OH$
26o: X = Cl, R = NHC_6H_4-3Cl, R^1 = $N(CH_2CH_2OH)_2$
26p: X = Br, R = NHC_6H_4-3Cl, R^1 = $NHCH_2CH_2OH$
26q: X = H, R = 4-morpholinyl, R^1 = $NHCH_2CH_2OH$
26r: X = H, R = 4-morpholinyl, R^1 = $N(CH_2CH_2OH)_2$
26s: X = H, R = 4-morpholinyl, R^1 = $NHCH_2CH_2NH_2$
26t: X = H, R = 4-morpholinyl, R^1 = OCH_2CH_2OH

Method A: Appropriate amine, DMSO/n-butanol, or DMSO, or an. DMF, 90 °C, 12 h (to obtain **26a,b, f,g, i-s** and SI113).
Method B: $HOCH_2CH_2OH$, NaH, an DMF, 1h, rt (to obtain **26c** and **26t**).

It is interesting to report that during the first attempt to obtain compound **26j**, we observed the formation of a by-product. We characterized it, and we disclosed that it was the buthylether derivate **26h** (**Scheme 4**). For a better understanding, we repeated this reaction different times, and we observed that prolonging the reaction time, in the same conditions of solvent and temperature, the conversion of **26h** in **26j** was complete. To avoid the formation of this by-product, we removed n-butanol and used only DMSO as a solvent for the synthesis of other diethanolamine derivatives. This problem never appeared during the synthesis of ethanolamine derivatives.

Scheme 4: Conditions of reaction affording the synthesis of compound **26j** and the by-product **26h**.

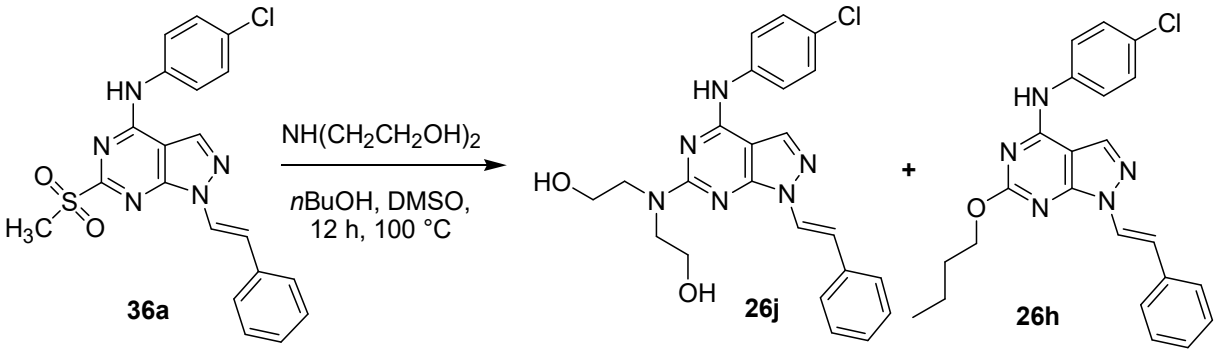

To obtain compounds **26d,e**, (route 2) intermediate **33a** was first oxidized with *m*CPBA, giving the sulfone derivative **37**. Then, the latter was reacted with morpholine in DMSO affording compound **38**, which in turn was chlorinated in C4 and on the N1 side chain with the Vilsmeier complex. The obtained intermediate **39** was reacted with the appropriate amines, affording **40a** and **40b**. These intermediates were finally dehydrohalogenated in basic conditions to obtain the desired compounds **26d** and **26e** (**Scheme 5**). This route allows to introduce the variability in C4 just in the pre-final step, minimizing the number of steps needed to obtain the desired compounds **26d,e**. Differently, for the synthesis of compounds **26a-c** and **26f-t**, we had first to functionalize the C4 position, and then to introduce the C6 amino alcohol chain, in order to prevent the chlorination of the primary alcohol by the Vilsmeier complex.

Scheme 5: Preparation of final compounds **26d**,**e.**

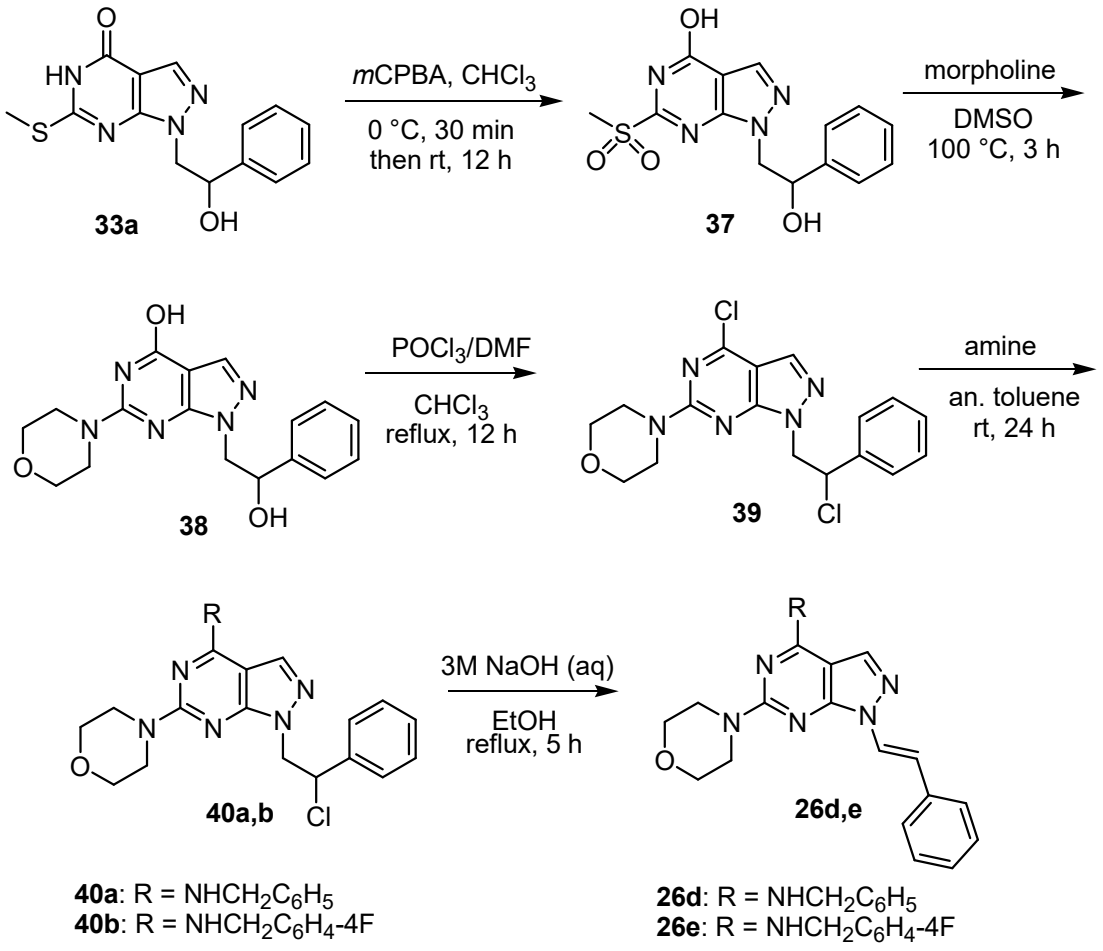

5.3.2 Biology

Preliminary enzymatic assays on SGK1 have been performed by Prof. Perrotti's group at the University Magna Graecia of Catanzaro. To date, a set of ten compounds which includes **26d, i, o, e, n, j, q, h, l** and **27d**, has been tested on SGK1, at a concentration of 600 nM, which is the IC_{50} value of SI113. The assay was performed incubating the enzyme, the inhibitor, the peptide substrate and [γ32P]ATP. To determine the kinase activity in presence of different inhibitors, the radioactivity expressed in count per minute (CPM) was measured using a scintillation counter. SI113 has been used as the reference compound.

As it is shown in graph (**Fig.21**), the majority of compounds show an activity similar to SI113. Interestingly, the buthylether derivate **26h**, which was not planned to be synthesized, showed to have an activity slightly better than the lead compound SI113.

Therefore, it will be interesting to compare **26h** activities both on kinase and cell assays to establish how much the presence of the lipophilic chain can affect the permeability into the cells. Moreover, compound **26n** and the morpholino-derivative **26q** resulted about three folds more active on the enzyme compared to SI113.

The lower inhibitory activity performed by intermediate **27d** let us think that probably a bulky group is necessary on the C6 position for the correct collocation and consequent inhibition of the enzyme.

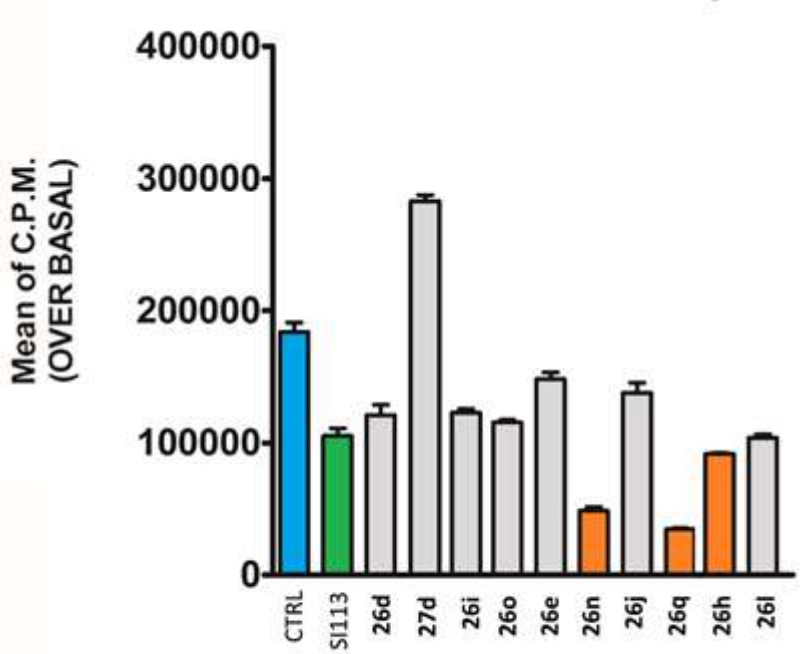

Fig.21. Activity of compounds **26d, i, o, e, n, j, q, h, l** and **27d** on SGK1.

5.4 Conclusions

In conclusion, the SGK1 inhibitor, SI113 which is endowed with a strong anticancer activity, has been identified using a multidisciplinary approach based on association of molecular modeling, organic synthesis, molecular biology, cell biology and pharmacological skills.

Thanks to this study, during my PhD course I synthesized a new library of 28 SI113 derivatives endowed with a potential activity on inhibiting SGK1.

Among them, ten compounds have been tested until now on the isolate enzyme SGK1 and the biological assays on the other derivatives are still in progress. Anyway, the first results are already very interesting: indeed, three compounds (**26n**, **q**, **h**) resulted more active than the lead compound SI113. In particular, the most active compound **26q** resulted about 3-fold more active than S1113 on SGK1. These preliminary results have brought me to the synthesis of new set of morpholino derivative **26r-t**.

Moreover, a scale-up synthesis for SI113 was also performed with the aim to submit this interesting compound to other *in vitro* and *in vivo* assays. Further results on SI113 and derivatives will orient future work.

CHAPTER 6

Synthesis of pyrazolo[3,4-d]pyrimidines as potential Fyn inhibitors

6.1 Background

Because of the involvement of Fyn in different tauopathies and tumors, the design and synthesis of Fyn inhibitors represent an expanding field of research.

Molecular modeling studies, performed in collaboration with the University of Siena, were combined with organic synthesis with the aim of developing novel Fyn kinase inhibitors. A docking study was employed with the purpose of identifying novel ATP-competitive Fyn kinase inhibitors. An in-house library of pyrazolo[3,4-*d*]pyrimidines **41** was chosen for this purpose, using the experimental pose of the known active ligands PP1 **7** and PP2 **8**, selected as the reference compounds. Pyrazolo[3,4-*d*]pyrimidines were virtually screened against the active site of Fyn and then tested in an enzymatic assay towards this kinase. Derivative **42** emerged as the most active compound with a K_i of 0.9 μM on Fyn. An increase in the *in vitro* binding affinity of such compound toward Fyn was then rapidly obtained by the synthesis of a small family of analogues. Among these new compounds, the best Fyn inhibitor resulted to be the previously cited SI308 **24**, having a K_i value of 70 nM[124]. Then SI308 was also tested against a panel of kinases including other SFK members (Hck, Blk, Fgr, Fyn, Src, Lck, Lyn, and Yes), TKs (Abl, EGFR, IGF1R, Jak2, PDGFR, KDR), as well as some STKs. This compound proved to be more efficient against SFK members than towards the other investigated kinases, confirming such a compound as a useful probe to study the SFK functions. Furthermore, a high activity against Abl was also detected, as expected because of the high structural similarity between Abl and SFKs.

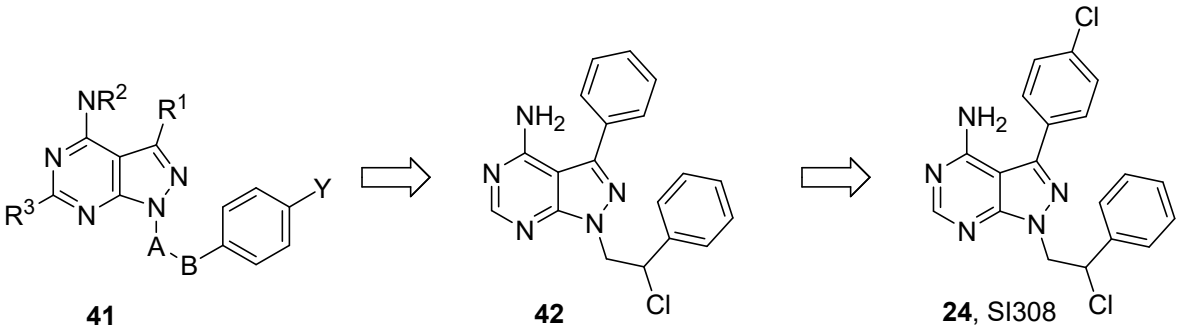

A-B = $CH_2CH(Cl)$, $CH_2CH(Br)$,
CH_2CH_2, CH=CH
Y = H, F, Cl, Br
R^1 = alkyl and aryl groups
R^2 = alkyl and aryl groups
R^3 = H, alkyl, S-alkyl, amino groups

6.1.1 Anticancer activity of SI308

Compound SI308 and derivatives were then evaluated for their antiproliferative activity on the human CML cell line K562. Interestingly, SI308 inhibited cell viability with an IC_{50} value in the submicromolar range. Moreover, the antiproliferative effect of SI308 was evaluated through cell cycle analysis (**Fig.22**).

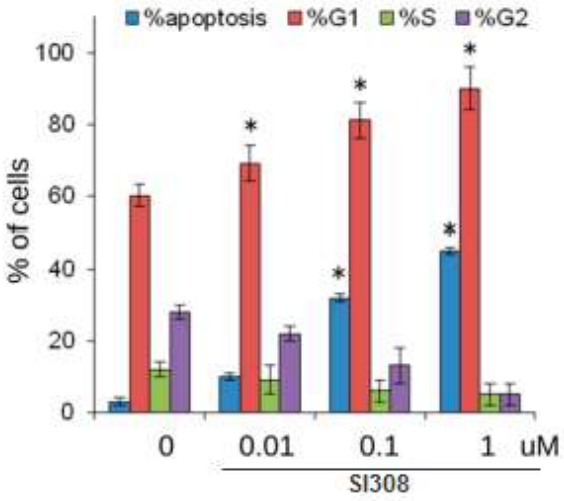

Fig.22. Analysis of the cell cycle distribution of K562 cells after treatment with increasing concentrations of SI308.

Notably, the treatment with 0.1 μM of SI308 induced apoptosis in about 50% of treated K562 cells. Compounds SI308 was also tested on early hematopoietic progenitor cells (CD34+) from Ph+ CML patients who developed resistance to both imatinib mesylate and dasatinib. The percentage of apoptotic CD34+ after imatinib treatment was found equal to control, confirming drug resistance. By contrast, SI308 increased apoptotic levels to 35%. It is important to note that this compound, when tested in human normal fibroblasts, did not show any sign of cell toxicity. Furthermore, compound SI308 was also evaluated on two solid human tumor cell lines, MDA-MD-231 (human breast cancer cell line) and U87 (human GBM cell line). These cell lines, treated with SI308, showed similar response profiles, with a significant difference in cell growth starting from 20 h after treatment with respect to control cells, and a more evident inhibition of cell viability from 70 h after treatment. U87 cells resulted particularly responsive showing IC_{50} values of 0.074 μM (**Fig.23**)[124].

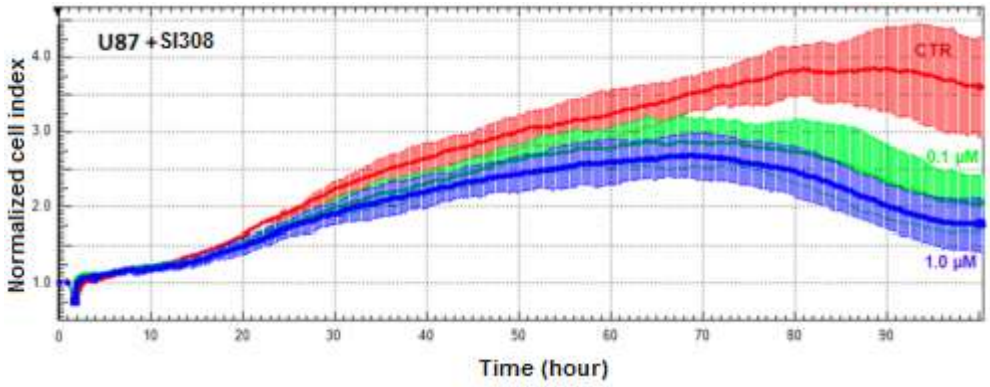

Fig.23. In the graph, a representative growth profile (with SD) obtained with U87 cells treated with 0.1 (green line) and 1 μM (blue line) SI308 with respect to control cells (red line) are shown.

6.1.2 SI308 activity on AD model

In AD, Fyn mediates the phosphorylation of Tau protein on the Tyr18 residue, an early and crucial step in the disease progression[125]. For this reason, SI308 was also evaluated for its ability to inhibit the Fyn mediated phosphorylation of residue Tyr18 of Tau in a cellular model of AD. To this aim, neuroblastoma SH-SY-5Y cells were differentiated to mature neurons with the administration of retinoic acid, followed by brain derived neurotrophic factor, neuregulin β1,

nerve growth factor, and vitamin D3 treatment. Once differentiated, SH-SY-5Y cells were treated[175] with amyloid beta 1–42 ($A\beta_{42}$) oligomer/protofibril in order to induce AD-like neurotoxicity[176]. The compound significantly affected amyloid beta 1-42 (Aβ42) induced Tyr18-Tau phosphorylation in a dose dependent manner. Moreover, the inhibitory activity of SI308 resulted constant over time, being effective up to 6 h after compound administration[124].

6.2 Project

On the basis of these interesting results, we decided to expand the SAR of this inhibitor and planned the synthesis of a new generation of SI308 derivatives. Since the introduction of a methyl group in C6 was not yet explored, we thought to evaluate the effect of this new feature. In fact, sometimes the presence or absence of a small group as a methyl can contribute to a significant change on the activity.

Furthermore, as emerged in the previous studies, a substituent on the para position of the C3 phenyl ring may contribute to enhance the activity. For this reason, the evaluation of para substituted and unsubstituted phenyl ring on C3 has been assessed.

6.3 Results and discussion

In this context during my PhD course, I planned the synthesis of the small set of SI308 derivatives **43a-c**. The final compounds mainly differ from the lead compound SI308 for the presence of a methyl group in C6.

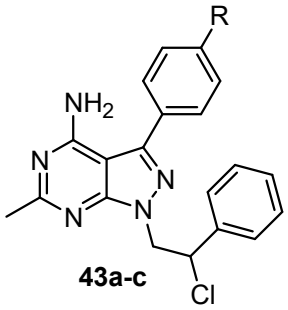

43a-c

43a: R = H
43b: R = CH_3
43c: R = Cl

6.3.1 Chemistry

For the synthesis of Fyn inhibitors **43a-c**, a three-component one-pot synthesis was performed, since it was faster, cheaper and more efficient in term of yield than the corresponding step-by-step route. Sodium hydride was added in small batches to a solution of malononitrile in dry THF precooled at 0/5 °C; after 30 min, the suitable acyl chloride was added and the solution stirred at room temperature for 2-12 h. Then dimethylsulfate was added, and the solution was refluxed for 3-6 h. Finally, 2-hydrazino-1-phenylethanol **29a** (previously reported in **Scheme 1**) dissolved in dry THF was added and the reaction was refluxed for 4 h to afford intermediates **44a-c**, then purified by flash chromatography. Intermediates **44a-c** were cyclized by reaction with acetonitrile in the presence of sodium ethoxide at reflux for 8 h, affording the derivatives **45a-c**. The latter were reacted with thionyl chloride in dry CH_2Cl_2 at room temperature for 12 h under nitrogen atmosphere to give the final compounds **43a-c** (**Scheme 6**).

Scheme 6: preparation of final compounds **43a-c.**

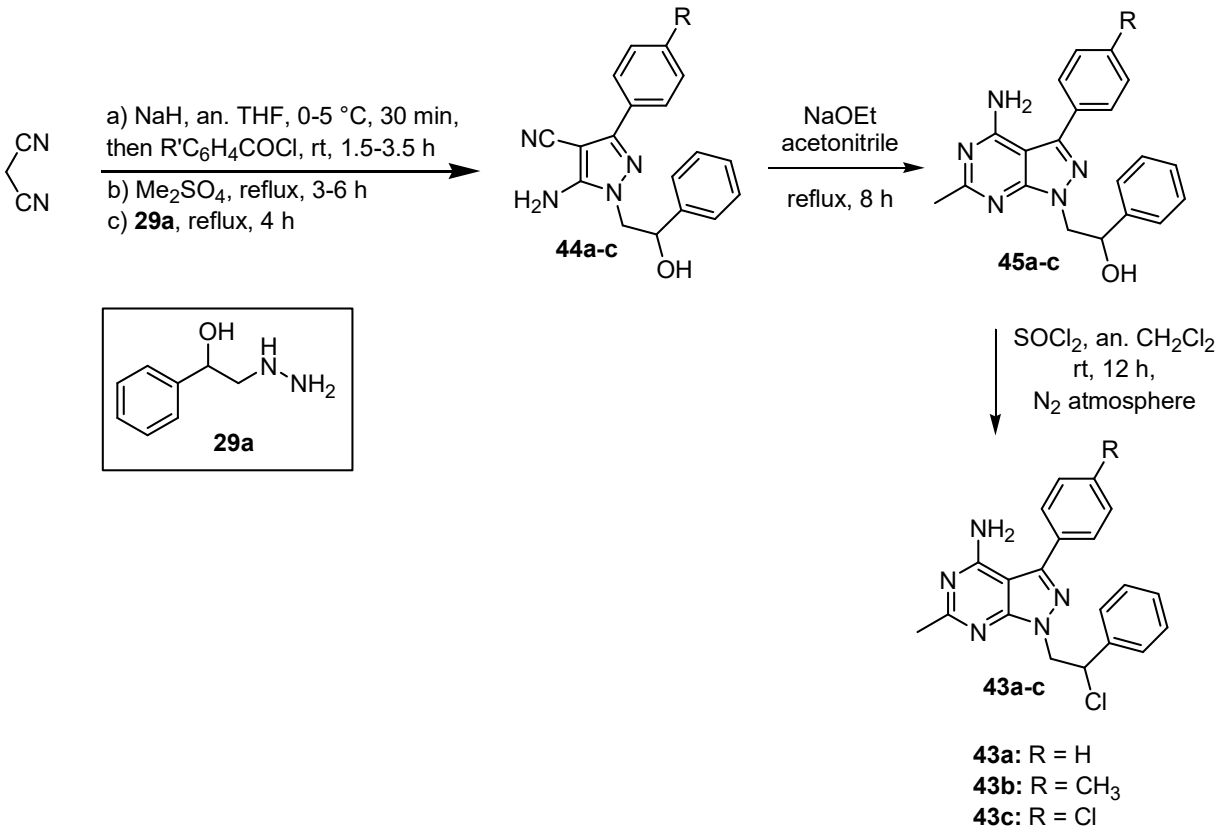

6.3.2 Biology

Enzymatic assay on isolated kinases have been performed by Dr Maga's group of the Institute Genetic Molecular of Pavia (Italy). Since the high homology among kinase members,

compounds have been tested on Fyn, Abl and Src (the main targets of the in-house pyrazolo[3,4-*d*]pyrimidine library) (**Table 3**). Kinase assays were performed in the presence of active, recombinant Fyn/Abl/Src, the specific peptide substrate and [γ32P]ATP. Compounds **43a,c** have been tested only on Fyn because of their low solubility. Therefore, their percentage of inhibition on Fyn has to be considered as a preliminary data which deserve a further evaluation using appropriate formulations that make these compounds more soluble.

Table 3. Percentage of inhibition of Fyn, Abl and Src of **43a-c** compared to SI308.

Cpd	**% inhibition of Fyn**		**% inhibition of Abl**		**% inhibition of Src**	
	10 μM	1 μM	10 μM	1 μM	10 μM	1 μM
SI308	99	70[a]	81	ND[b]	98	ND
43a	NA[c]	NA	ND	ND	ND	ND
43b	42	NA	24	NA	24	24
43c	51	16	ND	ND	ND	ND

[a] K_i value expressed as nM

[b] ND = Not Determined

[c] NA = Not Active

6.4 Conclusions

This work led to the synthesis of new Fyn inhibitors. The compounds have been obtained through a multistep approach. Compounds **43a-c** have been already tested on Fyn and also on Abl and Src, other two cytoplasmic TKs. Unfortunately, these molecules are less active than the first generation in-house inhibitor SI308. Nevertheless, compounds **43b,c** maintained a certain activity in inhibiting Fyn and 10 μM. Since the main issue related to these compounds seems to be the poor solubility, it would be interesting to develop formulations of these compounds to overcome this problem. Recently, the group has already used this approach for other in-house compounds with excellent results[177].

CHAPTER 7

Synthesis of the pyrazolo[3,4-d]pyrimidine SI306 and subsequent evaluation in NB cell lines

7.1 Background

NB is a childhood solid tumor originating from progenitor cells of the sympathetic nervous system and accounts for 15% of deaths from pediatric cancer[178]. It is characterized by a plethora of biological behaviors which range from tumors which regress or differentiate spontaneously into ganglioneuromas to highly aggressive forms which are frequently fatal. High-risk NB is characterized by metastatic disease and/or amplification of the MYCN proto-oncogene that is a biomarker still used today to stratify the disease risk[179]. Current treatment for high-risk NB patients includes intensive and toxic chemotherapy followed by surgical resection, myeloablation and autologous stem cell rescue, radiation, and intensive immunotherapy[180]. Although most high-risk patients initially respond to chemotherapy, the majority of them relapse and succumb to the therapy-resistant disease[181]. Recently, it has been shown that c-Src inhibitors exhibit strong anti-proliferative and pro-apoptotic effects toward several cancer cell lines, including NB[182]. Starting from the crystallographic complex of an in-house pyrazolo[3,4-*d*]pyrimidine derivative and c-Src, an efficient optimization study was performed to obtain new c-Src inhibitors endowed with a better activity and pharmacokinetic profile. Among them, compound **46**, called SI306, resulted one of the most promising for development against NB[92].

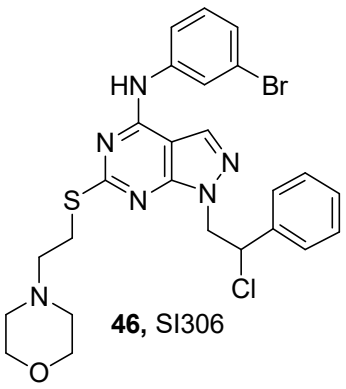

46, SI306

7.1.1 SI306 activity on NB *in vitro* and *in vivo* studies

In this context, our previous studies demonstrated that 72 h treatment with SI306 markedly affected the proliferation of SH-SY-5Y neuroblastoma cells by inhibiting the spheroid formation. Moreover, this effect was concentration-dependent, and the compound showed an IC_{50} value of 0.34 μM[92].

In addition, SI306 exposure led to a dose-dependent accumulation of SH-SY-5Y cells in the G1 phase of cell cycle (**Fig.24**) and a progressive induction of apoptosis.

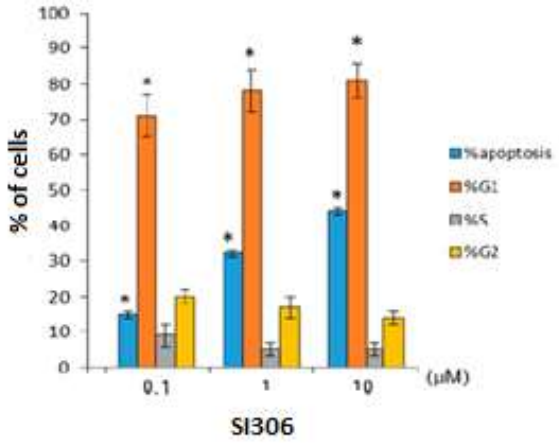

Fig.24. Analysis of the cell cycle distribution of SH-SY-5Y cells after treatment with increasing concentrations of SI306. The percentage of cells in each phase of cell cycle was evaluated by cytofluorimetric analysis of DNA content.

The anticancer activity of SI306 was confirmed by *in vivo* studies using a xenograft mouse model. Mice were inoculated with SH-SY-5Y NB cells and, starting from the appearance of a visible tumor mass, were treated daily with 50 mg/kg SI306. Tumor volume was evaluated at regular intervals and interestingly, SI306 has been found to reduce the tumor volume by 50% in treated mice in comparison with placebo treated mice. Moreover, the observed reduction in tumor volume was associated with a significantly compromised angiogenesis, further demonstrated by a three-dimensional *in vitro* sprouting assay on endothelial cells. Notably, after treatments mice did not show any sign of toxicity.

7.2 Project

In order to further investigate the potential of SI306 as a promising compound able to counteract NB growth, I started to collaborate with Professor Domenicotti's group (Department of Experimental Medicine of the University of Genova) which has been involved for many years in the study of molecular mechanisms underlying chemoresistance in NB.

For the realisation of this project, carried out during my PhD course, first, I synthesized compound SI306 and then I performed the biological assays for this inhibitor on three human NB cell lines characterized by a different MYCN status: HTLA-230 and SK-N-BE-2C with MYCN amplification and SH-SY-5Y without MYCN amplification.

7.3 Results and discussion

7.3.1 Chemistry

Preparation of compound **32a** has been previously described in **scheme 1**. Alkylation with 4-(2-chloroethyl)morpholine at position C6 in the presence of NaOH in anhydrous DMF and absolute ethanol at reflux for 6 hours gave compound **47**. This intermediate was treated with the Vilsmeier complex ($POCl_3$/DMF, 1:1) in $CHCl_3$ at reflux for 8 h to obtain the halogenated derivative **48**. Finally, the reaction of **48** with *m*-bromoaniline in ethanol for 4h at reflux, afforded the desired compound SI306 (**Scheme 7**).

Scheme 7: preparation of compound SI306.

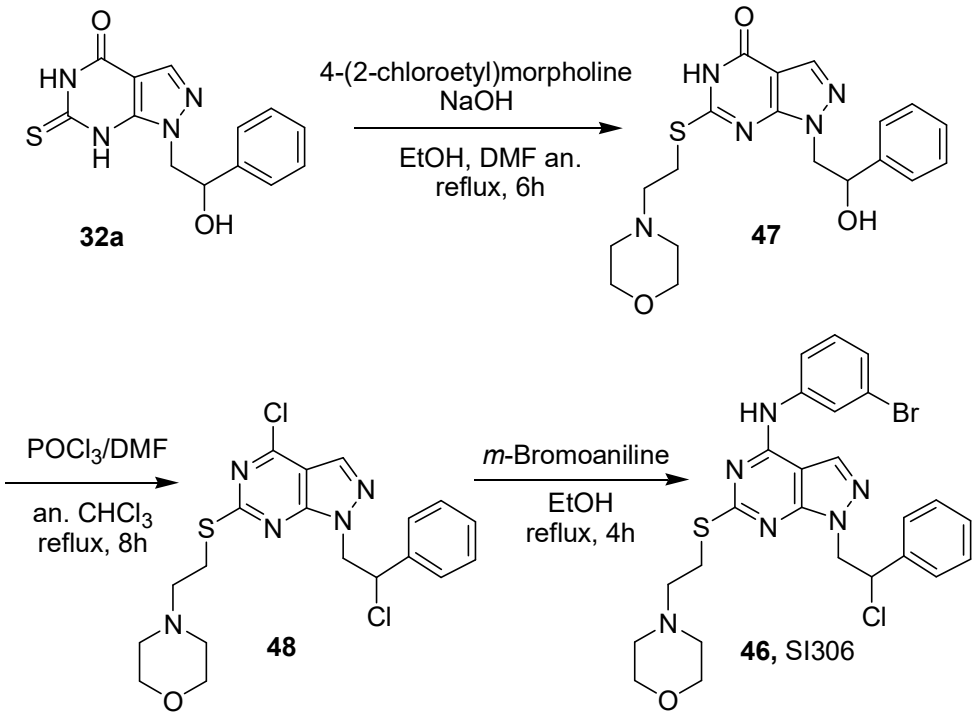

7.3.2 Biology

In order to investigate if the anticancer effect of SI306 on NB cells can be influenced by a different MYCN status, HTLA-230, SK-N-BE-2C and SH-SY-5Y cells were treated with increasing concentrations (0.1-20 μM) of the drug for 72 hrs. As shown in graphs (**Fig.25**), SI306 differently affected the viability of three NB cell lines. In detail, SI306 exerted a cytotoxic effect on HTLA-230 cells already at 1 μM (**Fig.25A**), while it was able to affect the viability of both SK-N-BE-2C and SH-SY-5Y starting from 7μM concentration (**Fig.25 B and C**).

Notably, the IC_{50} value was similar for MYCN-amplified NB cells (IC_{50}=11.83 for HTLA-230 and 12.62 for SK-N-BE-2C) and it was higher by 30% than the IC_{50} calculated in non amplified SH-SY-5Y cells (IC_{50}=8.47).

In addition, a 20 μM concentration, the maximal dose used in these experiments, was more cytotoxic for SH-SY-5Y cells, with a reduction of viability by 90%, in comparison with HTLA-230 and SK-N-BE-2C, whose cell viability was reduced by 70% (**Fig.25**).

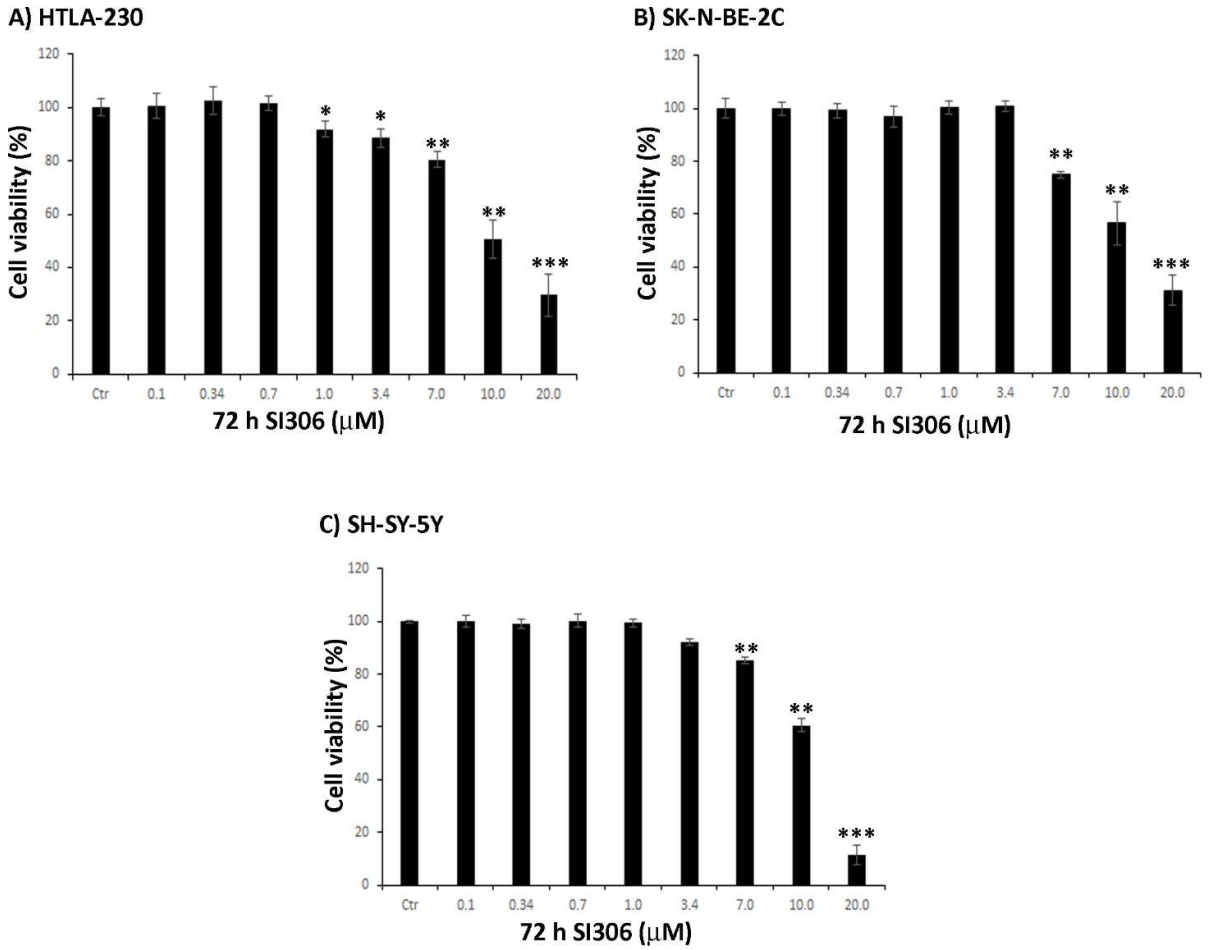

Fig.25. Effects of SI306 on NB cell viability. Cell viability was evaluated by MTT assay in HTLA-230 (A), SK-N-BE-2C (B) and SH-SY-5Y (C) cells exposed to increasing concentrations (0.1 - 20 μM) of SI306 for 72 h. The graph summarizes quantitative data of the means ± S.E.M. of three independent experiments. *p<0.05 vs Ctr cells; **p< 0.01 vs Ctr cells; ***p< 0.001 vs Ctr cells.

7.4 Materials and methods

7.4.1 Cell lines and treatments

NB cell lines were kindly provided by Dr. Raffaghello L. (G Gaslini Institute, Genoa, Italy). NB cells were tested for mycoplasma contamination (Mycoplasma Reagent Set; Euroclone s.p.a, Pavia, Italy) and were cultured in RPMI1640 media (Euroclone) supplemented with 10% fetal bovine serum (FBS; Euroclone), 2 mM glutamine (Euroclone), 1% penicillin/streptomycin (Euroclone), 1% sodium pyruvate (Sigma), and 1% of aminoacid solution (Sigma). NB cells were treated for 72 h with SI306 doses ranging from 0.1 to 20 μM. The stock solution of SI306

prepared in DMSO and pilot experiments demonstrated that the final DMSO concentrations did not alter cell viability.

7.4.2 Viability assay

Cell viability was evaluated by using the dimethylthiazolyl-2-5-diphenyltetrazolium bromide (MTT; Sigma) staining. Cells were seeded into 96 well plates (Corning) and then treated with SI306. After 72 hours, NB cells were incubated with 0.5 mg/ml MTT for 3 h at 37°C. After incubation, the supernatant was discarded, insoluble formazan precipitates were dissolved in HCl (0.1 N in isopropanol) and the absorbance at 570/630 nm was recorded using a microplate reader (EL-808; BioTek Instruments Inc., Winooski, VT, USA).

7.5 Conclusions

The results obtained from the biological studies carried out in NB cell lines displaying a different status of MYCN confirm the anticancer activity of SI306 further supporting its role as a promising candidate for NB treatment and encouraging the search for new SI306 derivatives.

CHAPTER 8

Polymer-carried pyrazolo[3,4-d]pyrimidine kinase inhibitors as feasible treatments against GBM recurrence

8.1 Background

8.1.1 Glioblastoma multiforme

GBM is the most common, malignant and aggressive primary brain tumor in adults, mainly due to its rapid proliferation and ability to penetrate and diffusely infiltrate healthy brain parenchyma (**Fig.26**). Standard of care treatment currently involves a combination of surgery, radiotherapy and chemotherapy[183]. Yet, despite this multimodal treatment, the median survival remains poor at less than 15 months[184]. Problems with existing treatment approaches include:

- increased resistance to chemotherapeutic drugs caused by the heterogeneity of the tumor micro-environment and subsequent variation in tumor sub-clones,
- inability or impairment of drugs to cross the blood-brain barrier (BBB),
- lack of penetration of locally delivered therapeutic agents deep into the brain parenchyma beyond the resection cavity at sufficient therapeutic concentrations to therapeutically target residual tumor cells[185,186].

It is important to note that the residual cells at the tumor margin are responsible for 85% of GBMs that locally relapse after maximal safe surgical resection followed by the standard combination protocol of temozolomide and radiotherapy[187]. For these reasons, superior and more innovative treatment methods are necessary to eradicate invasive tumor cells which remain beyond the resection cavity lining post-surgery, and to block or impair GBM recurrence, which is inevitable with current treatment methods.

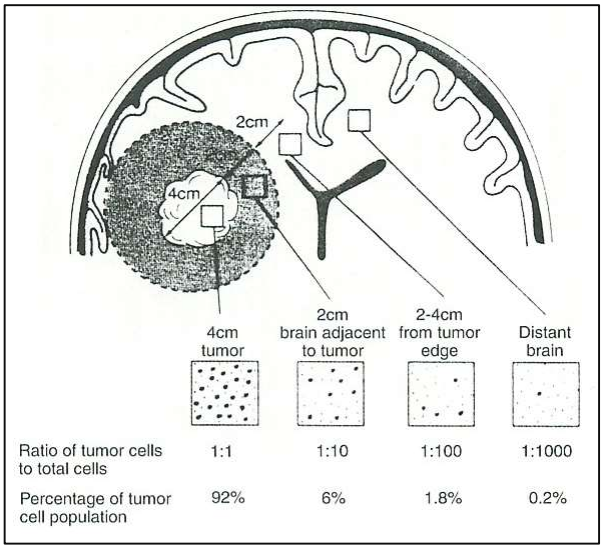

Fig.26. Schematic presentation of cell's ability to penetrate and diffusely infiltrate healthy brain parenchyma in GBM.

8.1.2 Use of kinase inhibitors in GBM

The implication of kinases in GBM pathogenesis and drug resistance has led to the evaluation of small molecule kinase inhibitors as possible treatment options[188,189]. Crucially, kinase inhibitors, acting specifically on molecular targets, are supposed to reduce off- site toxicity during antitumor treatments[190].

As previously reported, deregulated SFK signaling can induce multiple pro-tumorigenic effects in glioma biology, including reduced apoptosis, increased angiogenesis, and increased proliferation[120,191,122]. Furthermore, evidence suggests that SFKs play roles in cancer cell invasion and metastasis[192,193]. Preclinical data confirmed that Src kinase, which is in general frequently overexpressed in brain tumors[85], plays a key role in GBM proliferation and invasion[194], leading the way for the use of Src inhibitors in clinical studies. Fyn, as it was widely discussed in chapter 3, has also been reported to be an effector of oncogenic signaling in GBM patients. In 2009, Lu *et al.* demonstrated that persistent EGFR signaling activated both Fyn and Src to increase GBM invasion and tumor survival *in vivo*[119]. More recently, Comba *et al.* reported the correlation of Fyn expression with malignant features of GBM tumors, including pseudopalisades, necrosis, and hypervascularization[122].

In 2013, the broad spectrum SFK inhibitor dasatinib **9** was proposed as a therapeutic option in recurrent GBM[192]. Dasatinib was well tolerated in clinical trials but failed to improve the overall survival either as a monotherapy or in combination therapy for GBM patients[195,196]. This result can be attributed to dasatinib susceptibility to cellular efflux by transporters and subsequent poor accumulation in brain tissue[197].

8.1.3 Water solubility enhancement of pyrazolo[3,4-*d*]pyrimidines using an inkjet printing technology

The pyrazolo[3,4-*d*]pyrimidines are readily soluble in DMSO and other organic solvents, but the limited solubility in water adversely affects their bioavailability and efficacy. Thus, in order to avoid the use of toxic organic solvents for *in vitro* and *in vivo* tests, as well as to develop oral formulations, several strategies have been sought to improve the aqueous solubility and pharmacokinetics of pyrazolo[3,4-*d*]pyrimidine derivatives, including formation of complexes with cyclodextrins[198], encapsulation into liposomes[199], formulation with albumin into nanoparticles[200] and synthesis of prodrug derivatives[201]. Additionally, a simple and promising methods is represented by the preparation of an amorphous solid dispersion, where the compound is molecularly dispersed in an inert carrier, typically a hydrophilic polymer[202], such that the resulting stabilized amorphous compound shows a higher water solubility than the crystal form[203].

Accordingly, a new miniaturized screening process, based on an inkjet printing technology, have been developed by Sanna *et al*. to evaluate pyrazolo[3,4-*d*]pyrimidines water solubility enhancement into hydrophilic polymer carriers[177].

This formulation strategy, which is briefly summarized in figure 27, can be used to increase the water solubility of pyrazolo[3,4-*d*]pyrimidine derivatives, requiring only a few micrograms of compounds, in a manner that does not compromise potency, and thus provides a viable approach for development of oral formulations.

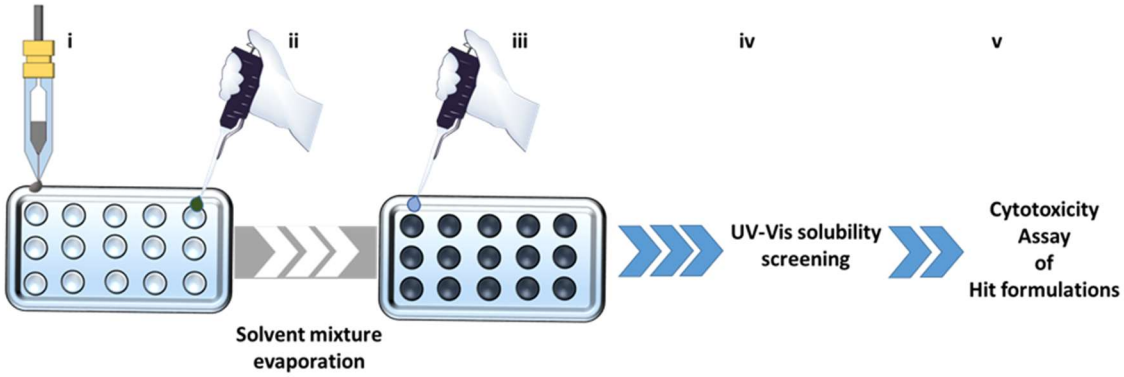

Fig.27. i. Highthroughput dispensing of DMSO drug solutions by an inkjet 2D printer; **ii.** Sequential addition of polymeric aqueous solutions and evaporation of water and DMSO; **iii.** Resuspension with water of the dry solid dispersions; **iv.** Evaluation of the apparent-solubility of the drugs in water from the polymeric matrixes via multiwell-reader UV-vis analysis; and **v.** Cytotoxicity assay of the hit formulations.

8.2 Project

During my visiting research fellowship period at the School of Pharmacy in Nottingham, under the supervision of Prof. Cameron Alexander, I had the opportunity to focus my research on the biological activity of a set of in house kinase inhibitors on a range of patient-derived GBM cell lines and to explore an appropriate formulation method.

In particular, I selected three pyrazolo[3,4-*d*]pyrimidines, SI113, SI308 and SI306 (**Fig.28**) which are inhibitors of SGK1[141], Fyn[124] and Src[92], respectively, and have also demonstrated anticancer effects on different commercial (established) GBM cell lines[124,86,67]. Importantly, most commercial GBM cell lines have historically been derived from the core region of tumors, which does not allow a realistic, phenotypically accurate representation of the infiltrative cells which, due to their difficult surgical removing, ultimately result in GBM recurrence[185].

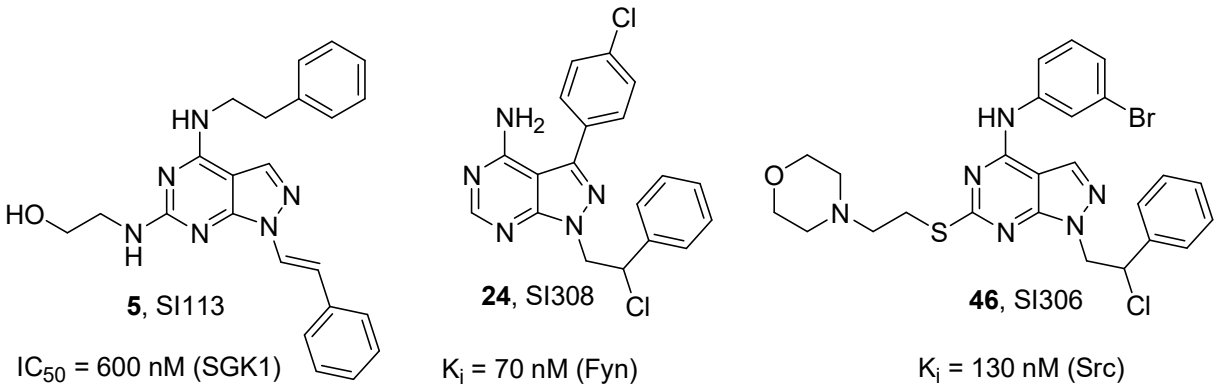

Fig.28. Structures of in-house kinase inhibitors SI306, SI308 and SI113 and their activity towards SGK1, Fyn and Src.

This time the three selected kinase inhibitors have been tested on a series of patient derived GBM cell lines isolated from both the central tumor core (GCE28) and from the invasive margin of the tumor (GIN28 and GIN8), kindly provided by Dr. Rahman at the Medical School in Nottingham.

In vitro studies on invasive margin derived cells represent an important step in the discovery and development of drugs for the treatment of GBM, as these cells, which are associated with disease reoccurrence, are one the most relevant targets for pharmacotherapy.

Furthermore, the anticancer effects of our kinase inhibitors have been explored in mono- and combination-therapy. Finally, since our compounds can be considered in Biopharmaceutical Classification System (BCS) class II[204], demonstrating good permeability[205] (indicating a good probability of BBB permeation) but limited water solubility, I performed a formulation study, applying the innovative inkjet printing technology to generate solid dispersions of our lead compound in inert hydrophilic polymeric carriers.

8.3 Results and discussion

8.3.1 Preliminary cytotoxic evaluation

In *vitro* data demonstrated that the tested kinase inhibitors were cytotoxic, implicating Src, Fyn and SGK1 kinases as valid targets in the tested GBM cell lines. SI306 (Src inhibitor) was demonstrated to be the most potent compound with IC_{50} values of 11.2, 7.7 and 7.2 μM on the

GIN8, GIN28 and GCE28 cell lines, respectively. Compound SI113 (SGK1 inhibitor) exhibited a potency comparable to that of SI306 on the GIN8 line but was 1.9-fold and 1.5-fold less potent on GIN28 and GCE28 cells. The least potent compound was shown to be SI308 (Fyn inhibitor), with IC_{50} values 4.9-fold, 6.5-fold and 6.6-fold higher than the most potent compound (SI306) on GIN8, GIN28, and GCE28 cells, respectively (**Table 4**). However, despite being the least potent compound in monotherapy, SI308 demonstrated a promising application in synergistic combination-therapy with a Src inhibitor, as described later.

Table 4. IC_{50} values of kinase inhibitors on GBM cells. Data represent the mean of three independent experiments ± S.E.M.

cpd	GIN8 IC_{50} (µM)	GIN28 IC_{50} (µM)	GCE28 IC_{50} (µM)
SI306	11.2 ± 3.8	7.7 ± 1.6	7.2 ± 2.0
SI308	54.7 ± 6.3	49.8 ± 4.2	47.6 ± 6.9
SI113	10.5 ± 3.5	14.4 ± 2.8	10.7 ± 1.2

8.3.2 Apoptosis investigation

After the confirmation of compound cytotoxicity, we next investigated the effect of our derivatives on caspases-3/7 to determine if cell death was apoptotic in nature[206].

Data in figure 29 demonstrates that at a cytotoxic concentration (12.5 µM), SI113 and SI306 induced a significant increase in caspase-3/7 activation in all GBM cell lines tested, with the exception of SI113 in the GIN28 line.

Staurosporine (10.0 µM), a known inducer of apoptosis[207], was also tested as a reference compound. It elicits significant increase in caspase activation at similar or lower levels than those of the kinase inhibitors. It can be noted that SI306 induces higher levels of effector caspase activation compared to SI113, a result that reflects the IC_{50} data (**Table 4**), which together indicate that SI306 is the most active compound we tested against these cell lines.

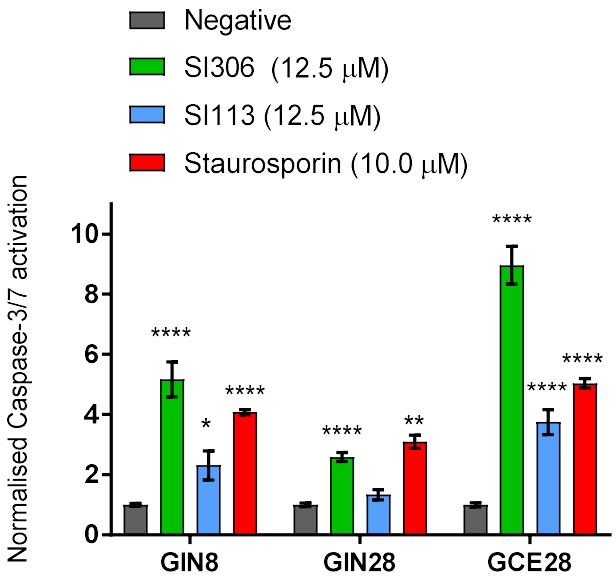

Fig.29. Effect of kinase inhibitors on levels of activated effector caspases-3/7 on GBM. Data represents mean ± S.E.M. (n=3). Statistical significance was determined via Two-way Anova followed by Dunnett's multiple comparisons test.

To further confirm the apoptotic death induced by SI306, the nuclear morphology and permeability was investigated by fluorescence microscopy using Hoechst 33342 (Ho) and propidium iodide (PI) double staining (**Fig.30**). Cells treated with SI306 at 12.5 μM exhibit signs of chromatid condensation, nuclear fragmentation and the presence of apoptotic bodies, which are well known pro-apoptotic features. SI306 treatment did not induce nuclear membrane permeability, as shown by PI negative staining (**Fig.30**), or nuclear swelling, indicators of necrotic cell death and caused by ethanol (EtOH) (**Fig.30**), a known inducer of necrosis[208]. These observations, taken together with the effective caspase activation, indicate that SI306 induces GBM cell death via an apoptotic mechanism.

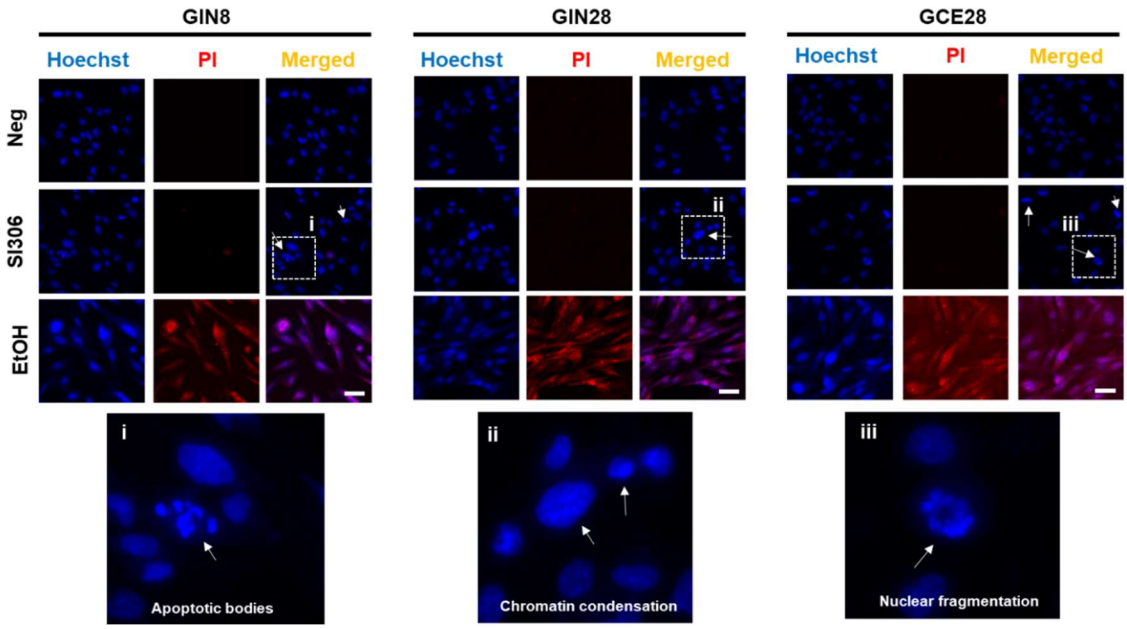

Fig.30. Ho/PI staining of nuclei. Effect of SI306 kinase inhibitor on apoptotic features of cellular nuclei. Scale bar indicates 30 µm. Images are representative of 3 sets of independent images. White arrows indicate the presence of apoptotic nuclei (chromatid condensation, apoptotic bodies).

8.3.3 Combination study

Previous evidence indicates that targeting more than one kinase may be beneficial in cancer treatment. This can offer the opportunity to achieve a synergistic effect and to overcome the development of resistance[209,210]. Therefore, we have investigated our novel compounds as combination therapies in order to assess if synergistic activity can be achieved. The median-effect algorithm based on the widely used method established by Chou and Talalay[211] was employed to calculate the combination index (CI) as outlined in the materials and methods section. The CI equation was used to generate CI values, which categorize the compound-compound combinations as synergistic, additive or antagonistic. Interestingly, the combination of SI308 with either SI306 or SI113 was determined to generate synergistic effects, SI308 having been demonstrated to be the least potent compound in monotherapy (**Fig.31**).

On the contrary, SI113 and SI306 co-therapy exhibited only additive action. Therefore, the observed effects suggest that a co-inhibition of the Fyn kinase and SGK1 or Src kinases can provide a synergistic action that cannot be achieved via inhibiting SGK1 and Src together. Of

further note is the observation that in the GIN8 line, co-therapy with SI113 and SI308 produced an antagonistic effect despite synergy being observed in the GIN28 and GCE28 lines with this combination; the reasons for this remain unclear, however, patient genetic variation may play a role (GIN28 and GCE28 lines are derived from the same patient, and the GIN8 line from a separate patient). Taken together, the evidence for synergistic action with our compounds may promote the adoption of combination therapies in the field of kinase inhibitors for the treatment of resistant GBM.

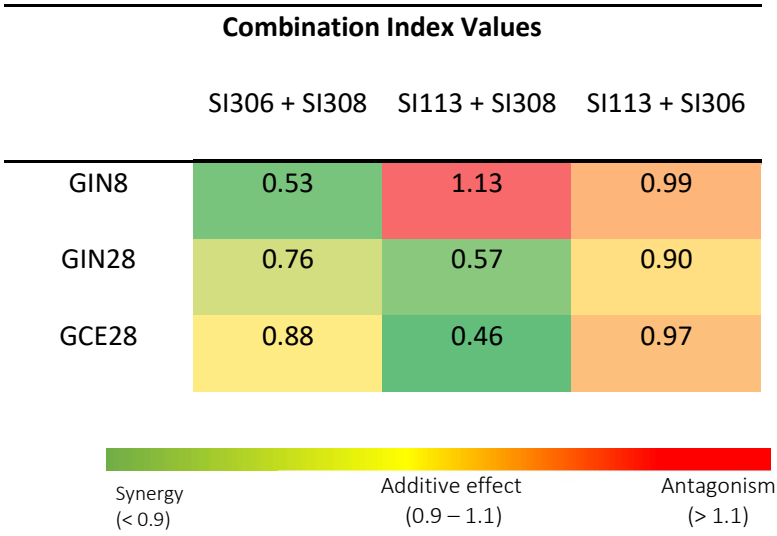

Fig.31. Combination index values. Each CI value was calculated, and a heat map generated on the basis of three independent IC_{50} experiments (n=3).

8.3.4 SI306 formulation

The promising *in vitro* data highlights pyrazolo[3,4-*d*]pyrimidine kinase inhibitors as potential therapies for eradicating invasive GBM cell lines. To further investigate the possibility of the development of these derivatives for clinical application, the formulation of our lead compound SI306 has been evaluated. To overcome the water solubility limitation of SI306, which may affect further *in vivo* studies and future oral administration routes, I performed a preliminary formulation screening process based on 2D inkjet printing, building on an approach previously validated by our group[177,212,213]. Different commercial polymers (PEG8000, PEG20000,

Pluronic F-68, Tween 80, PVPVA) were combined with SI306 (at a "drug"/polymer ratio of 10/90% w/w) and the apparent-solubility (ΔA%) value of each formulation was calculated in order to identify the polymers able to solubilise our lead compound. Data demonstrated that two surfactants (Pluronic F-68 and Tween 80) and the amphiphilic co-polymer PVPVA showed notably higher ΔA% average values compared to the highly hydrophilic homopolymers (PEG8000-20000) (**Fig.32**).

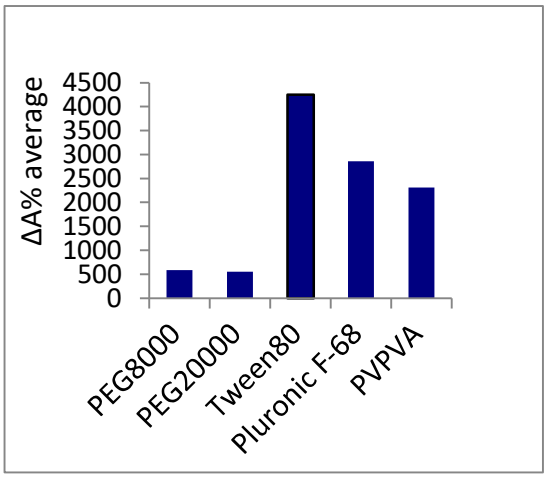

Fig.32. ΔA% average of SI306-polymer formulation ranked according to their water apparent-solubility enhancement (high ΔA% is related with a high compound water solubility). Samples were diluted until the final concentration of 100 µg/mL and 900 µg/mL for SI306 and the polymers, respectively.

These results suggest that solubilization of the hydrophobic compound SI306 is due to associative interactions between hydrophobic blocks in Pluronic F-68, Tween 80 and PVPVA and the lipophilic regions in SI306[177]. Dynamic Light Scattering (DLS) measurements were performed on the formulation of SI306 with the three candidate polymers Pluronic F-68, Tween 80 and PVPVA (**Fig.33**) in order to evaluate the particulate nature of the drug-polymer assemblies.

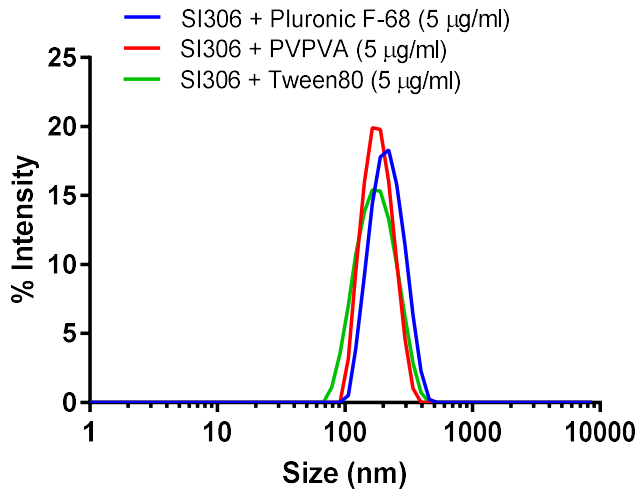

Fig.33. DLS traces in PBS of SI306 as a formulation. Light scattering measurements were collected on suspensions prepared with a final concentration of 5 μg/mL.

As can be observed from figure 33, all the formulations produced well-defined nanoaggregates, characterised by a single monomodal and monodispersed population with sizes ranging from 180 to 200 nm. The absence of a second peak or species related to aggregation confirmed the quality of the nanoformulation obtained, due to the interactions between the small molecules and the different polymers. The amphiphilic nature of the macromolecules facilitated the interactions with the hydrophobic active compounds leading to an improvement of the self-assembly properties.

To further validate the water solubility enhancement, we performed a cytotoxicity assay using a concentration of 5 μg/mL (8.7 μM) of SI306 either dissolved in DMSO or printed into the selected polymers at a "drug"/polymer ratio of 10/90% w/w. Negative control, polymers alone and SI306 suspended in cell culture medium DMEM (to highlight SI306 poor water solubility and consequent *in vitro* inactivity) had no effect on cell viability. On the contrary, formulated SI306 resuspended in DMEM and SI306 dissolved in DMSO treatments had comparable cytotoxic effects on all GBM cell lines (**Fig.34**). Therefore, the described SI306 formulations can successfully increase the apparent water solubility of the inhibitor without affecting its potency, and this provides a further step into the development of our lead compound.

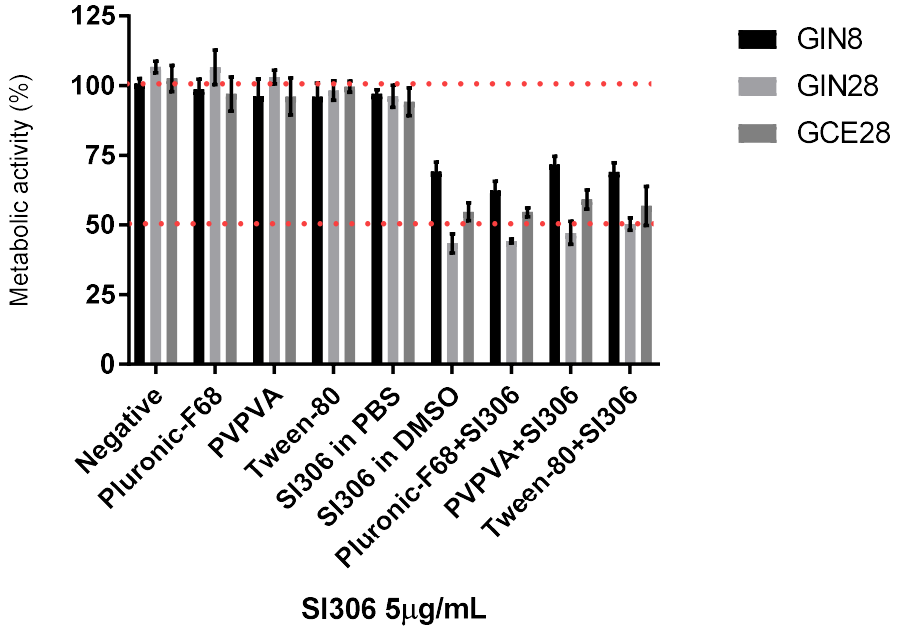

Fig.34. The compounds formulated with the selected best polymers were then tested against the patients derived GBM cell lines and the potency compared to the compounds solubilized in 1% DMSO. Data represents mean ± S.D.

8.4 Materials and methods

8.4.1 Chemicals

Polyvinylpyrrolidone-vinyl acetate copolymer (PVPVA), Tween 80, Pluronic F-68 and DMSO were purchased from SIGMA Aldrich and the latter used as a common solvent to dissolve all the printable materials. Synthesis of pyrazolo[3,4-*d*]pyrimidines kinase inhibitors were performed by our research group[92,124,205]. Synthesis of SI113 and SI306 has been previously reported in **scheme 3** and **scheme 7** respectively.

8.4.2 Formulation

8.4.2.1 Printing

The drug solutions were dispensed into 96-well plate, via a piezoelectric inkjet printer (Sciflexarray S5, Scienion) using a 90 µm orifice nozzle. The droplet size was controlled by the values of the voltage and electrical pulse. A fixed amount of drug (20 µg) was dispensed

for each well, by adjusting the number of drops. The number of drops per spot were selected in such way that the volume aspired delivered by the nozzle (max 10 µL) at the beginning of a run was sufficient to print the whole print pattern. In a routine experiment DMSO solution (10 mg/mL) droplets with nominal volumes ranging from 250-280 pL, were dispensed at a 300 Hz jetting frequency by adjusting the voltage and pulse between 98-105 Volt (Voltage) and 45-55 µs (Pulse) respectively. The nozzle was washed with DMF, in between each printing cycle, as part of the automated printing-washing loop. DMSO was chosen for its high evaporation point that avoids nozzle blockage and its ability to dissolve the selected drug. SI306 and polymer solutions were prepared by dissolving the desired amount of compound in DMSO and, separately, the polymers in deionized (DI) water.

8.4.2.2 Dynamic Light Scattering

DLS measurements were conducted in triplicate using a Malvern Zetasizer Nano ZS at 25 ºC (scattering angle 173º, laser of 633 nm) or a Viscotek 802 DLS with a laser wavelength of 830 nm at 20 ºC. Formulations were prepared as above at 5 µg/mL (with respect to drug) in PBS. Data was analyzed using OmniSIZE software. A minimum of 10 measurements were collected per sample.

8.4.2.3 UV screening

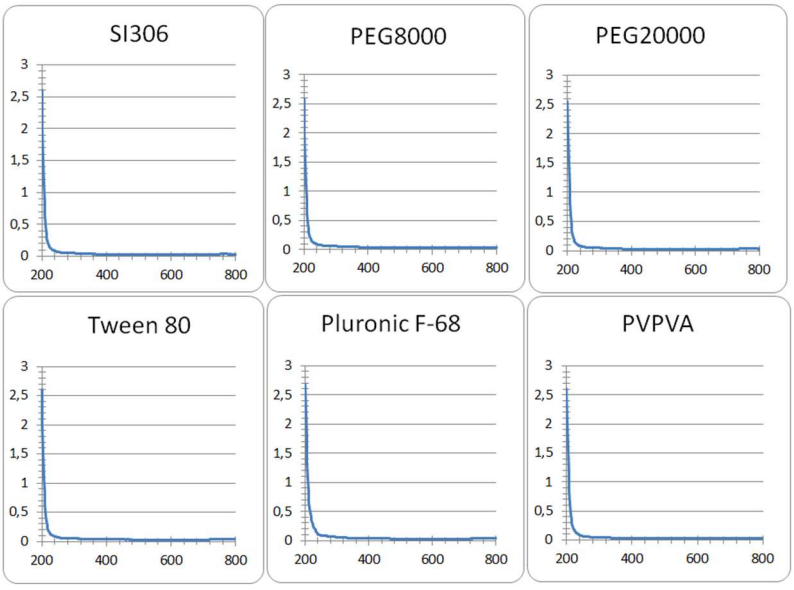

Fig.35. UV-vis spectra of SI306 (concentration 100 μg/mL) and selected commercial polymers (concentration 900 μg/mL) in PBS. We already demonstrated that solutions of in-house pyrazolo[3,4-*d*]pyrimidines in DMSO absorb in the UV region[177].

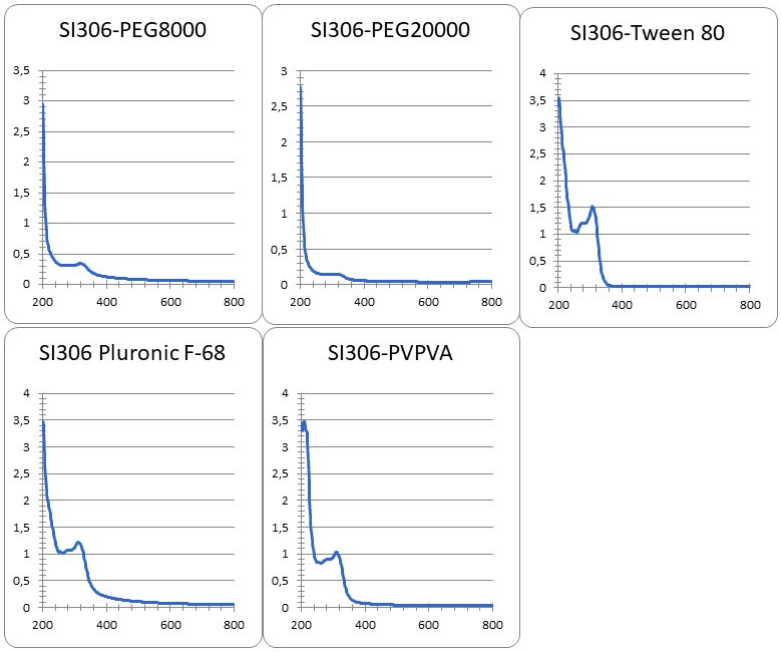

Fig.36.UV-vis spectra of SI306-polymer formulations in PBS (100 μg/mL of SI306 and 900 μg/mL of polymer).

8.4.2.4 ΔA% determination

ΔA% was calculated according the following equation[177]:

$$\Delta A\% = \frac{A - A_0}{A_0} \cdot 100$$

Where:

A_0 is the absorbance of the polymer solutions in water (used as blank),

A is the absorbance of the aqueous solutions of drug/polymer blends.

No signal was observed from the presence of water-insoluble SI306 (**Fig.35**).

In **Table 5** the ΔA% is reported for every SI306-polymer formulation.

Table 5. ΔA% of SI306 and polymers. Absorbance has been measured at λ = 308 nm

	PEG8000	PEG20000	Tween80	Pluronic F68	PVPVA
ΔA%	584.5179	555.3168	4251.295	2857.245	2312.342

8.4.3 Biology

8.4.3.1 Cell lines

GIN8 (Glioma INvasive margin cells) isolated from medial front invasive margin, GIN28 isolated from 5-ALA fluorescence invasive margin and GCE28 (Glioma Contrast Enhanced core cells) isolated from central enhanced core region by Dr. Smith and Dr. Rahman, were used at passage range of 15-30 to maintain consistent cell performance . The samples were paraffin-embedded and sectioned by the Queen's Medical Centre Histopathology Department. Cell lines were cultured in Dulbecco's Modified Eagle Medium (DMEM; Sigma-Aldrich) supplemented with 10% HyClone™ Bovine Growth Serum (BGS; GE Healthcare), 1g/L glucose and 2 mM L-glutamine (Sigma-Aldrich) at 37°C with 5% CO_2.

8.4.3.2 Metabolic activity

Cells were seeded at a density of 1 x 10^4 cells per well in 96 well plates (Corning) for 24 hours prior to assaying. Dosing of cells was initiated by removing culture medium, washing cells with phosphate buffered saline (PBS; Sigma-Aldrich) and the application of 100 µL per well of treatment for 48 hours. Treatments were applied to cells in phenol red free DMEM (Thermo-Fisher) containing 10% BGS. Pyrazolo[3,4-*d*]pyrimidine-based kinase inhibitors were dosed at concentrations of 0.1 – 100.0 µM for determination of their half maximal inhibitory concentration (IC_{50}) values, and at 5 µg/ml for evaluation of SI306 activity in formulations. Additionally, to study the cytocompatibility of the DMSO concentration used to dissolve free drugs, medium containing 1% (v/v) DMSO was applied to cells. Cells were also treated with 0.1% (v/v) Triton-X 100 and DMEM with 10% BGS for 48 h for use as positive and negative controls, respectively. Following this treatment, cells were washed with PBS and incubated with 100 µl 10% PrestoBlue™ Cell Viability Reagent diluted in medium per well for 1 h.

Solution fluorescence was then measured at 560/600 nm λexcitation/ λemission (λex/λem), and relative metabolic activity calculated by setting the values of the negative control as 100% and the positive control (0.1% Triton X-100) as 0%.

8.4.3.3 Detection of activated caspase-3/7

The CellEvent caspase-3/7 green detection reagent (Thermo Fisher Scientific) was employed to evaluate the levels of activated caspase-3 or -7. After exposure to the drug solutions, 150 µL of 2% (v/v) CellEvent probe in PBS was applied per well for 30 min at 37 °C. Staurosporine was used at 10 µM as the apoptotic control. Fluorescent intensity was measured at 502/530 nm (λex/λem) and normalized to the untreated control (set as a value of 1).

8.4.3.4 Hoechst 33342/Propidium Iodide microscopy

Integrity of the nuclear membrane and nuclear fragmentation was measured by PI (Thermo Fisher Scientific) uptake. To do so, 6×10^4 GIN28 and GCE28 cells per well were seeded in 24-well plates (Corning) and cultured for 24h. Following this, the treatment solutions, including selected kinase inhibitors or 100% ice cold ethanol were applied for 48h. Treatments were then aspirated, and the cells were washed with PBS, followed by the addition of 1 µM Hoechst 33342 (Thermo Fisher Scientific) in PBS for 5 min and then 0.1 mg/mL of PI in PBS (final concentration ~2 µg/mL PI). The cells were incubated for another 5 min, after which the solution was removed, and the cells were washed with PBS. Cells were then imaged on an inverted Nikon Eclipse TE 300 microscope using a DAPI filter (357/447 nm; excitation/ emission) for detection of the Hoechst signal and the RFP filter (531/593 nm; excitation/emission) for the PI signal.

8.4.3.5 Statistical analysis

Dose-response curve fitting was performed using non-linear regression analysis to enable IC_{50} determination (GraphPad prism, version 7.03). Statistical analysis was performed by one-way ANOVA with Dunnett's multiple comparison post hoc test using GraphPad prism.

8.4.3.6 Determination of combination index values

CI values were determined according to a widely used method established by Chou and Talalay[211]. Briefly, in order to determine each CI value, the following cytotoxicity studied were

conducted: (1) SI113 as a single compound, (2) SI308 as a single compound, (3) SI306 as a single compound, (4) S306 + SI308 combination, (5) SI113 + SI308 combination and (6) SI113 + SI306 combination. Compounds were applied in combination at a molar ratio of 1:1 and dosed with a range of 0.1 – 100.0 μM per compound. IC_{50} values were then calculated from each study and used in the following equation to determine CI values;

$$\mathbf{CI} = \frac{\mathbf{D_{CA}}}{\mathbf{D_{SA}}} + \frac{\mathbf{D_{CB}}}{\mathbf{D_{SB}}} + \frac{\mathbf{D_{CA}}\,\mathbf{D_{CB}}}{\mathbf{D_{SA}}\,\mathbf{D_{SB}}}$$

Where D_{CA} represents the IC_{50} values of drug A in combination with drug B, and D_{SA} the IC_{50} of drug A as a single compound. Similarly, D_{CB} represents the IC_{50} values of drug B in combination with drug A, and D_{SB} the IC_{50} of drug B as a single compound. Based on this method, CI values are indicative of strong synergism (<0.7), synergism (0.7-0.9), additive effect (0.9-1.1), antagonism (1.1-3.3), or strong antagonism (>3.3)[214]. Microsoft Excel was then employed to produce a tricolor system based on these values, where antagonism is represented by red, additive effect by yellow, and synergism by green.

8.5 Conclusions

In conclusion, I have evaluated the potency of our pyrazolo[3,4-*d*]pyrimidines active as specific kinase inhibitors against patient derived cell lines from the invasive region and core of GBM, identifying the Src inhibitor SI306 as a lead compound. SI306 possesses an IC_{50} in the low micromolar range on all the three GBM cell lines tested in this work, and demonstrates the ability to induce apoptotic death. A combination study, using the Chou and Talalay method, has also been assessed and showed that, based on patient genetic variations, our kinase inhibitors possess a synergistic effect that could positively influence the success of GBM treatment. Lastly, a polymer formulation strategy involving the novel 2D inkjet printing technology was explored as a strategy to enhance SI306 water solubility. *In vitro* results illustrated that printing 5 μg/mL of our lead compound into dispersions of Pluronic F-68, Tween 80 or PVPVA at a level of 90% is a successful formulation method, resulting in a comparable potency to SI306 dissolved in DMSO. Accordingly, this methodology provides a viable approach for the development of oral formulations of our in-house kinase inhibitors.

Furthermore, since some of the chosen polymers, such as the Pluronic family, have been shown to facilitate transport across the BBB, a next challenge could be the selection of the best polymer for *in vivo* GBM studies.

Overall, these results encourage *in vivo* studies and promote polymer-carried pyrazolo[3,4-*d*]pyrimidine kinase inhibitors as oral feasible treatments against GBM recurrence.

CHAPTER 9

Evaluation of pyrazolo[3,4-d]pyrimidines against bacterial infections

9.1 Background

The increasing emergence of bacterial strains resistant to currently available antibiotics has created medical needs for antibacterial therapy that remain unmet today[215]. It is broadly accepted that new-class agents represent unique and valuable opportunities to achieve significant advances against bacterial resistance, because they should not be as susceptible to preexisting mechanisms of resistance, as seen with established antibacterial classes[216].

One new strategy is the pursuit of novel compounds that target microbial signaling cascades that are relatively overlooked by traditional methods of antibiotic development. Protein phosphorylation by bacterial kinases is one such process that has been garnering attention within the past decade as a potential target for truly novel antibiotics[217].

Differently from eukaryotic kinases which have been widely studied as pharmaceutical target, prokaryotic protein kinases have just begun to be investigated as potentially novel antibiotic targets.

Since the discovery of protein kinase n1 (Pkn1), a bacterial serine/threonine kinase with high structural homology to eukaryotic protein kinases[218], genomic studies have shown eukaryotic-like serine/threonine kinases (eSTKs) to be near ubiquitous in bacteria[219].

Specifically, many important Gram positive pathogens have transmembrane eSTKs, the penicillin-binding protein and serine/threonine kinase-associated (PASTA) kinases which play central roles in processes ranging from metabolism and basic bacterial physiology to regulation of virulence and lactam antibiotic susceptibility. As such, efforts are being put to identify small molecule inhibitors of the PASTA kinases[220,221,222], which are of particular interest due to their role in regulating resistance to β-lactam antibiotics. Very recently, the Akt kinase inhibitor, GSK690693 **49**[223], and other imidazopyridine aminofurazan derivatives demonstrated to increase the sensitivity to lactams, in a dose-dependent manner, of the pathogen *Listeria monocytogenes various* by inhibiting the PASTA kinase PrkA[224].

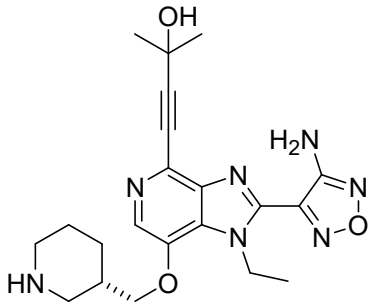

49, GSK690693

Besides the evident efforts in finding prokaryotic kinase inhibitors as possible new antibacterial agents, in literature are reported also a great number of pyrazolo[3,4-*d*]pyrimidine derivatives showing interesting activity against bacterial proliferation[225,226,227]. For example, in 2003, Ali A. *et al.* described how some pyrazolo[3,4-*d*]pyrimidin-4-ones **50** inhibit *Staphylococcus aureus* (*S. aureus*) DNA polymerase III and the growth of several other Gram positive bacteria in culture[228]. Later, other different compounds characterized by a pyrazolo[3,4-*d*]pyrimidine core have been reported to show an appreciable antibacterial activity[229]. However, the mechanism of action by which these compounds exert their antibacterial activity has not yet been clarified.

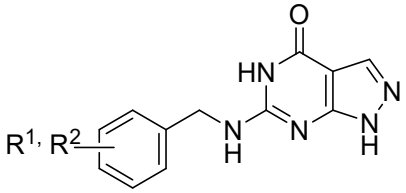

50

9.2 Project

In this context, we were interested in exploring possible antibacterial activity in our molecules, since they possess activity as kinase inhibitors and have a pyrazolo[3,4-*d*]pyrimidine structure. During my research period spent at the University of Nottingham, with the collaboration of Professor Alan Huett's research group of the Faculty of Medicine & Health Sciences, I had the opportunity to take this interesting challenge, by testing a set of our pyrazolo[3,4-*d*]pyrimidines on the Gram positive bacteria *S. aureus*, and the Gram negative bacteria *Escherichia coli* (*E. coli*). A representative number of pyrazolo[3,4-*d*]pyrimidines, presenting different substituents

in position N1, C4 and C6 (**Fig.37**) has been chosen to be evaluated as antibacterial agents, in order to obtain the widest information about the SAR.

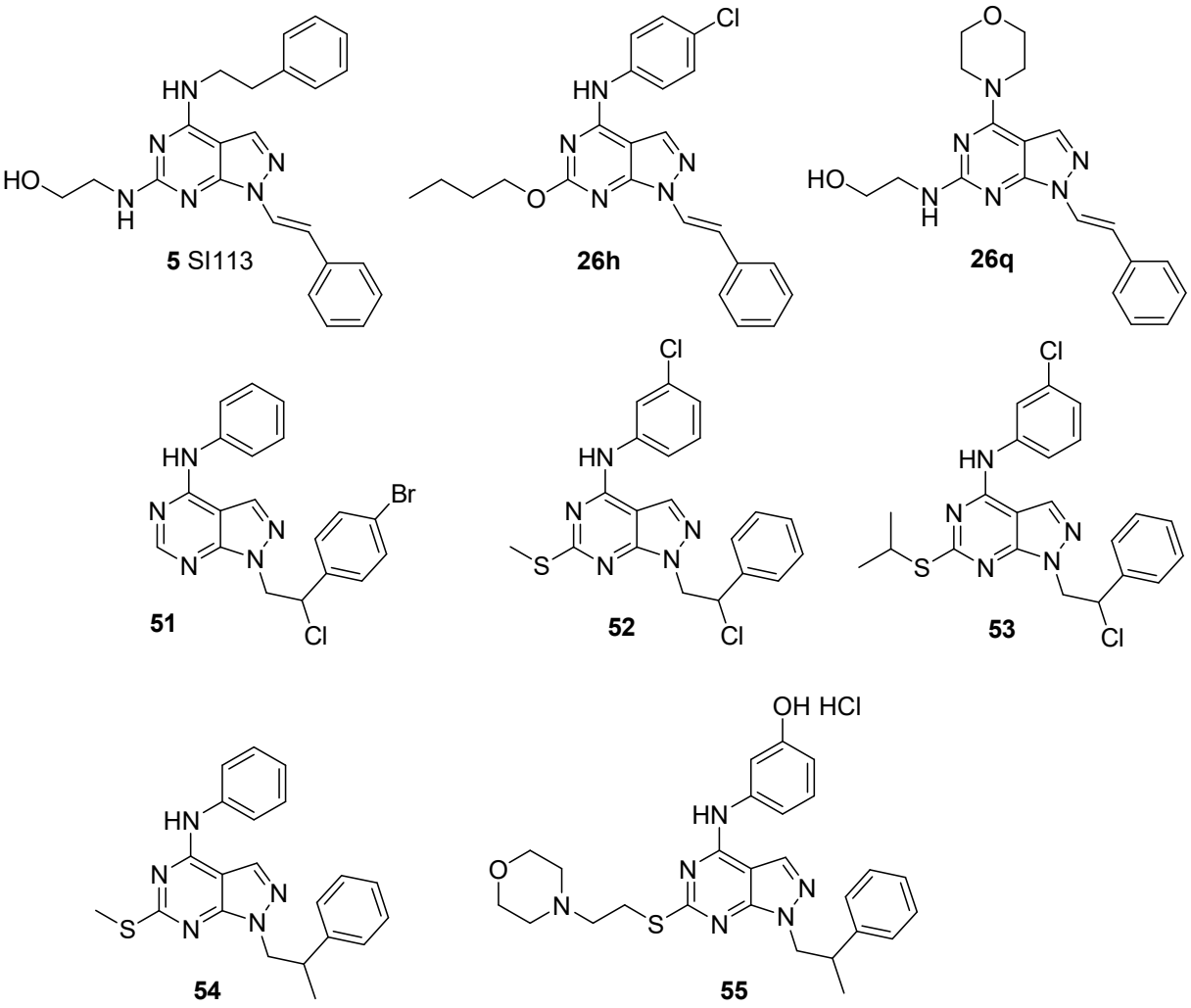

Fig.37. Structure of pyrazolo[3,4-*d*]pyrimidines tested on *S. aureus* and *E. coli.*

The first attempts allowed the identification of the most promising compounds that we subsequently chose for a deeper investigation in order to hypnotize a possible mechanism of action.

Inspired by research literature, we decided to try the combination with a well-known β-lactam antibiotic (ampicillin) to determine a variation on bacteria lactam sensitivity induced by a possible inhibition of the prokaryotic kinases PASTA. In fact, if our compounds inhibit the PASTA kinases, an enhancement of ampicillin activity should be observed.

To further validate our speculation, a combination with an antibiotic acting with a different mechanism, the aminoglycoside kanamycin which act by interfering with bacteria protein synthesis, has been included in the assays as the negative control.

9.3 Results and discussion

Initially the *in vitro* effects on *S. aureus* and on *E. coli* growth of the eight selected pyrazolo[3,4-*d*]pyrimidines has been evaluate at four different concentrations (200 µg/mL, 100 µg/mL, 50 µg/mL, 25 µg/mL). In this first attempt four compounds (SI113, **51**, **52**, **55**) have been individuated for their bacteriostatic activity, concentration dependent, as it is shown in graphs (**Fig.38**).

Interestingly, those compounds resulted more active on the Gram negative *E. coli*, leading to a remarkable decrease on bacteria growth. In particular, compound **52** was able to halve the bacterial growth of *E. coli* at the lowest concentration of 25 µg/mL. Regarding *S. aureus* the results are less exciting, but anyway the highest concentrations of all compounds showed a considerable effect on bacteria growth.

Another interesting fact to report is that among the most active compound tested, SI113 and **55** have been previously reported and studied for their anticancer activity *in vitro* and *in vivo*[92,40].

In this field is interesting to note that a possible antitumor/antibacterial dual activity of our kinase inhibitors could lead to multiple advantages such as a reduced drug administration in oncologic patients. In fact, bacterial infections during chemotherapy represent a serious complication for cancer patients which have lower resistance to infections[230].

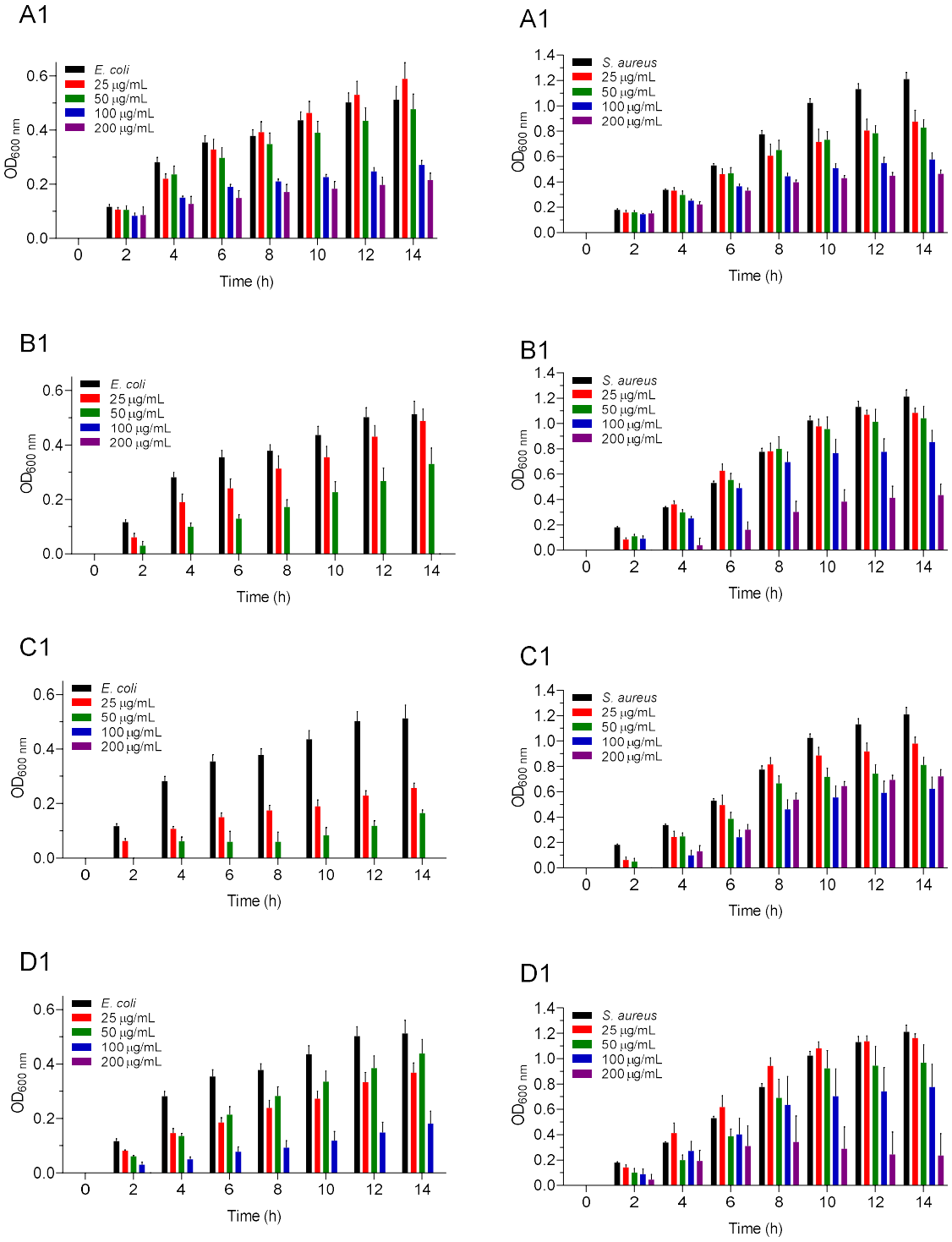

Fig.38. Dose-dependent growth inhibitions of *E. coli* XL-1 (left) and *S. aureus* Newman (right) in the presence of compound SI113 (A1), **51** (B1), **52** (C1) and **55** (D1) at increasing concentrations (25 µg/mL, 50 µg/mL, 100 µg/mL, 200 µg/mL). Error bars indicate S.E.M. OD: optical density.

Then, each compound has been tested at the two lowest concentrations in association whit 0.2 μg/mL of either ampicillin or kanamycin. Again, the best results were obtained in the assays performed on *E. coli*. as it is shown in graphs (**Fig.39**): all compounds were able to enhance the activity of both antibiotics even at the lowest concentrations. In particular, compounds **51**, **52** and **55** at 50 μg/mL, completely eradicate the bacteria *E. coli* in combination with kanamycin.
As already noted, the compounds are less potent on the Gram positive bacteria tested. However, the data reported do not allow a clear understanding of this result. Considering also that the concentration of ampicillin used for the experiment was high, this part of the work needs to be revisited.
The results obtained, showing more activity on Gram negative bacteria, and the positive results with the kanamycin combination, suggest that an antibiotic effect through the inhibition of PASTA kinases is probably unlikely. In any case, it is too early and the data are not complete enough to exclude the possibility of our compounds interacting with PASTA kinases.

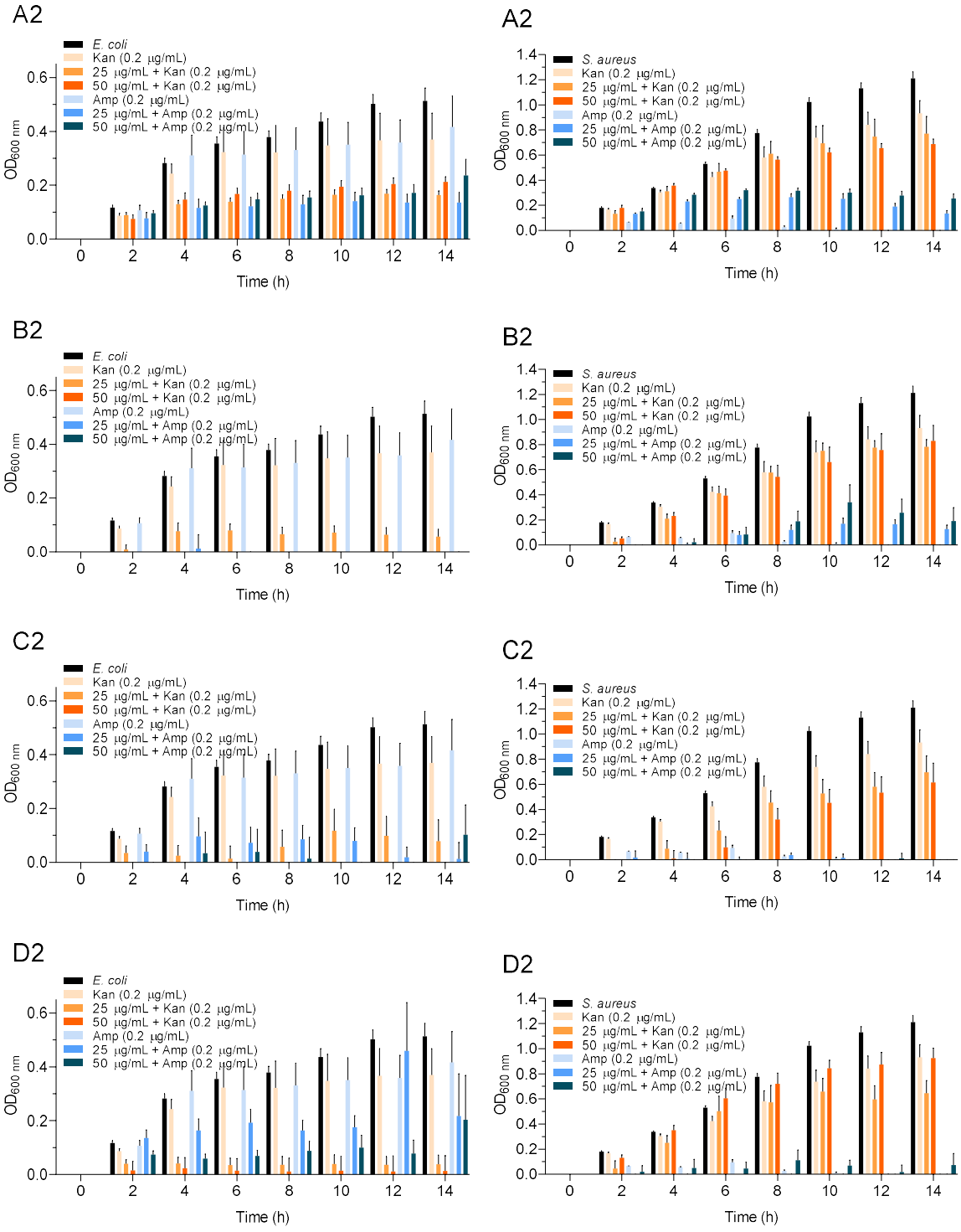

Fig.39. Dose-dependent growth inhibitions of *E. coli* XL-1 (left) and *S. aureus* Newman (right) in the presence of 0.2 μg/mL of kanamycin or ampicillin and increasing concentrations (25 μg/mL and 50 μg/mL) of compounds 113 (A2), **51** (B2), **52**(C2) and **55** (D2). Error bars indicate S.E.M. OD: optical density.

9.4 Materials and methods

Broth microdilution assays were performed according to the guidelines of the National Committee for Clinical Laboratory Standards (NCCLS), except that our drug stock solutions (20 mg/ml) were prepared in DMSO instead of in Mueller-Hinton broth (MHB).

Initially, the preinoculum of *E. coli* XL-1 and *S. aureus* Newman in Mueller-Hinton (MH) were grown at 37°C, shaking at 245 rpm for 12–14h; then the culture of each strain was adjusted appropriately by spectrophotometry at 600 nm to provide 105 colony-forming unit (CFU) ml^{-1} in fresh MH (2x); 100µl aliquots of these cell suspensions were mixed with 100 µl of drug solution in PBS at different drug concentrations (200 µg/mL, 100 µg/mL, 50 µg/mL, 25 µg/mL) in a 96 well plate and incubated at 37°C in an orbital shaker (245rpm for 14h). For the combination experiment, the procedure was the same except that 0.2 µg/mL of either kanamycin or ampicillin were added to the wells containing 25 and 50 µg/mL of each compound.

The growth kinetics of each microorganism was determined by triplicate measuring absorbance at 600nm in a Epoch 2 microplate reader (BioTek). The controls were (1) culture media, (2) culture media plus bacteria, (3) culture media plus bacteria with 2% of DMSO, (equivalent to the amount of DMSO in the 200 µg/ml concentration of drugs), (4) culture media plus 0.2 µg/mL of ampicillin, (5) culture media plus 0.2 µg/mL of kanamycin, (6) culture media plus bacteria and Gentamicin. Values given are averages from three independent cultures in triplicate ± S.E.M.

9.5 Conclusions

A preliminary study in antimicrobic context, performed on pyrazolo[3,4-*d*]pyrimidines active as kinase inhibitors and potential anticancer drugs, has been developed in collaboration with Professor Alan Huett's research group at the Faculty of Medicine & Health Sciences of Nottingham University.

Four pyrazolo[3,4-*d*]pyrimidines has been identified for their bacteriostatic activity in particular against the Gram negative bacteria *E. coli.* A subsequent study has allowed to highlight a favourable combination with kanamycin and ampicillin. In fact, the association with 0.2 µg/mL of antibiotics (which alone resulted not active) with 50 µg/mL of our compounds almost

completely eradicate *E. coli* growth. However, the limited amount of data collected from these preliminary experiments doesn't allow to establish neither a SAR evaluation nor a possible mechanism of actions. Nevertheless, we obtained promising results that needs to be further explored, with the aim to highlight a very useful dual activity of pyrazolo[3,4-*d*]pyrimidines in the context of bacterial infections in oncologic patients.

CHAPTER 10

Experimental section

Starting materials were purchased from Aldrich-Italia (Milan, Italy) and Alfa Aesar (Lancashire, UK). Melting points were determined with a Büchi 530 apparatus and are uncorrected. IR spectra were measured in KBr with a Perkin-Elmer 398 spectrophotometer. ^{1}H NMR spectra were recorded in a $(CD_3)_2SO$ or $CDCl_3$ solution on a Varian Gemini 200 (200 MHz) instrument. Chemical shifts are reported as δ (ppm) relative to TMS as the internal standard, J in Hz. ^{1}H patterns are described using the following abbreviations: s = singlet, d = doublet, t = triplet, q = quartet, quint = quintet, sex = sextet, m = multiplet, and br = broad. TLC was carried out using Merck TLC plates silica gel 60 F254. Chromatographic purifications were performed on columns packed with silica gel 60 Å, 220-440 mesh particle size, 35-75 μM, or using, for flash technique, the instrument Isolera™ One Biotage that works with cartridge Biotage® SNAP Ultra packed with Biotage® HP-Sphere™ spherical silica. Analyses for C, H, N, and S were effectuated with Thermo Scientific Flash 2000 within ± 0.4% of the theoretical value. All target compounds possessed a purity of ≥ 95% as verified by elemental analyses by comparison with the theoretical values.

General procedure for the synthesis of compounds 29a-d

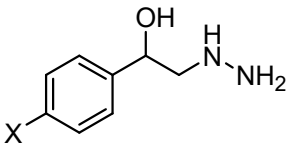

29a-d

29a: X = H
29b: X = F
29c: X = Cl
29d: X = Br

Styrene oxide or *para*-substitued styrene oxides **28a-d** (0.17 mol) were added to hydrazine monohydrate (30 mL, 0.60 mol) heated at 100 °C. The solutions were heated for 30 min at 100 °C and the excess of hydrazine was removed under reduced pressure. The obtained oils were purified by bulb to bulb distillation under high vacuum to obtain the pure products as pale yellow oils.

1-Hydrazino-2-phenylethanol 29a

Bp: 155-158 °C/0.6 mmHg.

Yield: 82%.

MW:152.19.

2-(4-Fluorophenyl)-1-hydrazinoethanol 29b

Bp: 175-178 °C/0.6 mmHg.

Yield: 85%.

MW: 170.18

2-(4-Clorophenyl)-1-hydrazinoethanol 29c

Bp: 170-175 °C/0.6 mmHg.

Yield: 80%.

MW: 186.64

2-(4-Bromophenyl)-1-hydrazinoethanol 29d

Bp: 175-180 °C/0.6 mmHg.

Yield: 60%.

MW: 231.09.

General procedure for the synthesis of compounds 30a-d

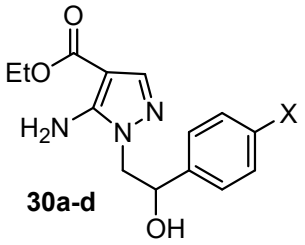

30a-d

30a: X = H
30b: X = F
30c: X = Cl
30d: X = Br

A solution of appropriate intermediates **29a-d** (122.5 mmol) and ethyl(ethoxymethylene)-cyanoacetate (20.40 g, 122.5 mmol) in anhydrous toluene (140 mL) was heated at 80 °C for 8 h. The solution was concentrated under reduced pressure to half of the volume and allowed to cool to room temperature. The yellow pale solids obtained were filtered and recrystallized from toluene to obtain the desired compounds **30a-d**.

Ethyl 5-amino-1-(2-phenylethyl)-1*H*-pyrazole-4-carboxylate 30a

Mp: 136-137 °C.

Yield: 54%.

MW: 275.30.

Anal. calcd. for $C_{14}H_{17}N_3O_3$: C 61.08, H 6.22, N 15.26; found C 61.07, H 6.22, N 15.31.

^{1}H NMR: δ 1.33 (t, *J* = 7.0 Hz, 3H, CH_3), 3.53 (br s, 1H, OH), 3.92-4.20 (m, 2H, CH_2N), 4.25 (q, *J* = 7.0 Hz, 2H, CH_2O), 5.02-5.13 (m, 1H, CHO), 5.30 (br s, 2H, NH_2), 7.23-7.42 (m, 5H Ar), 7.58 (s, 1H, H-3).

IR cm^{-1}: 3470-330 (NH_2), 3300-3000 (OH), 1685 (CO).

Ethyl 5-Amino-1-[2-(4-fluorophenyl)-2-hydroxyethyl]-1*H*-pyrazole-4-carboxylate 30b

Yield: 70%.

Mp: 163-164 °C.

MW: 293.29.

Anal. calcd. for $C_{14}H_{16}N_3O_3F$: C 57.33, H 5.50, N 14.33; found: C 57.31, H 5.31, N 14.25.

^{1}H NMR: δ 1.33 (t, *J* = 7.0 Hz, 3H, CH_3), 3.73 (br s, 1H, OH), 3.90-4.15 (m, 2H, CH_2N), 4.29 (q, J = 7.0 Hz, 2H, CH_2O), 5.01–5.18 (m, 1H, CHO), 5.36 (br s, 2H, NH_2), 7.03–7.40 (m, 4H Ar), 7.55 (s, 1H, H-3). IR cm^{-1}: 3448, 3446 (NH_2), 3300–3000 (OH), 1685 (CO).

Ethyl 5-amino-1-[2-(4-chlorophenyl)-2-hydroxyethyl]-1*H*-pyrazole-4-carboxylate 30c

Yield: 75%.

Mp: 168-169 °C.

MW: 309.75.

Anal. calcd. for $C_{14}H_{16}N_3O_3Cl$: C 54.29, H 5.21, N 13.57; found: C 54.27, H 5.16, N 13.48.

^{1}H NMR: δ 1.38 (t, *J* = 7.0 Hz, 3H, CH_3), 3.56 (br s, 1H, OH), 3.91-4.19 (m, 2H, CH_2N), 4.28 (q, *J* = 7.0 Hz, 2H, CH_2O), 5.05-5.18 (m, 1H, CHO), 5.33 (br s, 2H, NH_2), 7.25-7.46 (m, 4H Ar), 7.59 (s, 1H, H-3). IR cm^{-1}: 3412, 3291 (NH_2), 3219-3100 (OH), 1685 (CO).

Ethyl 5-amino-1-[2-(4-bromophenyl)-2-hydroxyethyl]-1*H*-pyrazole-4-carboxylate 30d

Yield: 65%.

Mp: 164-165 °C.

MW: 354.20.

Anal. calcd. for $C_{14}H_{16}N_3O_3Br$: C 47.47, H 4.55, N 11.87; found: C 47.55, H 4.75, N 12.03.

^{1}H NMR: δ 1.28 (t, *J* = 7.0 Hz, 3H, CH_3), 3.86-4.13 (m, 2H, CH_2N), 4.21 (q, *J* = 7.2 Hz, 2H, CH_2O), 5.03-5.12 (m, 1H, CHO), 7.15-7.24 and 7.37-7.47 (m, 4H Ar), 7.55 (s, 1H, H-3).

IR cm^{-1}: 3411, 3291 (NH2), 3157-2900 (OH), 1685 (CO).

General procedure for the synthesis of compounds 31a-d

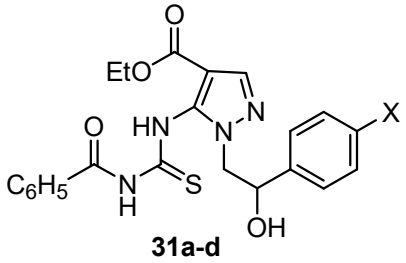

31a-d

31a: X = H
31b: X = F
31c: X = Cl
31d: X = Br

A solution of **30a-d** (15.0 mmol) and benzoyl isothiocyanate (2.2 mL, 16.5 mmol) in anhydrous THF (30 mL) was refluxed for 8 h. The solvent was evaporated under reduced pressure, and the crudes were crystallized as white solids by adding diethyl ether (30 mL). Compound **31c** was used as a crude in the subsequent step.

1-(2-Hydroxy-2-phenylethyl)-6-(methylthio)-1,5-dihydro-4*H*-pyrazolo[3,4-*d*]pyrimidin-4-one 31a

Mp: 170-172 °C.

Yield: 96 %.

MW: 438.50

Anal. calcd. for $C_{22}H_{22}N_4O_4S$: C 60.26, H 5.06, N 12.78, S 7.31; found: C 60.22, H 5.20, N 12.95, S 7.04.

^{1}H NMR: δ 1.29 (t, *J* = 7.0 Hz, 3H, CH_3), 3.97-4.20 (m, 5H, $2CH_2$ + OH), 4.58-4.68 (m, 1H, CHO), 7.05-7.98 (m, 10H Ar), 8.02 (s, 1H, H-3), 8.70 (s, 1H, NH), 12.05 (s, 1H, NH).

IR cm^{-1}: 3221 (NH), 3190-2940 (OH), 1708 (COOEt), 1671 (CO).

1-[2-(4-Fluorophenyl)-2-hydroxyethyl]-6-(methylthio)-1,5-dihydro-4*H*-pyrazolo[3,4-*d*]pyrimidin-4-one 31b

Mp: 129-130 °C.

Yield: 85%.

MW: 456.49.

Anal. calcd. for $C_{22}H_{21}N_4O_4SF$: C 57.88, H 4.64, N 12.27, S 7.02; found: C 57.99, H 4.70, N 12.41, S 7.19.

^{1}H NMR: δ 1.31 (t, *J* = 7.0 Hz, 3H, CH_3), 4.10-4.38 (m, 5H, $2CH_2$ + OH), 5.25-5.38 (m, 1H, CHO), 7.00-7.90 (m, 9H Ar), 8.05 (s, 1H, H-3), 9.36 (s, 1H, NH), 12.16 (s, 1H, NH).

IR cm^{-1}: 3444, 3261 (NH), 3190-2940 (OH), 1683 (CO).

1-[2-(4-Bromophenyl)-2-hydroxyethyl]-6-(methylthio)-1,5-dihydro-4*H*-pyrazolo[3,4-*d*]pyrimidin-4-one 31d

Mp: 159-161 °C.

Yield: 60%.

MW: 532.43.

Anal. calcd. for $C_{22}H_{21}N_4O_4SBr$: C 51.89, H 4.54, N 10.52, S 6.02; found: C 51.99, H 4.64, N 10.41, S 6.19.

^{1}H NMR: δ 1.35 (t, *J* = 7.0 Hz, 3H, CH_3), 4.26-4.40 (m, 5H, $2CH_2$ + OH), 5.20-5.30 (m, 1H, CHO), 7.30-7.98 (m, 9H Ar), 8.09 (s, 1H, H-3), 9.39 (s, 1H, NH), 12.15 (s, 1H, NH).

General procedure for the synthesis of compounds 32a-d

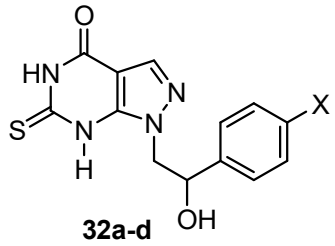

32a-d

32a: X = H
32b: X = F
32c: X = Cl
32d: X = Br

A solution of **31a-d** (14.0 mmol) in aqueous 2M NaOH (60 mL) was refluxed for 10 min and successively diluted with H_2O (40 mL). The solution was acidified with glacial acetic acid cooling with an ice bath. After 12 h of standing in a refrigerator, the crystallized solids were filtered and recrystallized from absolute ethanol to give white solids.

1-(2-Hydroxy-2-phenylethyl)-6-thinoxo-1,5,6,7-tetrahydro-4*H*-pyrazolo[3,4-*d*]pyrimidin-4-one 32a

Mp: 263-265 °C.

Yields: 63%.

MW: 288.32.

Anal. calcd. for $C_{13}H_{12}N_4O_2S$: C 54.15, H 4.20, N 19.43, S 11.12; found: C 54.28, H 4.27, N 19.70, S 11.03.

^{1}H NMR: δ 4.15-4.72 (m, 2H, CH_2N), 4.85-5.00 (m, 1H, CHO), 5.66 (br s, 1H, OH), 7.20-7.51 (m, 5H Ar), 8.02 (s, 1H, H-3), 12.20 (s, 1H, NH), 13.40 (s, 1H, NH).

IR cm^{-1}: 3362 (NH), 3142-2773 (OH), 1681 (CO).

1-[2-(4-Fluorophenyl)-2-hydroxyethyl]-6-thioxo-1,3a,5,6,7,7a-hexahydro-4*H*-pyrazolo[3,4-*d*]pyrimidin-4one 32b

Mp: 252-253 °C.

Yield: 75%.

MW: 306.17

Anal. calcd. for $C_{13}H_{11}N_4O_2SF$: C 50.97, H 3.62, N 18.29, S 10.47; found: C 51.08, H 4.00, N 18.12, S 10.22.

^{1}H NMR: δ 4.15-4.28 and 4.52-4.60 (2 m, 2H, CH_2N), 4.88-5.00 (m, 1H, CHO), 5.69 (s, 1H, OH), 7.12-7.29 and 7.40-7.52 (2m, 4H, Ar), 7.98 (s, 1H, H-3), 12.20 (s, 1H, NH), 13.36 (s, 1H, NH).

IR cm^{-1}: 3315, 3200 (NH), 3320, 2500 (OH), 1670 (CO).

1-[2-(4-Chlorophenyl)-2-hydroxyethyl]-6-thioxo-1,3a,5,6,7,7a-hexahydro-4*H*-pyrazolo[3,4-*d*]pyrimidin-4one 32c

Mp: 249-250 °C.

Yield: 70%.

MW: 322.81.

Anal. calcd. for $C_{13}H_{11}N_4ClO_2S$: C 48.37, H 3.44, N 17.36, S 9.55; found: C 48.12, H 3.23, N 17.55, S 9.87.

^{1}H NMR: δ 4.13-4.65 (m, 2H, CH_2N), 4.84-5.00 (m, 1H, CHO), 5.71 (br s, 1H, OH), 7.30-7.51 (m, 4H Ar), 7.97 (s, 1H, H-3), 12.19 (s, 1H, NH), 13.38 (s, 1H, NH).

IR cm^{-1}: 3390, 3220 (NH), 3100−2700 (OH), 1675 (CO).

1-[2-(4-Bromophenyl)-2-hydroxyethyl]-6-thioxo-1,3a,5,6,7,7a-hexahydro-4*H*-pyrazolo[3,4-*d*]pyrimidin-4-one 32d

Mp: 258-260 °C.

Yield: 60%.

MW: 369.27.

Anal. calcd. for $C_{13}H_{11}N_4BrO_2S$: C 42.29, H 3.55, N 15.16, S 8.65; found: C 42.12, H 3.23, N 15.55, S 9.17.

^{1}H NMR: δ 4.20-4.28 and 4.90-92 (2m, 2H, CH_2N), 4.58 (t, 1H, CHO), 5.73 (br s, 1H, OH), 7.39-7.59 (m, 4H, Ar), 7.99 (s, 1H, H-3), 12.23 (s, 1H, NH), 13.39 (s, 1H, NH).

General procedure for the synthesis of compounds 33a-d

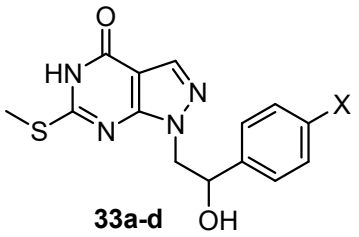

33a-d

33a: X = H
33b: X = F
33c: X = Cl
33d: X = Br

A solution of **32a-d** (6.9 mmol) and CH_3I (3.0 mL, 48.6 mmol) in anhydrous THF (150 mL) was refluxed for 12 h. The solvent was evaporated under reduced pressure, and the crudes were crystallized by adding diethyl ether (50 mL).

1-(2-Hydroxy-2-phenylethyl)-6-(methylsulfanyl)-1,5-dihydro-4*H*-pyrazolo[3,4-*d*]pyrimidin-4-one 33a

Mp: 208-209 °C.

Yield: 85 %.

MW: 302.35

Anal. calcd. for $C_{14}H_{14}N_4O_2S$: C 55.61, H 4.67, N 18.53, S 10.61; found: C 55.46, H 4.34, N 18.71, S 10.31.

^{1}H NMR: δ 2.52 (s, 3H, SCH_3), 4.27-4.50 (m, 2H, CH_2N), 5.04-5.18 (m, 1H, CHO), 5.68 (d, 1H, OH), 7.20-7.42 (m, 5H Ar), 7.97 (s, 1H, H-3).

IR cm^{-1}: 3544 (NH), 1678 (CO).

1-[2-(4-Fluorophenyl)-2-hydroxyethyl]-6-(methylsulfanyl)-1,5-dihydro-4*H*-pyrazolo[3,4-*d*]pyrimidin-4-one 33b

Mp: 217-218 °C.

Yield: 72%.

MW: 320.34.

Anal. calcd. for $C_{14}H_{13}N_4O_2SF$: C 52.49, H 4.09, N 17.49, S 10.01; found: C 52.19, H 4.29, N 17.31, S 9.85.

^{1}H NMR: δ 2.51 (s, 3H, CH_3S), 4.24-4.50 (m, 2H, CH_2N), 4.55 (br s, 1H, OH), 5.00-5.15 (m, 1H, CHO), 7.02-7.30 (m, 4H Ar), 7.96 (s, 1H, H-3), 12.33 (s, 1H, NH).

IR cm^{-1}: 3418 (NH), 3120-2850 (OH), 1668 (CO).

1-[2-(4-Chlorophenyl)-2-hydroxyethyl]-6-(methylsulfanyl)-1,5-dihydro-4*H*-pyrazolo[3,4-*d*]pyrimidin-4-one 33c

Mp: 210-211 °C.

Yield: 70%.

MW: 338.81.

Anal. calcd. for $C_{14}H_{13}N_4ClO_2$: C 49.93, H 3.9, N 16.69; found: C 49.68, H 4.03, N 16.51.

^{1}H NMR: δ 2.84 (s, 3H, CH_3S), 4.22−4.48 (m, 2H, CH_2N), 4.94−5.16 (m, 1H, CHO), 5.76 (d, 1H, OH), 7.07−7.22 (m, 4H Ar), 7.94 (s, 1H, H-3), 12.32 (s, 1H, NH).

IR cm^{-1}: 3427 (NH), 3120−2850 (OH), 1667 (CO).

1-[2-(4-Bromophenyl)-2-hydroxyethyl]-6-(methylsulfanyl)-1,5-dihydro-4*H*-pyrazolo[3,4-*d*]pyrimidin-4-one 33d

Mp: 214-216°C.

Yield: 50%.

MW: 381.25

Anal. calcd. for $C_{14}H_{13}N_4BrO_2S$: C 44.11, H 3.44, N 14.70, S 8.41; found: C 44.05, H 3.95, N 17.31, S 7.95.

^{1}H NMR, δ 2.50 (s, 3H, CH_3S), 4.32−4.42 (m, 2H, CH_2N), 5.05 (m, 1H, CHO), 5.76 (br s, 1H, OH), 7.17−7.49 (m, 4H Ar), 7.97 (s, 1H, H-3), 12.37 (s, 1H, NH).

General procedure for the synthesis of compounds 34a-d

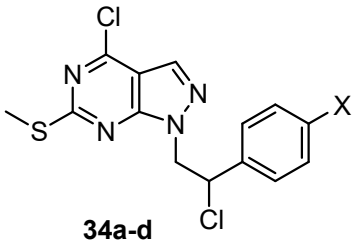

34a-d

34a: X = H
34b: X = F
34c: X = Cl
34d: X = Br

The Vilsmeier complex, previously prepared from $POCl_3$ (1.2 mL, 8.0 mmol) and anhydrous dimethylformamide (DMF) (1.1 mL, 8.0 mmol) was added to a suspension of **33a-d** (2.0 mmol) in $CHCl_3$ (15 mL). The mixture was refluxed for 8 h. The solution was washed with H_2O (2 × 20 mL), dried ($MgSO_4$), filtered, and concentrated under reduced pressure. The crude oils were purified by flash chromatography using the instrument Isolera™ One Biotage, (cartridge Biotage® SNAP Ultra packed with Biotage® HP-Sphere™), using a mixture of petroleum ether (bp 40-60 °C)/diethyl ether (9:1) as the eluant, to afford the pure products as white solids.

4-Chloro-1-(2-chloro-2-phenylethyl)-6-(methylthio)-1*H*-pyrazolo[3,4-*d*]pyrimidine 34a

Mp: 95-96 °C.

Yield: 88%.

MW: 339.24.

Anal. calcd. for $C_{14}H_{12}N_4SCl_2$: C 49.57, H 3.57, N 16.52, S 9.45; found: C 49.92, H 3.44, N 16.89, S 9.40.

^{1}H NMR: δ 2.62 (s, 3H, CH_3S), 4.77-5.05 (m, 2H, CH_2N), 5.45-5.56 (m, 1H, CHCl), 7.29-7.46 (m, 5H Ar), 8.02 (s, 1H, H-3).

4-Chloro-1-[2-chloro-2-(4-fluorophenyl)ethyl]-6-(methylthio)-1*H*-pyrazolo[3,4-*d*]pyrimidine 34b

Mp:136-137°C.

Yield:70%.

MW: 357.23

Anal. calcd. for $C_{14}H_{11}N_4Cl_2FS$: C 47.07, H 3.10, N 15.68, S 8.98; found: C 47.17, H 3.35, N 15.50, S 8.69.

^{1}HNMR: δ 2.65 (s, 3H, CH_3S), 4.74-5.03 (m, 2H, CH_2N), 5.42-5.54 (m, 1H, CHCl), 6.96-7.08 and 7.29-7.44 (2 m, 4H, Ar), 8.03 (s, 1H, H-3).

4-Chloro-1-[2-chloro-2-(4-chlorophenyl)ethyl]-6-(methylthio)-1*H*-pyrazolo[3,4-*d*]pyrimidine 34c

Mp: 142−143 °C.

Yield: 60%.

MW:373.69.

Anal. calcd. for $C_{14}H_{11}N_4Cl_3S$: C 45.55, H 2.97, N 14.99, S 8.58; found: C 44.99, H 3.21, N 14.82, S 8.45.

^{1}H NMR: δ 2.63 (s, 3H, CH_3S), 4.79−5.00 (m, 2H, CH_2N), 5.42−5.53 (m, 1H, CHCl), 7.25−7.42 (m, 4H Ar), 8.05 (s, 1H, H-3).

4-Chloro-1-[2-chloro-2-(4-bromophenyl)ethyl]-6-(methylthio)-1*H*-pyrazolo[3,4-*d*]pyrimidine 34d

Mp: 123-125°C.

Yield: 55%.

MW: 420.15.

Anal. calcd. for $C_{14}H_{11}N_4Cl_2BrS$: C 40.02, H 3.12, N 13.34, S 7.63; found: C 40.99, H 3.21, N 14.02, S 8.45.

^{1}H NMR: δ 2.50 (s, 3H, CH_3S), 4.04−4.53 (m, 2H, CH_2N), 5.69−5.73 (m, 1H, CHCl), 7.15−7.52 (m, 4H, Ar), 8.10 (s, 1H, H-3).

General procedure for the synthesis of compounds 35a,b,d,h

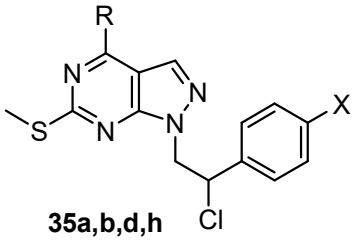

35a,b,d,h

35a: X = H, R = $NHCH_2CH_2C_6H_5$
35b: X = H, R = $NHCH_2C_6H_4$-4Cl
35d: X = F, R = $NHCH_2C_6H_4$-3F
35h: X = H, R = 4-morpholinyl

The appropriate amine (12.0 mmol) was added to a solution of **34a**,**b** (3.0 mmol) in anhydrous toluene (10 mL), and the reaction mixture was stirred at room temperature for 24 h. Water (50 mL) was added and the mixture was extracted with toluene (3 x 40 mL). Then the organic phase was washed with brine (50 mL), dried ($MgSO_4$) and evaporated under reduced pressure. To obtain pure compounds **35a,b,h** the crudes were purified by column chromatography (silica gel, 200-425 mesh), using a mixture of diethyl ether/petroleum ether (bp 40−60 °C) (3:7) as the eluant.

To obtain the desired product **35d,** the residue oil was crystallized by adding petroleum ether (bp 40-60 °C) (10 mL).

1-(2-Chloro-2-phenylethyl)-6-(methylthio)-N-(2-phenylethyl)-1*H*-pyrazolo[3,4-*d*]pyrimidin-4-amine 35a

Mp: 73-74°C.

Yield: 78%.

MW: 423.96.

Anal. calcd. for $C_{22}H_{22}N_5SCl$: C 62.33, H 5.23, N 16.52, S 7.56; found: C 62.40, H 5.24, N 16.40, S 7.43.

^{1}H NMR: δ 2.59 (s, 3H, CH_3), 2.98 (q, *J* = 6.0, 2H, CH_2Ar), 3.87 (q, *J* = 6.0, 2H, $\underline{CH_2}NH$), 4.70-4.95 (m, 2H, CH_2N), 5.30 (br s, 1H, NH, disappears with D_2O), 5.50-5.60 (m, 1H, CHCl), 7.19-7.48 (m, 10H Ar), 7.73 (s, 1H, H-3).

IR cm^{-1}: 3445 (NH).

N-(4-chlorobenzyl)-1-(2-chloro-2-phenylethyl)-6-(methylthio)-1*H*-pyrazol[3,4-*d*]pyrimidin-4-amine 35b

Mp: 126-127°C.

Yield: 75 %.

MW: 444.38.

Anal. calcd. for $C_{21}H_{19}N_5SCl_2$: C 56.76, H 4.31, N 15.76, S 7.22; found: C 56.81, H 4.45, N 16.40, S 7.29.

^{1}H NMR: δ 2.51 (s, 3H, CH_3S), 4.62-4.87 (m, 4H, CH_2N +CH_2Ar), 5.40-5.52 (m, 1H, CHCl), 7.09-7.48 (m, 9H Ar), 7.65 (s, 1H, H-3).

IR cm^{-1}: 3240 (NH).

1-[2-Chloro-2-(4-fluorophenyl)ethyl]-N-(3-fluorobenzyl)-6-(methylsulfanyl)-1*H*-pyrazolo[3,4-*d*]pyrimidin-4-amine 35d

Mp: 119-121 °C.

Yield: 68%.

MW: 445.91.

Anal. calcd. for $C_{21}H_{18}F_2N_5S$: C 56.56, H 4.07, N 15.71, S 7.19; found: C 56.67, H 4.35, N 15.58, S 6.00.

^{1}H NMR: δ 2.59 (s, 3H, CH_3S), 4.05-4.54 (m, 4H, CH_2N + CH_2Ar), 5.05-5.28 (m, 1H, CHCl), 7.65-7.83 (m, 8H Ar), 8.30 (s, 1H, H-3).

1-(2-Chloro-2-phenylethyl)-6-(methylthio)-4-morpholin-4-yl-1*H*-pyrazolo[3,4-*d*]pyrimidine 35h

Mp: 116-117 °C.

Yield: 75%.

MW: 389.90.

Anal. calcd. for $C_{18}H_{20}N_5OSCl$: C 55.45, H 5.17, N 17.96, S 8.22; found: C 55.48, H 5.32, N 18.19, S 8.09.

^{1}H NMR: δ 2.57 (s, 3H, CH_3), 3.77-3.87 and 3.89-3.98 (2m, 8H, 4CH_2morph.), 4.71-4.98 (m, 2H, CH_2N), 5.51-5.61 (m, 1H, CHCl), 7.26-7.49 (m, 5H Ar), 7.82 (s, 1H, H-3).

General procedure for the synthesis of compounds 35c,e-g

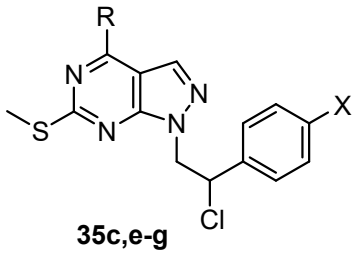

35c,e-g

35c: X = H, R = NHC_6H_4-4Cl
35e: X = F, R = NHC_6H_6
35f: X = Cl, R = NHC_6H_4-3Cl
35g: X = Br, R = NHC_6H_4-3Cl

The suitable aniline (1.3 mmol) was slowly added to a suspension of **34a-d** (0.9 mmol) in absolute ethanol (6.5 mL) and the mixture was refluxed for 5 h. The solution was washed with NaOH 1M (7 mL), H_2O (2 x 15 mL), dried ($MgSO_4$), filtered, and concentrated under reduced pressure. Compounds **35c**,**e-g** were crystallized with petroleum ether (bp 40-60 °C)/diethyl ether (1:1) and a solid was obtained. Then, compounds **35c**,**e-g** were purified by column chromatography (silica gel, 100 mesh) using DCM/n-hexane (9:1) as the eluant, to afford the pure products as white solids.

***N*-(4-chlorophenyl)-1-(2-chloro-2-phenylethyl)-6-(methylsulfanyl)-1*H*-pyrazolo[3,4-*d*]pyrimidin-4-amine 35c**

Mp: 226-228 °C.

Yield: 75 %.

MW: 430.35

Anal. calcd. for $C_{20}H_{17}Cl_2N_5S$: C 55.82, H 3.98, N 16.27, S 7.45 found: C 55.98, H 4.16, N 16.18, S 7.26.

^{1}H NMR: δ 2.42 (s, 3H, CH_3), 4.62-4.84 (m, 2H, CH_2N), 5.54-5.68 (m, 1H, CHCl), 7.03-8.12 (m, 9H Ar), 8.16 (s, 1H, H-3), 10.16 (s, 1H, NH).

1-[2-Chloro-2-(4-fluorophenyl)ethyl]-*N*-phenyl-6-(methylsulfanyl)-1*H*-pyrazolo[3,4-*d*]pyrimidin-4-amine 35e

Mp: 69-72 °C.

Yield: 60%.

MW: 413.90.

Anal. calcd. for $C_{20}H_{17}N_5ClFS$: C 58.04, H 4.14, N 16.92, S 7.75; found: C 57.93, H 4.40, N 16.53, S 6.53.

^{1}H NMR: δ 2.54 (s, 3H, CH_3S), 4.63-5.05 (m, 2H, CH_2N), 5.75 (t, 1H, CHCl), 7.13-7.81 (m, 9H, 9 Ar), 8.10 (s, 1H, H-3), 10.16 (s, 1H, NH).

1-[2-Chloro-2-(4-chlorophenyl)ethyl]-*N*-(3-chlorophenyl)-6-(methylsulfanyl)-1*H*-pyrazolo[3,4-*d*]pyrimidin4-amine 35f

Mp: 254-255 °C.

Yield: 78%.

MW: 464.80.

Anal. calcd. for $C_{20}H_{16}Cl_3N_5S$: C 51.68, H 3.47, N 15.07, S 6.90, found: C 51.52, H 3.51, N 15.02, S 7.01.

^{1}H NMR: δ 2.54 (s, 3H, SCH_3), 4.63-4.84 (m, 2H, CH_2N), 5.30-5.50 (m, 1H, CHCl), 6.79-7.51 (m, 9H, 8 Ar + H-3).

1-[2-(4-Bromophenyl)-2-chloroethyl]-*N*-(3-chlorophenyl)-6-(methylsulfanyl)-1*H*-pyrazolo[3,4-*d*]pyrimidin4-amine 35g

Mp: 203-205 °C.

Yield: 60%.

MW: 509.25.

Anal. calcd. for $C_{20}H_{16}BrCl_2N_5S$: C 47.17, H 3.17, N 13.75, S 6.30; found: C 47.28, H 3.50, N 13.38, S 6.01.

^{1}H NMR: δ 2.57 (s, 3H, SCH_3), 4.70-4.89(m, 2H, CH_2N), 5.38-5.50 (m, 1H, CHCl), 7.09-7.81 (m, 8H, 8 Ar), 8,08 (s,1H, H-3).

General procedure for the synthesis of compounds 27a-h

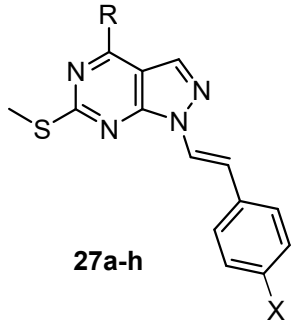

27a-h

27a: X = H, R = $NHCH_2CH_2C_6H_5$
27b: X = H, R = $NHCH_2C_6H_4$-4Cl
27c: X = H, R = NHC_6H_4-4Cl
27d: X = F, R = $NHCH_2C_6H_4$-3F
27e: X = F, R = NHC_6H_6
27f: X = Cl, R = NHC_6H_4-3Cl
27g: X = Br, R = NHC_6H_4-3Cl
27h: X = H, R = 4-morpholinyl

A solution of NaOH (0.28 g, 7.0 mmol) in water (2.1 mL) was added to a suspension of **35a-h** (0.9 mmol) in 95% ethanol (10 mL) and the mixture was refluxed for 5 h. After cooling, a white solid crystallized, then it was filtered and recrystallized from absolute ethanol to give a white solid.

6-(Methylthio)-*N*-(2-phenyletheyl)-1-(2-phenylvinyl)-1*H*-pyrazolo[3,4-*d*]pyrimidin-4-amine 27a

Mp: 121-122 °C.

Yields: 65%.

MW: 387.50.

Anal. calcd. for $C_{22}H_{21}N_5S$: C 68.19, H 5.46, N 18.07, S 8.28; found: C 68.42, H 5.24, N 18.09, S 8.00.

^{1}H NMR: δ 2.68 (s, 3H, CH_3S), 3.04 (t, 2H, CH_2Ar), 3.91 (q, 2H, CH_2N), 5.50 (br s, 1H, NH), 7.23-7.55 (m, 11H, 10H Ar + =CHAr), 7.85 (s, 1H, H-3), 7.99 (d, J_{trans} = 14.6, 1H, NCH=).

IR cm^{-1}: 3232 (NH), 1659 (C=C).

***N*-(4-Chlorobenzyl)-6-(methylthio)-1-[2-phenylvinyl]-1*H*-pyrazolo[3,4-*d*]pyrimidin-4-amine 27b**

Mp: 165-167 °C.

Yields: 94%.

MW: 407.92.

Anal. calcd. for $C_{21}H_{18}N_5SCl$: C 62.33, H 5.23, N 16.52, S 7.56; found: C 62.29, H 5.03, N 16.78, S 7.80.

^{1}H NMR: δ 2.65 (s, 3H, SCH_3), 4.85 (d, *J*= 8.0, 2H, $NHCH_2$), 7.34-7.44 and 7.50-7.55 (2m, 10H, 9H Ar + =CHAr), 7.92 (d, *J* = 8.8, 1H, NCH=), 8.00 (s, 1H, H-3).

_N_-(4-Chlorophenyl)-6-(methylthio)-1-[2-phenylvinyl]-1_H_-pyrazolo[3,4-_d_]pyrimidin-4-amine 27c

Mp: 121-123 °C.

Yields: 71%.

MW: 393.89.

Anal. calcd. for $C_{20}H_{16}ClN_5S$: C 60.98, H 4.09, N 17.78, S 8.14; found: C 60.74, H 4.00, N 17.59, S 6.22.

^{1}H NMR: δ 2.60 (s, 3H, SCH_3), 7.38-7.82 (m, 10H, 9H Ar + =CHAr), 8.00 (d, 1H, J_{trans} = 13.8 Hz, NCH=), 8.30 (s, 1H, H-3), 10.32 (br s, 1H, NH).

_N_-(3-Fluorobenzyl)-1-[2-(4-fluorophenyl)ethenyl]-6-(methylsulfanyl)-1_H_-pyrazolo[3,4-_d_]pyrimidin-4-amine 27d

Mp: 168-170 °C.

Yield: 73%.

MW: 409.45.

Anal. calcd. for $C_{21}H_{17}F_2N_5S$: C 61.60, H 4.18, N 17.10, S 7.83, found: C 61.50, H 4.49, N 17.40, S 6.70.

^{1}H NMR: δ 2.64 (s, 3H, SCH_3), 4.86 (d, *J* = 8.0 Hz, 2H, $NHCH_2$), 7.03-7.51 (m, 10H, 8H Ar + CH=CH), 7.93 (s, 1H, H-3).

_N_-Phenyl-1-[2-(4-fluorophenyl)ethenyl]-6-(methylsulfanyl)-1_H_-pyrazolo[3,4-_d_]pyrimidin-4-amine 27e

Mp: 187-190 °C.

Yield: 73%.

MW: 377.44.

Anal. calcd. for $C_{20}H_{16}FN_5S$: C 63.64, H 4.27, N 18.55, S 8.50, found: C 63.41, H 3.95, N 18.51, S 9.07.

^{1}H NMR: δ 2.67 (s, 3H, SCH_3), 6.99-7.52 (m, 11H, 9H Ar + CH=CH), 7.80 (s, 1H, H-3), 7.97 (s, 1H, NH).

_N_-(3-Chlorophenyl)-1-[(_E_)-2-(4-chlorophenyl)ethenyl]-6-(methylsulfanyl)-1_H_-pyrazolo[3,4-_d_]pyrimidin-4-amine 27f

Mp: 176-179 °C.

Yield: 70 %.

MW: 428.34.

Anal. calcd. for $C_{20}H_{15}Cl_2N_5S$: C 55.82, H 3.98, N 16.27, S 7.45; found: C 55.96, H 4.16, N 16.28, S 7.29.

^{1}H NMR: δ 2.69 (s, 3H, SCH_3), 7.28-7.43 (m, 8H, 7H Ar + =CHAr), 7.59 (s,1H, Ar), 7.70 (s, 1H, H-3), 7.90 (d, 1H, J_{trans} = 16 Hz, NCH=).

_N_-(3-Chlorophenyl)-1-[(_E_)-2-(4-bromophenyl)ethenyl]-6-(methylsulfanyl)-1_H_-pyrazolo[3,4-_d_]pyrimidin-4-amine 27g

Mp: 197-200 °C.

Yield: 40%.

MW: 472.79.

Anal. calcd. for $C_{20}H_{15}BrClN_5S$: C 50.81, H 3.20, N 14.81, S 6.75; found: C 50.84, H 3.52, N 14.53, S 5.00.

^{1}H NMR: δ 2.68(s, 3H, SCH_3), 7.29-7.47 (m, 9H, 8H Ar + =CHAr), 7.78 (s, 1H, H-3), 7.90 (d, 1H, J_{trans} = 16 Hz, NCH=).

6-(Methylthio)-4-morpholin-4-yl-1-(-2-phenylvinyl)-1_H_-pyrazolo[3,4-_d_]pyrimidine 27h

Mp: 161-162 °C.

Yield: 75%.

MW: 353.44.

Anal. calcd. for $C_{18}H_{19}N_5OS$: C 61.17, H 5.42, N 19.81, S 9.07; found: C 61.25, H 5.48, N 19.81, S 8.88.

^{1}H-NMR: δ 2.63 (s, 3H, CH_3S), 3.80-3.89 and 3.91-3.99 (2m, 8H, $4CH_2$ morph.), 7.21-7.55 (m, 6H, 5H Ar + CH=), 7.95 (s, 1H, H-3), 8.01 (d, J_{trans} = 14.6, 1H, NCH=).

IR cm^{-1}: 1658 (C=C).

General procedure for the synthesis of compounds 36a-h

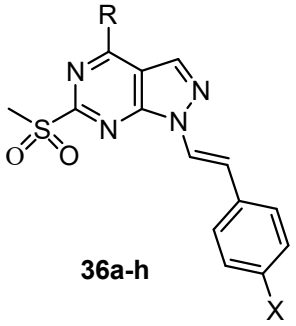

36a-h

36a: X = H, R = $NHCH_2CH_2C_6H_5$
36b: X = H, R = $NHCH_2C_6H_4$-4Cl
36c: X = H, R = NHC_6H_4-4Cl
36d: X = F, R = $NHCH_2C_6H_4$-3F
36e: X = F, R = NHC_6H_6
36f: X = Cl, R = NHC_6H_4-3Cl
36g: X = Br, R = NHC_6H_4-3Cl
36h: X = H, R = 4-morpholinyl

meta-Chloroperoxybenzoic acid 77% suspension in mineral oil (475 mg, 2.1 mmol) was added portion-wise to a suspension of **35a-h** (1.1 mmol) in anhydrous $CHCl_3$ (10 mL) at 0 °C. Then the mixture was stirred at room temperature for 6 h. The solvent was evaporated under reduced pressure and a solid was formed. The solution was washed with $NaHCO_3$ 1M (30 mL) till obtain a pH ~9, H_2O (2 x 15 mL), dried ($MgSO_4$), filtered, and concentrated under reduced pressure. Compounds **36a-d** and **36h** were purified by column chromatography (silica gel, 100 mesh) using ethyl acetate/n-hexane (7:3) as the eluant, to afford the pure products as white solids. Compounds **36e-g** because of their low solubility, were not purified and were used as a crude in the subsequent step.

6-(Methylsulfonyl)-*N*-(2-phenylethyl)-1-(2-phenylvinyl)-1*H*-pyrazolo-[3,4-*d*]pyrimidin-4-amine 36a

Mp: 138-139 °C.

Yield: 57%.

MW: 419.50.

Anal. calcd. for $C_{22}H_{21}N_5O_2S$: C 62.99, H 5.05, N 16.69, S 7.64; found: C 63.00, H 5.01, N 16.72, S 7.72.

^{1}H NMR: δ 3.05 (t, J = 6.0, 2H, CH_2Ar), 3.40 (s, 3H, SO_2CH_3), 3.98 (q, J = 6.0, 2H, $\underline{CH_2}NH$), 6.18 (br s, 1H, NH), 7.18-7.57 (m, 11H, 10Ar + =CHAr), 8.02 (d, J_{trans} = 14.4, 1H, NCH=), 8.13 (s, 1H, H-3).

IR cm^{-1}: 3348 (NH), 1713 (C=C), 1298, 1127 (SO_2).

_N_-(4-Chlorobenzyl)-6-(methylsulfonyl)-1-[2-phenylvinyl]-1_H_-pyrazolo[3,4-_d_]pyrimidin-4-amine 36b

Mp: 194-197 °C.

Yield: 28%.

MW: 439.92.

Anal. calcd. for $C_{21}H_{18}N_5O_2SCl$: C 57.33, H 4.12, N 15.92, S 7.29; found: C 57.33, H 4.07, N 15.68, S 6.80.

^{1}H NMR: δ 3.41 (s, 3H, SO_2CH_3), 4.81 (d, J = 5.4 Hz, 2H, CH_2), 7.36-7.46 and 7.64-7.70 (2m, 9H, Ar), 8.08 (d, J_{trans} = 16.5, 1H, NCH=), 8.50 (s, 1H, H-3), 9.73 (br s, 1H, NH).

_N_-(4-Chlorophenyl)-6-(methylsulfonyl)-1-[2-phenylvinyl]-1_H_-pyrazolo[3,4-_d_]pyrimidin-4-amine 36c

Mp: 225-227 °C.

Yield: 57%.

MW: 425.89

Anal. calcd. for $C_{20}H_{16}ClN_5O_2S$: C 56.40, H 3.79, N 16.44, S 7.53; found: C 56.52, H 3.88, N 16.27, S 6.23.

^{1}H NMR: δ 3.48 (s, 3H, SO_2CH_3), 7.23-7.90 (m, 10H, 9Ar + =CHAr), 7.96 (s, 1H, H-3), 8.10 (d, 1H, J_{trans} = 16 Hz, NCH=), 10.89 (s, 1H, NH).

_N_-(3-Fluorobenzyl)-1-[2-(4-fluorophenyl)ethenyl]-6-(methylsulfonyl)-1_H_-pyrazolo[3,4-_d_]pyrimidin-4-amine 36d

Mp: 215-218 °C.

Yield: 73%.

MW: 441.45

Anal. calcd. for $C_{21}H_{17}F_2N_5O_2S$: C 57.14, H 3.88, N 15.86, S 7.26; found: C 57.42, H 3.90, N 16.00, S 6.58.

^{1}H NMR: δ 3.40 (s, 3H, SO_2CH_3), 4.83 (d, 2H, J = 8 Hz, CH_2NH), 7.19-7.73 (m, 9H, 8Ar + =CHAr), 8.05 (d, 1H, J_{trans} = 16 Hz, NCH=), 8.48(s, 1H, H-3), 9.70 (s , 1H, NH).

6-(Methylsulfonyl)-4-morpholin-4-yl-1-(2-phenylvinyl)-1_H_-pyrazolo[3,4-_d_]pyrimidine 36h

Mp: 215-216 °C.

Yield: 87%.

MW: 385.44.

Anal. calcd. for $C_{18}H_{19}N_5O_3S$: C 56.09, H 4.97, N 18.17, S 8.32; found: C 56.25, H 5.07, N 17.86, S 8.64.

^{1}H NMR: 3.41 (s, 3H, SO_2CH_3), 3.86-3.97 and 4.02-4.16 (2m, 8H, $4CH_2$ morph.), 7.27-7.59 (m, 6H, 5Ar + =CHAr), 8.04 (d, J_{trans} = 14.4, 1H, NCH=), 8.16 (s, 1H, H-3).

IR cm^{-1}: 1658 (C=C), 1315, 1128 (SO_2).

General procedure for the synthesis of compounds SI113 and 26f,i,k,n,p,q

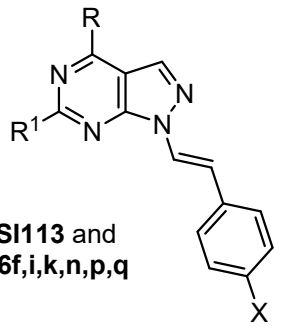

SI113 and **26f,i,k,n,p,q**

SI113: X = H, R = $NHCH_2CH_2C_6H_5$, R^1 = $NHCH_2CH_2OH$
26f: X = H, R = $NHCH_2C_6H_4$-4Cl, R^1 = $NHCH_2CH_2OH$
26i: X = H, R = NHC_6H_4-4Cl, R^1 = $NHCH_2CH_2OH$
26k: X = F, R = $NHCH_2C_6H_4$-3F, R^1 = $NHCH_2CH_2OH$
26n: X = Cl, R = NHC_6H_4-3Cl, R^1 = $NHCH_2CH_2OH$
26p: X = Br, R = NHC_6H_4-3Cl, R^1 = $NHCH_2CH_2OH$
26q: X = H, R = 4-morpholinyl, R^1 = $NHCH_2CH_2OH$

2-Amminoethanol (0.2 mL, 1.05 mmol) was added to a suspension of **36a-d** and **36f-h** (0.35 mmol) in butanol (5.6 mL) and DMSO (1.4 mL) and the mixture was heated at 90 °C for 12 h. The solvent was evaporated under reduced pressure. The solution was washed with water (2 x 15 mL), dried ($MgSO_4$), filtered, and concentrated under reduced pressure. The crude brown oils were purified by column chromatography (silica gel, 100 mesh) using ethyl acetate/n-hexane (1:1) as the eluant, to afford the pure products as white solids.

2-({4-[(2-Phenylethyl)amino]-1-(2-phenylvinyl)-1*H*-pyrazolo[3,4-*d*]pyrimidin-6-yl}-amino)ethanol SI113

Yield: 65%.

Mp: 83-84 °C.

MW: 400.48

Anal. calcd. for $C_{23}H_{24}N_6O$: C 68.98, H 6.04, N 20.99; found C 68.78, H 6.29, N 20.79.

^{1}H NMR: δ 2.99 (t, J = 7.0 Hz, 2H, CH_2Ar), 3.62-3.96 (m, 6H, $\underline{CH_2}NH$ + $NH\underline{CH_2}\underline{CH_2}OH$), 5.40 (br s, 1H, OH disappears with D_2O), 5.61 (br s, 1H, disappears with D_2O), 7.18-7.44 (m, 11H, 10H Ar + =CHAr), 7.75 (s, 1H, H-3), 7.82 (d, J_{trans} = 14.4 Hz, 1H, NCH=).
IR cm^{-1}: 3250-3150 (OH + NH), 1656 (C=C).

2-({4-[(4-Chlorobenzyl)amino]-1-[(*E*)-2-phenylvinyl]-1*H*-pyrazolo[3,4-*d*]pyrimidin-6-yl}amino)ethanol 26f

Mp: 150-152 °C.

Yield: 30 %.

MW: 420.89.

Anal. calcd. for $C_{22}H_{21}N_6OCl$: C 62.78, H 5.03, N 19.97; found: C 62.65, H 5.36, N 19.77.

^{1}H NMR: δ 3.30-3.50 (m, 4H, $NH\underline{CH_2}\underline{CH_2}OH$), 4.68 (d, J = 5.2 Hz, 2H, CH_2Ar), 7.16-7.40 and 7.42-7.59 (2m, 9H, Ar), 7.84 (d, J_{trans} = 17.6 Hz, 1H, NCH=), 8.15 (s, 1H, H-3), 8,50 (s, 1H, NH).

2-({4-[(4-Chlorophenyl)amino]-1-[2-phenylvinyl]-1*H*-pyrazolo[3,4-*d*]pyrimidin-6-yl}amino)ethanol 26i

Mp: 207-210 °C.

Yield: 57%.

MW: 406.87.

Anal. calcd. for $C_{21}H_{19}ClN_6O$: C 61.99, H 4.71, N 20.66; found: C 61.90, H 4.70, N, 20.31.

^{1}H NMR: δ 3.45-3.50 (m, 2H, $\underline{CH_2}NH$), 3.61-3.64 (m, 2H, $\underline{CH_2}OH$), 4.74 (s, 1H, OH), 7.26-7.82 (m, 9H, Ar), 7.92-7.98 (m, 2H, CH=CH), 8.25 (s, 1H, H-3), 9.80 (s, 1H, NH).

2-({4-[(3-Fluorophenyl)benzilamino]-1-[2-(4-fluorophenyl)vinyl]-1*H*-pyrazolo[3,4-*d*]pyrimidin-6yl}amino)ethanol 26k

Mp: 215-218 °C.

Yield: 32%.

MW: 422.43.

Anal. calcd. for $C_{22}H_{20}F_2N_6O$: C 62.55, H 4.77, N 19.89; found: C 62.76, H 4.72, N 20.10.

^{1}H NMR: δ 3.37-3.40 (m, 2H, $\underline{CH_2}$NH), 3.43-3.48 (m, 2H, $\underline{CH_2}$OH), 4.69 (s, 1H, OH), 6.80-7.60 (m, 9H, 8Ar + =CHAr), 7.80 (d, 1H, J_{trans} = 16 Hz, NCH=) 8.10 (s, 1H, H-3), 9.20 (s, 1H, NH).

2-({4-[(3-Chlorophenyl)amino]-1-[2-(4-chlorophenyl)vinyl]-1*H*-pyrazolo[3,4-*d*]pyrimidin-6yl}amino)ethanol 26n

Mp: 214-216 °C.

Yield: 13%.

MW: 441.31.

Anal. Calcd. for $C_{21}H_{18}Cl_2N_6O$: C 57.15, H 4.11, N 19.04; found: C 57.30, H 4.01, N 19.34.

^{1}H NMR: δ 3.51-3.60 (m, 2H, $\underline{CH_2}$NH), 3.43-3.65 (m, 2H, $\underline{CH_2}$OH), 4.73 (s, 1H, OH), 7.10-7.61 (m, 9H, 8Ar + =CHAr), 7.90 (d, 1H, J_{trans} = 16 Hz, NCH=), 8.26 (s, 1H, H-3), 9.90 (s, 1H, NH).

2-({4-[(3-Chlorophenyl)amino]-1-[2-(4-bromophenyl)vinyl]-1*H*-pyrazolo[3,4-*d*]pyrimidin-6yl}amino)ethanol 26p

Mp: 218-220 °C.

Yield: 13%.

MW: 484.77.

Anal. calcd. for $C_{21}H_{18}BrClN_6O$: C 51.92, H 3.73, N 17.30; found: C 51.87, H 3.45, N 17.59.

^{1}H NMR: δ 3.20-3.80 (m, 4H, NH$\underline{CH_2CH_2}$OH), 4.80 (s, 1H, OH), 7.00-8.61 (m, 12H, 9Ar + CH=CH + H-3), 9.90 (s, 1H, NH).

2-{[4-Morpholin-4-yl-1-(2-phenylvinyl)-1H-pyrazolo[3,4-*d*]pyrimidin-6-yl]amino}ethanol 26q

Mp: 177-178 °C.

Yield: 68%.

MW: 366.42.

Anal. calcd. for $C_{19}H_{22}N_6O_2$: C 62.28, H 6.05, N 22.94; found: C 62.23, H 6.19, N 23.25.

^{1}H NMR: δ 3.70 (q, J = 4.0 Hz, 2H, $\underline{CH_2}$NH), 3.81-3.96 (m, 10H, 4CH_2 morph. + $\underline{CH_2}$OH), 4.06 (br s, 1H, disappears with D_2O), 5.52 (br s, 1H, disappears with D_2O), 7.19-7.52 (m, 6H,

5H Ar + =CHAr), 7.87 (s, 1H, H-3), 7.88 (d, J_{trans} = 14.4 Hz, 1H, NCH=).

IR cm^{-1}: 3250-3150 (OH + NH), 1656 (C=C).

General procedure for the synthesis of compounds 26a,g,h,j,l,m,o,r

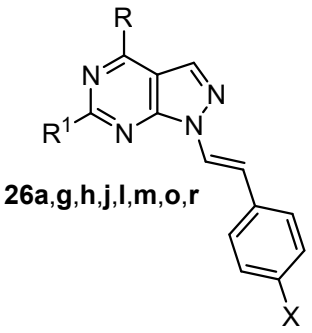

26a,**g**,**h**,**j**,**l**,**m**,**o**,**r**

26a: X = H, R = $NHCH_2CH_2C_6H_5$, R^1 = $N(CH_2CH_2OH)_2$
26g: X = H, R = $NHCH_2C_6H_4$-4Cl, R^1 = $N(CH_2CH_2OH)_2$
26h: X = H, R = $NHCH_2C_6H_4$-4Cl, R^1 = $OCH_2CH_2CH_2CH_3$
26j: X = H, R = NHC_6H_4-4Cl, R^1 = $N(CH_2CH_2OH)_2$
26l: X = F, R = $NHCH_2C_6H_4$-3F, R^1 = $N(CH_2CH_2OH)_2$
26m: X = F, R = NHC_6H_5, R^1 = $N(CH_2CH_2OH)_2$
26o: X = Cl, R = NHC_6H_4-3Cl, R^1 = $N(CH_2CH_2OH)_2$
26r: X = H, R = 4-morpholinyl, R^1 = $N(CH_2CH_2OH)_2$

Diethanolamine (0.3 mL, 1.29 mmol) was added to a solution of **36a-f** and **36h** (0.43 mmol) in DMSO (4 mL) and the mixture was heated at 90 °C for 24 h. The solution was washed with water (2 x 15 mL), dried ($MgSO_4$), filtered, and concentrated under reduced pressure. The crude yellow oils were purified by column chromatography (silica gel, 100 mesh) using ethyl acetate/n-hexane (6:4) as the eluant, to afford the pure products as white solids. In a first attempt, the reaction was performed in the presence of n-butanol (10 mL) and compound **26h** was isolated as a by-product.

2-({4-[(2-Phenylethyl)amino]-1-(2-phenylvinyl)-1*H*-pyrazolo[3,4-*d*]pyrimidin-6-yl}-amino)diethanol 26a

Mp: 133-134 °C.

Yield: 12 %.

MW: 444.53.

Anal.calcd. for $C_{25}H_{28}N_6O_2$: C 67.55, H 6.35, N 18.91; found: C 67.56, H 6.39, N 19.20.

^{1}H NMR: δ 2.96 (t, J = 8.0 Hz, 2H, CH_2Ar), 3.58-4.00 (m, 10H, $\underline{CH_2}NH$ + $N(\underline{CH_2CH_2}OH)_2$), 4.82 (br s, 2H, 2OH), 7.24-7.43 and 7.51-7.59 (2m, 11H, 10 H Ar + =CHAr), 7.86 (d, J_{trans} = 16.4 Hz, 1H, NCH=), 8.03 (s, 1H, H-3), 8.18 (t, J = 8 Hz, NH).

2-({4-[(4-Chlorobenzyl)amino]-1-[2-phenylvinyl]-1*H*-pyrazolo[3,4-*d*]pyrimidin-6-yl}amino)diethanol 26g

Mp: 144-145 °C.

Yield: 5 %. MW: 464.95

Anal. calcd. for $C_{24}H_{25}N_6OCl$: C 62.00, H 5.42, N 18.08; found: C 61.94, H 5.43, N 17.77.

^{1}H NMR: δ 3.81-3.90 (br s, 8H, N($\underline{CH_2CH_2}OH)_2$, 4.70 (s, 2H, CH_2Ar), 7.20-7.35 and 7.46-7.48 (2m, 10H, 9Ar + =CHAr), 7.82 (d, J_{trans} = 14.8 Hz, 1H, NCH=), 7.86 (s, 1H, H-3), 7.95 (s, 1H, NH).

***N*-(4-Chlorophenyl)-6-butoxy-1-[2-phenylethenyl]-1*H*-pyrazolo[3,4-*d*]pyrimidin-4-amine 26h**

Mp: 196-199 °C.

Yield: 30%.

MW: 419.90.

Anal. calcd. for $C_{23}H_{22}ClN_5O$: C 65.79, H 5.28, N 16.68; found: C 64.81, H 5.00, N 17.06.

^{1}H NMR: δ 0.99 (t, 3H, J = 6.3 Hz, CH_3), 1.48 (sx, 2H, J = 6.3 Hz, $CH_3\underline{CH_2}$), 1.71 (quint, 2H, J = 6.3 Hz, $CH_2\underline{CH_2}CH_2$), 4.41 (t, 2H, J = 6.3 Hz, CH_2O), 7.28-7-54 (m, 11H, 9Ar + =CHAr + H-3), 7.95 (d, 1H, J_{trans} = 16 Hz, NCH=).

2-({4-[(4-Chlorophenyl)amino]-1-[2-phenylvinyl]-1*H*-pyrazolo[3,4-*d*]pyrimidin-6-yl}amino)diethanol 26j

Mp: 215-217 °C.

Yield: 7%.

MW: 450.92.

Anal. calcd. for $C_{23}H_{23}ClN_6O_2$: C 61.26, H 5.14, N 18.64; found: C 61.20, H 4.99, N 18.51.

^{1}H NMR: δ 3.58-3.84 (m, 8H, N($\underline{CH_2CH_2}OH)_2$), 7.21-7.44, 7.54-7.60 and 7.87-7.92 (3m, 11H, 9Ar + CH=CH), 8.28 (s, 1H, H-3), 9.96 (s, 1H, NH).

2-({4-[(3-Fluorophenyl)benzilamino]-1-[2-(4-fluorophenyl)vinyl]-1*H*-pyrazolo[3,4-*d*]pyrimidin-6-yl}amino)diethanol 26l

Mp: 171-173 °C.

Yield: 28%.

MW: 466.48.

Anal. calcd. for $C_{24}H_{24}F_2N_6O_2$: C 61.79, H 5.19, N 18.02, found: C 61.62, H 5.04, N 18.00.

^{1}H NMR: δ 3.55-3.71 (m, 8H, N($\underline{CH_2CH_2}$OH)$_2$), 4.63-4.78 (m, 2H, 2OH), 7.18-7.40, 7.59-7.62 and 7.78-8.13 (3m, 12H, 9Ar + CH=CH + H-3), 8.61 (br s, 1H, NH).

2-({4-Phenylamino-1-[2-(4-fluorophenyl)vinyl]-1*H*-pyrazolo[3,4-*d*]pyrimidin-6-yl}amino)diethanol 26m

Mp: 200-202 °C.

Yield: 32%.

MW: 434.48.

Anal. calcd. for $C_{23}H_{23}FN_6O_2$: C 63.98, H 5.34, N 19.34; found: C 63.66, H 4.72, N 19.27.

^{1}H NMR: δ 3.60-4.00 (m, 8H, N($\underline{CH_2CH_2}$OH)$_2$), 4.80 (s, 2H, OH), 7.05-7.90 (m, 12H, 9Ar + CH=CH), 8.25 (s, 1H, H-3), 9.80 (s, 1H, NH).

2-({4-[(3-Chlorophenyl)amino]-1-[2-(4-chlorophenyl)vinyl]-1*H*-pyrazolo[3,4-*d*]pyrimidin-6yl}amino)diethanol 26o

Mp: 216-219 °C.

Yield: 10%.

MW: 485.36.

Anal. calcd. for $C_{23}H_{22}Cl_2N_6O_2$: C 56.92, H 4.57, N 17.31.; found: C 56.56, H 4.72, N 17.67.

^{1}H NMR: δ 3.76 (m, 8H, N($\underline{CH_2CH_2}$OH)$_2$), 4.83 (br s, 2H, 2OH), 7.09-7.15, 7.40-7.45 and 7.59-7.71 (3m, 8H, 7Ar+ =CHAr), 7.95 (d, 1H, J_{trans} = 16 Hz, NCH=), 8.28 (s, 1H, H-3), 9.96 (s, 1H, NH).

2-{[4-(Morpholin-4-yl)-1-(2-phenylvinyl)-1*H*-pyrazolo[3,4-*d*]pyrimidin-6-yl]amino}diethanol 26r

Mp: 178-180 °C.

Yield: 45%.

MW: 410.47.

Anal. calcd. for $C_{21}H_{26}N_6O_3$: C 61.45, H 6.38, N 20.47; found: C 61.56, H 6.14, N 21.25.

^{1}H NMR: δ 3.34-3.84(m, 16H, 4CH_2 morph. + N($\underline{CH_2CH_2}$OH)$_2$), 4.90 (br s, 2H, 2OH, disappear with D_2O), 7.30-7.55(m, 7H, 5Ar + CH=CH), 8.17 (s, 1H, H-3).

General procedure for the synthesis of compounds 26b,s

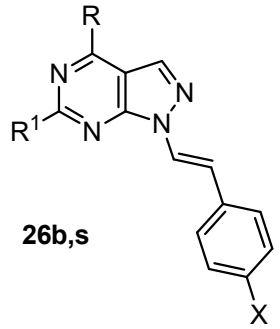

26b,s

26b: X = H, R = $NHCH_2CH_2C_6H_5$, R^1 = $NHCH_2CH_2NH_2$
26s: X = H, R = 4-morpholinyl, R^1 = $NHCH_2CH_2NH_2$

Ethylenediamine (1.05 mmol) was added to a suspension of **36a**,**h** in DMF (5 mL). The mixture was heated at 90 °C for 12 h. After cooling, water was added (20 mL), and the solution was extracted with ethyl acetate (3 x 20 mL); the organic phase was washed with brine (40 mL), dried ($MgSO_4$), and evaporated under reduced pressure. White solids were purified by a column chromatography with diethyl ether as the eluant.

***N*^{6}-(2-aminoethyl)-N4-(2-phenylethyl)-1-[2-phenylvinyl]-1*H*-pyrazolo[3,4-*d*]pyrimidine-4,6-diamine 26b**

Mp: 74-76 °C.

Yield: 8%.

MW: 399.49.

Anal. calcd. for $C_{23}H_{25}N_7$: C 69.15, H 6.31, N 24.54; found: C 69.07, H 6.40, N 24.21.

^{1}H NMR: δ 2.97 (t, *J* = 7.2 Hz, 2H, CH_2Ar), 3.51 (quint, *J* = 6.0, 2H, $NH_2\underline{CH_2}$), 3.61 (q, *J* = 6.0, 2H, $NH_2CH_2\underline{CH_2}NH$), 3.76 (t, *J* = 7.2, 2H $NH\underline{CH_2}CH_2Ar$), 7.18-7.36 and 7.48-7.50 (2m, 11H, 10Ar + =CHAr), 7.86-7.89 (m, 2H, H-3 + NCH=), 8.08 (s, 1H, NH).

***N*-[4-(Morpholin-4-yl)-1-(2-phenylvinyl)-1*H*-pyrazolo[3,4-*d*]pyrimidin-6-yl]ethane-1,2-diamine 26s**

Mp: 170-173 °C.

Yield: 20%.

MW: 365.43.

Anal. calcd. for $C_{19}H_{23}N_7O$: C 62.45, H 6.34, N 26.83; found: C 62.33, H 6.10, N 23.85. ^{1}H NMR: δ 3.20-3.39 (m, 4H, $NH_2\underline{CH_2CH_2}NH$), 3.75-3.85 (m, 8H, $4CH_2$ morph.), 7.26-8.028(m, 7H, 5H Ar + CH=CH), 8.25 (s, 1H, H-3).

General procedure for the synthesis of compounds 26c,t

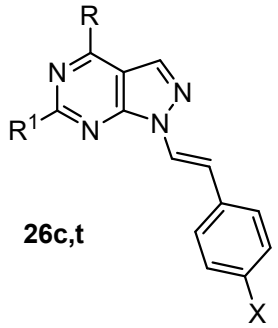

26c,t

26c: X = H, R = $NHCH_2CH_2C_6H_5$, R^1 = OCH_2CH_2OH
26t: X = H, R = 4-morpholinyl, R^1 = OCH_2CH_2OH

Ethylene glycol (1.14 mL, 20.6 mmol) and NaH 60% dispersion in mineral oil (91.2 mg, 2.28 mmol) were added to a suspension of **36a**,**h** (1.14 mmol) in anhydrous DMF (10 mL) precooled in an ice-water bath. The mixture was stirred at room temperature 1.5 h. Then the reaction was quenched with a 30% acetic acid solution (10 mL) and DMF was removed under reduced pressure. The aqueous solution was extracted with ethyl acetate (3 x 20 mL); the organic phase was washed with brine (40 mL), dried ($MgSO_4$), and evaporated under reduced pressure. White solids were purified by a column chromatography with petroleum ether (bp 40-60 °C)/diethyl ether (9:1→ diethyl ether alone) as the eluant to afford the desired compounds as pure solids.

2-({4-[(2-Phenylethyl)amino]-1-[2-phenylvinyl]-1*H*-pyrazolo[3,4-*d*]pyrimidin-6-yl}oxy)ethanol 26c

Mp: 150.5-151.8 °C.

Yield: 47 %.

MW: 401.46.

Anal. calcd. for $C_{23}H_{23}N_5O_2$: C 68.81, H 5.77, N 17.44; found: C 68.60, H 5.99, N 17.52.

^{1}H NMR: δ 2.86-3.01 (m, 2H, CH_2Ar), 3.59-3.80 (m, 4H, $\underline{CH_2}NH$ + CH_2O), 4.25, 4.42 (m, 2H, $\underline{CH_2}OH$), 4.84 (t, *J* = 6.3 Hz, 1H, NH), 7.24-7.35 and 7.55-7.58 (2m, 11H, 10 Ar + =CHAr), 7.83 (d, J_{trans} = 15.7 Hz, 1H, NCH=), 8.17 (s, 1H, H-3), 8.58 (br s, 1H, OH), 9.96 (s, 1H, NH).

2-({4-[Morpholin-4-yl]-1-[2-phenylvinyl]-1*H*-pyrazolo[3,4-*d*]pyrimidin-6-yl}oxy)ethanol 26t

Mp: 187-188 °C.

Yield: 88%.

MW: 367.40.

Anal. calcd. for $C_{19}H_{21}N_5O_3$: C 62.11, H 5.76, N 19.06; found: C 62.13, H 6.19, N 18.25.

^{1}H NMR: δ 3.74-3.91 (m, 10H, $4CH_2$ morph. + CH_2O), 4.36-4.41 (t, 2H, $\underline{CH_2}OH$), 4.90 (t, 1H, OH), 7.26-7.63 (m, 6H Ar + =CHAr), 7.93-8.00 (d, J_{trans} = 14 Hz, 1H, NCH=), 8.44(s, 1H, H-3).

Synthesis of 1-(2-hydroxy-2-phenylethyl)-6-(methylsulfonyl)-1,5-dihydro-4*H*-pyrazolo[3,4-*d*]pyrimidin-4one 37

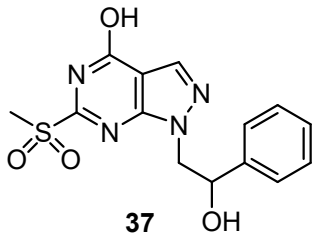

37

meta-Chloroperoxybenzoic acid 77% suspension in mineral oil (4.45 g, 20.0 mmol) was added portion-wise to a solution of **33a** (3.0 g, 10.0 mmol) in anhydrous DMF (5 mL) and $CHCl_3$ (50 mL) at 0 °C. Then the mixture was stirred at room temperature for 12 h. The solvent was evaporated under reduced pressure, and diethyl ether (20 mL) was added. By standing in a refrigerator for 2 h, a white solid was precipitated, which was filtered and recrystallized from absolute ethanol.

Mp: 170-171 °C.

Yield: 84%.

MW: 334.35

Anal.calcd. for $C_{14}H_{14}N_4O_4S$: C 50.29, H 4.22, N 16.76, S 9.59 found: C 50.44, H 4.28, N 12.90, S 6.50.

^{1}H NMR: δ 3.69 (s, 3H, SO_2CH_3), 4.22-4.52 (m, 2H, NCH_2), 4.91-5.09 (m, 1H, CHO), 5.60 (br s, 1H, OH), 7.09-7.28 (m, 5H, Ar), 8.15 (s, 1H, H-3), 13.20 (br s, 1H, NH).

IR cm^{-1}: 3540 (NH), 3150-2900 (OH), 1693 (CO).

Synthesis of 1-(2-hydroxy-2-phenylethyl)-6-morpholin-4-yl-1*H*-pyrazolo[3,4-*d*]pyrimidin-4-ol 38

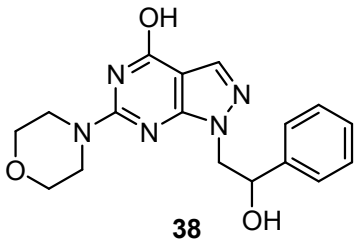

38

Morpholine (2.6 mL, 30.0 mmol) was added to a solution of **37** (2.0 g, 6.0 mmol) in DMSO (18 mL) and the mixture was heated at 100 °C for 3 h. After cooling to room temperature, cold water was added; the pale yellow solid was filtered, washed with H_2O, and recrystallized from absolute ethanol.

Mp: 247-248 °C.

Yields: 83 %.

MW: 341.36.

Anal. calcd. for $C_{17}H_{19}N_5O_3$: C 59.81, H 5.61, N 20.52; found: C 59.59, H 5.58, N 20.49.

^{1}H NMR: δ 3.36-3.49 and 3.51-3.62 (2 m, 8H, 4CH_2 morph), 3.99-4.25 (m, 2H, NCH_2), 4.90-5.03 (m, 1H, CHO), 5.50-5.55 (m, 1H, OH), 7.03-7.24 (m, 5H Ar), 7.70 (s, 1H, H-3), 10.75 (br s, 1H, NH).

IR cm^{-1}: 3380, 3168, 3113 (NH + OH), 1702 (CO).

Synthesis of 4-chloro-1-(2-chloro-2-phenylethyl)-6-(morpholin-4-yl)-1*H*-pyrazolo[3,4-*d*]pyrimidine 39

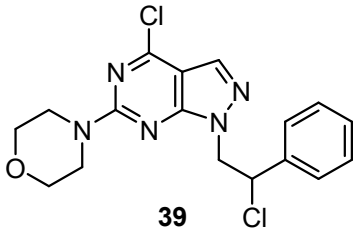

39

The Vilsmeier complex, previously prepared from $POCl_3$ (5.5 mL, 58.6 mmol) and anhydrous DMF (4.5 mL, 58.6 mmol) was added to a suspension of **38** (1.0 g, 2.9 mmol) in $CHCl_3$ (30 mL). The mixture was refluxed for 12 h. The solution was washed with 4M NaOH (2 × 20 mL), and with H_2O (20 mL), dried ($MgSO_4$) and concentrated under reduced pressure. The crude was purified by column chromatography (silica gel, 100 mesh) using a mixture of petroleum ether (bp 40-60 °C) /diethyl ether (8:2) as the eluant, to afford the pure product **39** as a yellow oil, which was crystallized as a white solid by adding a mixture of petroleum ether (bp 40-60 °C)/diethyl ether (1:1) and standing in a refrigerator.

Mp: 117-118 °C.
Yields: 87 %.
MW: 378.25.
Anal. calcd. for $C_{17}H_{17}Cl_2N_5O$: C 53.98, H 4.53, N 18.51; found: C 54.05, H 4.77, N 18.35.
^{1}H NMR: δ 3.47-3.56 and 3.60-3.68 (2 m, 8H, 4CH_2 morph), 4.53-4.70 (m, 2H, NCH_2), 5.40-5.50 (m, 1H, CHCl), 7.15-7.38 (m, 5H Ar), 7.73 (s, 1H, H-3).

General procedure for the synthesis of compounds 40a,b

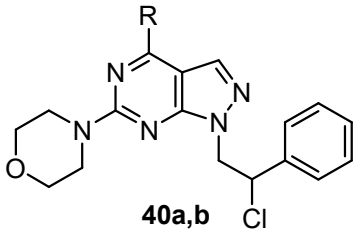

40a,b

40a: R = $NHCH_2C_6H_5$
40b: R = $NHCH_2C_6H_4$-4F

The appropriate amine (3.5 mmol) was added to a solution of **39** (0.30 g, 0.9 mmol) in anhydrous toluene (5 mL) and the mixture was stirred at room temperature for 24 h. The organic phase was washed with water (2 x 10 mL), dried ($MgSO_4$) and concentrated under reduced pressure. The crude oil **40b** was recrystallized by adding diethyl ether. Compound **40a** crystallized by adding a mixture of CH_2Cl_2/n-hexane (1:1).

***N*-Benzyl-1-(2-chloro-2-phenylethyl)-6-morpholin-4-yl-1*H*-pyrazolo[3,4-*d*]pyrimidin-4-amine 40a**

Mp: 90-93 °C.

Yield: 57%.

MW: 448.95.

Anal. calcd. for $C_{24}H_{25}ClN_6O$: C 64.21, H5.61, N 18.72; found: C 64.42, H 5.97, N 18.44.

^{1}H NMR: δ 3.61-3.81 (m, 8H, 4CH_2 morph.), 4.32-4.80 (m, 4H, CH_2H + CH_2Ar), 5.36-5.54 (m, 1H, CHCl), 7.17-7.42 (m, 10H Ar), 7.56 (s, 1H, H-3).

1-(2-Chloro-2-phenylethyl)-*N*-(4-fluorobenzyl)-6-morpholin-4-yl-1*H*-pyrazolo[3,4-*d*]pyrimidin-4-amine 40b

Mp: 85-88 °C.

Yield: 62%.

MW: 466.94.

Anal. calcd. for $C_{24}H_{24}ClFN_6O$: C 61.73, H 5.18, N 18.00; found: C 61.05, H 5.71, N 17.56.

^{1}H NMR: δ 2.31-2.61 (m, 8H, 4CH_2 morph.), 4.12-4.20 (m, 4H, NCH_2 + CH_2Ar), 5.04-5.20 (m, 1H, CHCl), 7.20-7.52 (m, 9H Ar), 7.80 (s, 1H, H-3).

General procedure for the synthesis of compounds 26d,e

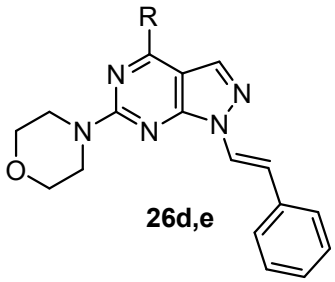

26d,e

26d: R = $NHCH_2C_6H_5$
26e: R = $NHCH_2C_6H_4$-4F

A solution of NaOH (0.14 g, 3.4 mmol) in water (1 mL) was added to a suspension of derivatives **40a,b** (0.48 mmol) in 95% ethanol (5 mL) and the mixture was refluxed for 10 h. After cooling, the white solids were washed with water. Compound **26d** was obtained as a white pure solid and it did not need further purification. Compound **26e** was purified by column chromatography (silica gel, 100 mesh) using a mixture of diethyl ether/petroleum ether (bp 40-60 °C) (7:3) as the eluant, to afford the pure product as white solid.

***N*-Benzyl-6-morpholin-4-yl-1-[2-phenylvinyl]-1*H*-pyrazolo[3,4-*d*]pyrimidin-4-amine 26d**

Mp: 163-166 °C.

Yield: 67%.

MW: 412.48.

Anal. calcd. for $C_{24}H_{24}N_6O$: C 69.88, H 5.86, N 20.37; found: C 69.68, H 5.72, N 20.35.

^{1}H NMR: δ 3.80-3.83 (m, 4H, $2CH_2N$ morph.), 3.91-3.93 (m, 4H, $2CH_2O$ morph), 4.81 (d, J = 5.6 Hz, 2H, CH_2Ar), 5.65 (s, 1H, NH), 7.26-7.34 and 7.50-7.54 (2m, 11H, 10 Ar + =CHAr), 7.78 (s, 1H, H-3), 7.91 (d, 1H, J_{trans} = 14.6 Hz, NCH=).

***N*-(4-Fluorobenzyl)-6-morpholin-4-yl-1-[2-phenylvinyl]-1*H*-pyrazolo[3,4-*d*]pyrimidin-4-amine 26e**

Mp: 174-176 °C.

Yield: 55%.

MW: 430.47.

Anal. calcd. for $C_{24}H_{23}FN_6O$: C 66.96, H 5.39, N 19.52; found: C 67.08, H 5.36, N 19.34.

^{1}H NMR: δ 3.80-3.83 (m, 4H, CH_2N morph.), 3.90-3.93 (m, 4H, CH_2O morph.), 4.78 (d, 2H, *J* = 5.6 Hz, CH_2 Ar), 5.70 (br s, 1H, NH), 7.03-7.12, 7.26-7.38 and 7.41-7.78 (3m, 10H, 9 Ar + =CHAr), 7.78 (s, 1H, H-3), 7.91 (d, 1H, J_{trans} = 14.6 Hz, NCH=).

General procedure for the synthesis of compounds 44a-c

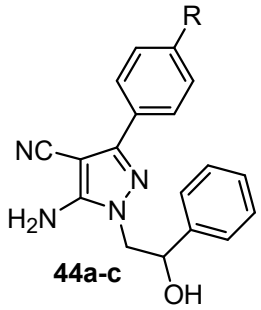

44a-c

44a: R = H
44b: R = CH_3
44c: R = Cl

A 60% sodium hydride dispersion in mineral oil (1.21 g, 30.3 mmol) was added in small batches to a solution of malonitrile (1.00 g, 15.1 mmol) in dry THF (25 mL) precooled at 0−5 °C. After 30 min at 0−5 °C, the suitable acyl chloride (15.1 mmol) was added dropwise. The orange solution was stirred at room temperature for 2−12 h, then dimethylsulfate (1.75 mL, 18.2 mmol) was slowly added and the solution was refluxed for 3−6 h. Finally, 2-hydrazinyl-1-phenylethanol 7 (4.62 g, 30.2 mmol) dissolved in dry THF (2 mL) was added and the reaction was refluxed for 3−6 h. After cooling to room temperature, water (25 mL) and conc. NH_3 (5 mL) were added under stirring. After 15 min, THF was removed under reduced pressure and the aqueous phase was extracted with CH_2Cl_2 (30 mL). Organic phases were washed with water (15 mL) and brine (15 mL), dried (Na_2SO_4), and evaporated under reduced pressure. The crudes were purified by flash chromatography using diethyl ether/petroleum ether (bp 40-60 °C) as the eluant, with a gradient elution (3:1 → 9:1).

5-Amino-1-(2-hydroxy-2-phenylethyl)-3-phenyl-1*H*-pyrazole-4-carbonitrile 44a

Mp: 165-166 °C.

Yield: 40%.

MW: 304.35.

Anal. calcd. for $C_{18}H_{16}N_4O$: C 71.04, H 5.30, N 18.41; found: C 70.91, H 5.40, N 18.49.

^{1}H NMR: δ 3.95-4.23 (m, 2H, CH_2), 5.10-5.18 (m, 1H, CH), 7.20-7.37 and 7.79-7.81 (2m, 10H Ar).

IR cm^{-1}: 3560-3240 (OH), 3358, 3350 (NH2), 2204 (CN).

5-Amino-1-(2-hydroxy-2-phenylethyl)-3-(4-methylphenyl)-1*H*-yrazole-4-carbonitrile 44b

Mp: 172-174 °C.

Yield: 42%.

MW: 318.37.

Anal. calcd. for $C_{19}H_{18}N_4O$: C 71.68, H 5.70, N 17.60; found: C 71.77, H 5.76, N 17.44.

^{1}H NMR: δ 2.36 (s, 3H, CH_3), 4.00-4.05 and 4.12-4.15 (2m, 2H, CH_2), 5.10-5.15 (m, 1H, CH), 7.20-7.34 and 7.57-7.91 (2m, 9H Ar).

IR cm^{-1}: 3400-3200 (OH), 3400, 3322 (NH_2), 2221 (CN).

5-Amino-3-(4-chlorophenyl)-1-(2-hydroxy-2-phenylethyl)-1*H*-pyrazole-4-carbonitrile 44c

Mp: 173-174 °C.

Yield: 49%.

MW: 338.39.

Anal. calcd. for $C_{18}H_{15}N_4OCl$: C 63.81, H 4.46, N 16.54; found: C 63.86, H 4.76, N 16.43.

^{1}H NMR: δ 2.99 (brs, 1H, OH), 3.99-4.15 (m, 2H, CH_2), 4.85 (brs, 2H, NH_2), 5.18-5.22 (m, 1H, CHOH), 7.37-7.51 and 7.79-7.90 (2m, 9H Ar).

IR cm^{-1}: 3450−3100 (OH), 3388, 3322 (NH_2), 2223 (CN).

General procedure for the synthesis of compounds 45a-c

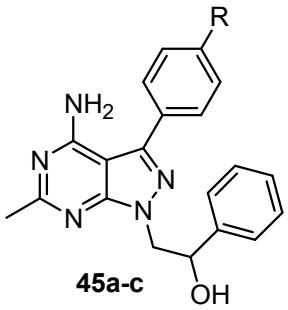

45a-c

45a: R = H
45b: R = CH_3
45c: R = Cl

A solution of sodium ethoxyde (190 mg, 8.25 mmol of sodium in 5 mL of absolute ethanol) was added to the suspension of the suitable intermediate **44a-c** (1.65 mmol) in acetonitrile (10 mL). The reaction was refluxed 8 h. Acetonitrile and ethanol were removed under reduced pressure. Water (50 mL) was added, and the aqueous phase was extracted with ethyl acetate (3 x 50 mL). Then the organic phase was washed with brine (70 mL). Brine was in turn extracted with ethyl acetate (35 mL) and the organic solution was added to the previously obtained ethyl acetate extracts. The organic phase was dried and concentrated under reduced pressure. All crudes were purified by column chromatography using diethyl ether/methanol (95:5) as the eluant.

2-(4-Amino-6-methyl-3-phenyl-1*H*-pyrazolo[3,4-*d*]pyrimidin-1-yl)-1-phenylethanol 45a

Mp: 193-194 °C.

Yield: 41%.

MW: 345.40

Anal. calcd. for $C_{20}H_{19}N_5O$: C 69.55, H 5.54, N 20.28; found: C 69.55, H 5.59, N 20.39.

^{1}H NMR: δ 2.66 (s, 3H, CH_3), 4.60-4.77 (m, 2H, CH_2), 5.26-5.37 (m, 1H, CHOH), 7.36-7.71 (m, 10H Ar).

2-[4-Amino-6-methyl-3-(4-methylphenyl)-1*H*-pyrazolo[3,4-*d*]pyrimidin-1-yl]-1-phenylethanol 45b

Mp: 175-176 °C.

Yield: 25%.

MW: 359.42

Anal. calcd. for $C_{21}H_{21}N_5O$: C 70.17, H 5.89, N 19.48; found: C 70.47, H 6.20, N 19.39.

^{1}H NMR: δ 2.40 and 2.44 (2s, 6H, $2CH_3$), 4.22-4.37 and 4.35-4.60 (2m, 2H, CH_2), 5.20 (br s, 1H, OH), 5.61-5.69 (m, 1H, CHOH), 6.70 (br s, 2H, NH_2), 7.26-7.42 and 7.50-7.60 (2m, 9H Ar).

2-[4-Amino-3-(4-chlorophenyl)-6-methyl-1*H*-pyrazolo[3,4-*d*]pyrimidin-1-yl]-1-phenylethanol 45c

Mp: 176-178 °C.

Yield: 57%.

MW: 379.84

Anal. calcd. for $C_{20}H_{18}N_5OCl$: C 63.24, H 4.87, N 18.44; found: C 63.23, H 4.57, N 18.27.

^{1}H NMR: δ 2.60 (s, 3H, CH_3), 4.59-4.76 (m, 2H, CH_2), 5.27-5.32 (m, 1H, CHOH), 5.68 (br s, 2H, NH_2) 7.30-7.45 and 7.50-7.68 (2m, 9H Ar).

General procedure for the synthesis of compounds 43a-c

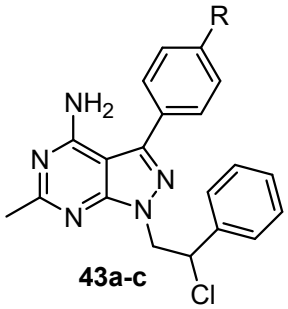

43a-c

43a: R = H
43b: R = CH_3
43c: R = Cl

$SOCl_2$ (220 μL, 3 mmol) was added dropwise to a solution of the suitable intermediate **45a-c** (0.4 mmol) in dry CH_2Cl_2 (5 mL), and the reaction was stirred at room temperature for 12 h under nitrogen atmosphere. The reaction was cautiously washed with 1N NaOH (2 x 15 mL) and then the aqueous phases were extracted twice with CH_2Cl_2 (2 x 10 mL). Organic phases

were washed with brine (30 mL). Brine was in turn extracted with CH_2Cl_2 (15 mL), and the organic solution was added to the previously obtained CH_2Cl_2 extracts. The organic phase was dried (Na_2SO_4) and concentrated under reduced pressure. All the crudes were purified by chromatography using CH_2Cl_2/methanol as the eluant.

1-(2-Chloro-2-phenylethyl)-6-methyl-3-phenyl-1*H*-pyrazolo[3,4-*d*]pyrimidin-4-amine 43a

Mp: 148-150 °C.

Yield: 19%.

MW: 363.84

Anal. calcd. for $C_{20}H_{18}N_5Cl$: C 66.02, H 4.99, N 19.25; found: C 66.20, H 4.88, N 19.04.

^{1}H NMR: δ 2.47 (s, 3H, CH_3), 4.69-4.83 and 4.94-5.10 (2m, 2H, CH_2), 5.69-5.80 (m, 1H, CHCl), 7.31-7.48 and 7.50-7.72 (2m, 10H Ar).

1-(2-Chloro-2-phenylethyl)-6-methyl-3-(4-methylphenyl)-1*H*-pyrazolo[3,4-*d*]pyrimidin-4-amine 43b

Mp: 207-209 °C.

Yield: 32%.

MW: 377.87

Anal. calcd. for $C_{21}H_{20}N_5Cl$: C 66.75, H 5.33, N 18.53; found: C 66.84, H 5.12, N 18.48.

^{1}H NMR: δ 2.39, 2.45 (2s, 6H, $2CH_3$), 4.69-4.81 and 4.90-5.07 (2m, 2H, CH_2), 5.68-5.78 (m, 1H, CHCl), 7.34-7.42 and 7.52-7.62 (2m, 9H Ar).

3-(4-Chlorophenyl)-1-(2-chloro-2-phenylethyl)-6-methyl-1*H*-pyrazolo[3,4-*d*]pyrimidin-4-amine 43c

Mp: 203-205 °C.

Yield: 28%.

MW: 398.29

Anal. calcd. for $C_{20}H_{17}N_5Cl_2$: C 60.31, H 4.30, N 17.58; found: C 60.50, H 5.50, N 17.80.

^{1}H NMR: δ 2.66 (s, 3H, CH_3), 4.70-4.85 and 5.00-5.18 (2m, 2H, CH_2), 5.57-5.63 (m, 1H, CHCl), 7.30-7.40 and 7.45-7.63 (2m, 9H Ar).

Synthesis of 1-(2-hydroxy-2-phenylethyl)-6-((2-morpholinoethyl)thio)-1*H*-pyrazolo[3,4-*d*]pyrimidin4(5H)-one 47

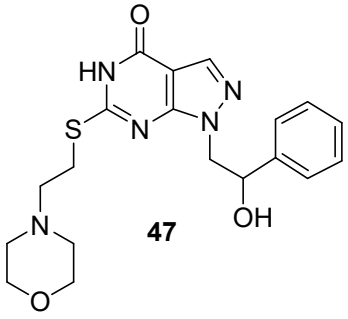

47

NaOH (0.4 g, 10 mmol) dissolved in absolute ethanol (5 mL) and 4-(2-chloroethyl)morpholine (2.24 g, 15 mmol) were added to a solution of intermediates **32a** (2.88 g, 10 mmol) in anhydrous DMF (5 mL). The solution was refluxed for 6 h. After cooling, the solvent was evaporated under reduced pressure, and the crude was poured into cold water. The white solid was filtered, washed with water, and recrystallized from absolute ethanol.

Yield: 63%.

Mp: 201-202 °C.

MW: 401.48.

Anal. calcd for $C_{19}H_{23}N_5O_3S$: C 56.84, H 5.77, N 17.44, S 7.99, found C 56.68, H 5.55, N 17.48, S 8.00.

^{1}H NMR: δ 2.36-2.50 (m, 4H, 2CH_2N morph.), 3.10-3.40 (m, 4H, CH_2S + $\underline{CH_2}CH_2$S), 3.45-3.56 (m, 4H, 2CH_2O morph.), 4.13-4.40 (m, 2H, CH_2N), 4.83-5.06 (m, 1H, CHO), 5.55 (d, 1H, OH disappears with D_2O), 7.10-7.28 (m, 5H Ar), 7.89 (s, 1H, H-3).

IR cm^{-1}: 3100-2850 (NH + OH), 1664 (CO).

Synthesis of 4-(2-((4-chloro-1-(2-chloro-2-phenylethyl)-1*H*-pyrazolo[3,4-*d*]pyrimidin-6yl)thio)ethyl)morpholine 48

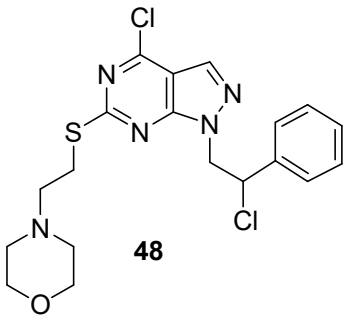

48

The Vilsmeier complex, previously prepared from $POCl_3$ (12.27 g, 80 mmol) and anhydrous DMF (5.85 g, 80 mmol) was added to a suspension of intermediate 84c (4.01 g, 10 mmol) in $CHCl_3$ (50 mL). The mixture was refluxed for 8 h. The solution was washed with 4 M NaOH (2 x 20 mL), then with water (20 mL), dried ($MgSO_4$), and concentrated under reduced pressure. The yellow crude oil was crystallized as a brown solid by adding absolute ethanol and standing in a refrigerator.

Yield: 75%.

Mp: 106-107 °C.

MW: 438.37.

Anal. calcd for $C_{19}H_{21}N_5Cl_2OS$: C 52.06, H 4.83, N 15.98, S 7.31, found C 52.00, H 4.91, N 16.01, S 7.52.

^{1}H NMR: δ 2.81-3.12 (m, 4H, $2CH_2N$ morph.), 3.18-3.81 (m, 4H, CH_2S + $\underline{CH_2}CH_2S$), 3.86-4.10 (m, 4H, $2CH_2O$ morph.), 4.60-4.78 and 5.12-5.30 (2m, 2H, CH_2N), 5.36-5.50 (m, 1H, CHCl), 7.16-7.50 (m, 5H Ar), 8.00 (s, 1H, H-3).

Synthesis of *N*-(3-bromophenyl)-1-(2-chloro-2-phenylethyl)-6-((2-morpholinoethyl)thio)-1*H*-pyrazolo[3,4-*d*]pyrimidin-4-amine SI306

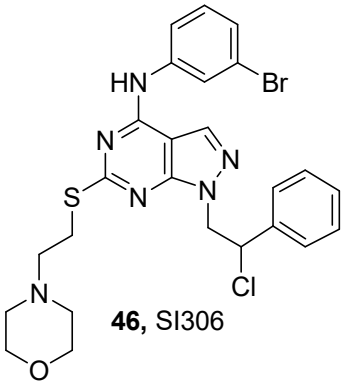

46, SI306

Yield: 61%

Mp: 232-233 °C

MW: 573.94

Anal. calcd for $C_{25}H_{26}N_6BrClOS$: C 52.32, H 4.57, N 14.64, S 5.59, found C 52.12, H 4.52, N 14.55, S 5.52.

^{1}H NMR: δ 2.90-3.99 (m, 12H, 4CH_2 morph. + CH_2N + CH_2S), 4.63-4.85 and 5.045.21 (2m, 2H, CH_2N pyraz.), 5.55-5.70 (m, 1H, CHCl), 7.03-8.52 (m, 10H, 9 Ar + H-3), 11.33 (s all., 1H, NH disappears with D_2O).

IR cm^{-1}: 3450 (NH).

BIBLIOGRAPHY

1. Adams, J. A. Kinetic and catalytic mechanisms of protein Structural Biology of Protein Tyrosine Kinases kinases. *Chem. Rev.* **101**, 2271–2290 (2001).
2. Manning, G., Whyte, D. B., Martinez, R., Hunter, T. & Sudarsanam, S. The protein kinase complement of the human genome. *Science (80-.).* **298**, 1912–1934 (2002).
3. Hanks, S. K. & Hunter, T. The eukaryotic protein kinase superfamily: Kinase (catalytic) domain structure and classification. *FASEB J.* **9**, 576–596 (1995).
4. Taylor, S. S. & Kornev, A. P. Protein kinases: Evolution of dynamic regulatory proteins. *Trends in Biochemical Sciences* **36**, 65–77 (2011).
5. Roskoski, R. Properties of FDA-approved small molecule protein kinase inhibitors. *Pharmacol. Res.* **144**, 19–50 (2019).
6. Carles, F., Bourg, S., Meyer, C. & Bonnet, P. PKIDB: A curated, annotated and updated database of protein kinase inhibitors in clinical trials. *Molecules* **23**, 1–18 (2018).
7. Bhullar, K. S. *et al.* Kinase-targeted cancer therapies: Progress, challenges and future directions. *Mol. Cancer* **17**, 1–20 (2018).
8. Edelman, A. Protein Serine Threonine Kinases. *Annu. Rev. Biochem.* **56**, 567–613 (1987).
9. Arencibia, J. M., Pastor-Flores, D., Bauer, A. F., Schulze, J. O. & Biondi, R. M. AGC protein kinases: From structural mechanism of regulation to allosteric drug development for the treatment of human diseases. *Biochimica et Biophysica Acta - Proteins and Proteomics* **1834**, 1302–1321 (2013).
10. Carolina, N., Hook, S. S. & Means, A. R. Ca2+/CaM-Dependent kinases: From activation to function. *Ann. Rev. Pharmacol. Toxicol.* 471–505 (2001).
11. Varjosalo, M. *et al.* The Protein Interaction Landscape of the Human CMGC Kinase Group. *Cell Rep.* **3**, 1306–1320 (2013).
12. Josso, N. & Di Clemente, N. Serine/threonine kinase receptors and ligands. *Curr. Opin. Genet. Dev.* **7**, 371–377 (1997).
13. Rozpędek, W. *et al.* Breaking the DNA Damage Response via Serine/Threonine Kinase Inhibitors to Improve Cancer Treatment. *Curr. Med. Chem.* **26**, 1425–1445 (2018).
14. Capra, M. *et al.* Frequent alterations in the expression of serine/threonine kinases in human cancers. *Cancer Res.* **66**, 8147–8154 (2006).
15. Hubbard, S. R. & Till, J. H. Protein Tyrosine Kinase Structure and Function. *Annu. Rev. Biochem.* **69**, 373–398 (2000).
16. Maruyama, I. Mechanisms of Activation of Receptor Tyrosine Kinases: Monomers or Dimers. *Cells* **3**, 304–330 (2014).

17. Takeuchi, K. & Ito, F. Receptor tyrosine kinases and targeted cancer therapeutics. *Biol. Pharm. Bull.* **34**, 1774–1780 (2011).

18. Cowan-Jacob, S. W. Structural biology of protein tyrosine kinases. *Cell. Mol. Life Sci.* **63**, 2608–2625 (2006).

19. Jiao, Q. *et al.* Advances in studies of tyrosine kinase inhibitors and their acquired resistance. *Mol. Cancer* **17**, 1–12 (2018).

20. Marum, J. E. & Branford, S. Current developments in molecular monitoring in chronic myeloid leukemia. *Ther. Adv. Hematol.* **7**, 237–251 (2016).

21. Di Cristofano, A. SGK1: The Dark Side of PI3K Signaling. *Curr. Top. Dev. Biol.* **123**, 49–71 (2017).

22. Pearce, L. R., Komander, D. & Alessi, D. R. The nuts and bolts of AGC protein kinases. *Nat. Rev. Mol. Cell Biol.* **11**, 9–22 (2010).

23. Bruhn, M. A., Pearson, R. B., Hannan, R. D. & Sheppard, K. E. Second AKT: The rise of SGK in cancer signalling. *Growth Factors* **28**, 394–408 (2010).

24. Lang, F. *et al.* (Patho)physiological significance of the serum- and glucocorticoid-inducible kinase isoforms. *Physiol. Rev.* **86**, 1151–1178 (2006).

25. Castel, P. & Scaltriti, M. The emerging role of serum/glucocorticoid-regulated kinases in cancer. *Cell Cycle* **16**, 5–6 (2017).

26. Lang, F. & Stournaras, C. Serum and glucocorticoid inducible kinase, metabolic syndrome, inflammation, and tumor growth. *Hormones* **12**, 160–171 (2013).

27. Lang, F., Stournaras, C., Zacharopoulou, N., Voelkl, J. & Alesutan, I. Serum- and glucocorticoid-inducible kinase 1 and the response to cell stress. *Cell Stress* **3**, 1–8 (2019).

28. Webster, M. K., Goya, L., Ge, Y., Maiyar, A. C. & Firestone, G. L. Characterization of sgk, a novel member of the serine/threonine protein kinase gene family which is transcriptionally induced by glucocorticoids and serum. *Mol. Cell. Biol.* **13**, 2031–2040 (1993).

29. Waldegger, S., Barth, P., Raber, G. & Lang, F. Cloning and characterization of a putative human serine/threonine protein kinase transcriptionally modified during anisotonic and isotonic alterations of cell volume. *Proc. Natl. Acad. Sci. U. S. A.* **94**, 4440–4445 (1997).

30. Zhao, B. *et al.* Crystal structure of the kinase domain of serum and glucocorticoid-regulated kinase 1 in complex with AMP-PNP. *Protein Sci.* **16**, 2761–2769 (2007).

31. Cheng, S. & Niv, M. Y. Molecular Dynamics Simulations and Elastic Network Analysis of Protein Kinase B (Akt/PKB) Inactivation. *J. Chem. Inf. Model.* **50**, 1602–1610 (2010).

32. Park, J. *et al.* Serum and glucocorticoid-inducible kinase (SGK) is a target of the PI 3-kinase-stimulated signaling pathway. *EMBO J.* **18**, 3024–3033 (1999).

33. García-Martínez, J. M. & Alessi, D. R. mTOR complex 2 (mTORC2) controls hydrophobic motif phosphorylation and activation of serum- and glucocorticoid-induced protein kinase 1 (SGK1). *Biochem. J.* **416**, 375–385 (2008).

34. Perrotti, N., He, R. A., Phillips, S. A., Haft, C. R. & Taylor, S. I. Activation of Serum- and Glucocorticoid-induced Protein Kinase (Sgk) by Cyclic AMP and Insulin. *J. Biol. Chem.* (2001). doi:10.1074/jbc.M007052200

35. Amato, R. *et al.* IL-2 signals through Sgk1 and inhibits proliferation and apoptosis in kidney cancer cells. *J. Mol. Med.* (2007). doi:10.1007/s00109-007-0205-2

36. Faletti, C. J., Perrotti, N., Taylor, S. I. & Blazer-Yost, B. L. sgk: An essential convergence point for peptide and steroid hormone regulation of ENaC-mediated Na+ transport. *Am. J. Physiol. - Cell Physiol.* **282**, (2002).

37. Amato, R. *et al.* Sgk1 activates MDM2-dependent p53 degradation and affects cell proliferation, survival, and differentiation. *J. Mol. Med.* **87**, 1221–1239 (2009).

38. Murakami, Y. *et al.* Identification of sites subjected to serine/threonine phosphorylation by SGK1 affecting N-myc downstream-regulated gene 1 (NDRG1)/Cap43-dependent suppression of angiogenic CXC chemokine expression in human pancreatic cancer cells. *Biochem. Biophys. Res. Commun.* **396**, 376–381 (2010).

39. Lang, F. & Shumilina, E. Regulation of ion channels by the serum- and glucocorticoid-inducible kinase SGK1. *FASEB J.* **27**, 3–12 (2013).

40. D'Antona, L. *et al.* In Preclinical Model of Ovarian Cancer, the SGK1 Inhibitor SI113 Counteracts the Development of Paclitaxel Resistance and Restores Drug Sensitivity. *Transl. Oncol.* **12**, 1045–1055 (2019).

41. Liu, W. *et al.* SGK1 inhibition induces autophagy-dependent apoptosis via the mTOR-Foxo3a pathway. *Br. J. Cancer* (2017). doi:10.1038/bjc.2017.293

42. Tang, Z. *et al.* Serum and glucocorticoid-regulated kinase 1 (SGK1) is a predictor of poor prognosis in non-small cell lung cancer, and its dynamic pattern following treatment with SGK1 inhibitor and γ-ray irradiation was elucidated. *Oncol. Rep.* **39**, 1505–1515 (2018).

43. Talarico, C. *et al.* SI113, a SGK1 inhibitor, potentiates the effects of radiotherapy, modulates the response to oxidative stress and induces cytotoxic autophagy in human glioblastoma multiforme cells. *Oncotarget* **7**, 15868–15884 (2016).

44. Davidson, B. *et al.* Gene expression signatures of primary and metastatic uterine leiomyosarcoma. *Hum. Pathol.* **45**, 691–700 (2014).

45. Xiaobo, Y. *et al.* Serum and glucocorticoid kinase 1 promoted the growth and migration of non-small cell lung cancer cells. *Gene* **576**, 339–346 (2016).

46. Talarico, C. *et al.* SGK1, the New Player in the Game of Resistance: Chemo-Radio Molecular Target and Strategy for Inhibition. *Cellular Physiology and Biochemistry* **39**, 1863–1876 (2016).

47. Sherk, A. B. *et al.* Development of a small-molecule serum- and glucocorticoid-regulated kinase-1 antagonist and its evaluation as a prostate cancer therapeutic. *Cancer Res.* **68**, 7475–7483 (2008).

48. Szmulewitz, R. Z. *et al.* Serum/glucocorticoid-regulated kinase 1 expression in primary human prostate cancers. *Prostate* **72**, 157–164 (2012).

49. Isikbay, M. *et al.* Glucocorticoid Receptor Activity Contributes to Resistance to Androgen-Targeted Therapy in Prostate Cancer. *Horm. Cancer* **5**, 72–89 (2014).

50. Chen, F. *et al.* Radiation-induced glucocorticoid receptor promotes CD44+ prostate cancer stem cell growth through activation of SGK1-Wnt/β-catenin signaling. *J. Mol. Med.* **97**, 1169–1182 (2019).

51. Nasir, O. *et al.* Relative resistance of SGK1 knockout mice against chemical carcinogenesis. *IUBMB Life* (2009). doi:10.1002/iub.209

52. Amato, R. *et al.* Sgk1 enhances RANBP1 transcript levels and decreases taxol sensitivity in RKO colon carcinoma cells. *Oncogene* **32**, 4572–4578 (2013).

53. D'Antona, L. *et al.* SI113, a specific inhibitor of the Sgk1 kinase activity that counteracts cancer cell proliferation. *Cell. Physiol. Biochem.* **35**, 2006–2018 (2015).

54. Liang, X. *et al.* Development of a new analog of SGK1 inhibitor and its evaluation as a therapeutic molecule of colorectal cancer. *J. Cancer* **8**, 2256–2262 (2017).

55. Zhu, J. *et al.* Knockdown of long non-coding RNA XIST inhibited doxorubicin resistance in colorectal cancer by upregulation of miR-124 and downregulation of SGK1. *Cell. Physiol. Biochem.* **51**, 113–128 (2018).

56. Conza, D. *et al.* The SGK1 inhibitor SI113 induces autophagy, apoptosis, and endoplasmic reticulum stress in endometrial cancer cells. *J. Cell. Physiol.* **232**, 3735–3743 (2017).

57. Wang, M. *et al.* Inhibition of SGK1 confers vulnerability to redox dysregulation in cervical cancer. *Redox Biol.* **24**, 101225 (2019).

58. Sommer, E. M. *et al.* Elevated SGK1 predicts resistance of breast cancer cells to Akt inhibitors. *Biochem. J.* **452**, 499–508 (2013).

59. Salis, O. *et al.* Cytotoxic effect of fluvastatin on MCF-7 cells possibly through a reduction of the mRNA expression levels of SGK1 and CAV1. *Cancer Biother. Radiopharm.* **29**, 368–375 (2014).

60. Castel, P. *et al.* PDK1-SGK1 Signaling Sustains AKT-Independent mTORC1 Activation and Confers Resistance to PI3Kα Inhibition. *Cancer Cell* **30**, 229–242 (2016).

61. Ma, X. *et al.* Characterization of the Src-regulated kinome identifies SGK1 as a key mediator of Src-induced transformation. *Nat. Commun.* **10**, 1–16 (2019).

62. Won, M. *et al.* Protein kinase SGK1 enhances MEK/ERK complex formation through the phosphorylation of ERK2: Implication for the positive regulatory role of SGK1 on the ERK function during liver regeneration. *J. Hepatol.* **51**, 67–76 (2009).

63. Salis, O. *et al.* Antimetastatic effect of fluvastatin on breast and hepatocellular carcinoma cells in relation to SGK1 and NDRG1 genes. *Tumor Biol.* **37**, 3017–3024 (2016).

64. Talarico, C. *et al.* Preclinical model in HCC: The SGK1 kinase inhibitor SI113 blocks tumor progression in vitro and in vivo and synergizes with radiotherapy. *Oncotarget* **6**, 37511–37525 (2015).

65. Catalogna, G. *et al.* The SGK1 Kinase Inhibitor SI113 Sensitizes Theranostic Effects of

the 64CuCl2 in Human Glioblastoma Multiforme Cells. *Cell. Physiol. Biochem.* **43**, 108–119 (2017).

66. Kulkarni, S., Goel-Bhattacharya, S., Sengupta, S. & Cochran, B. H. A large-scale RNAi screen identifies SGK1 as a key survival kinase for GBM stem cells. *Mol. Cancer Res.* **16**, 103–114 (2018).

67. Matteoni, S. *et al.* The kinase inhibitor SI113 induces autophagy and synergizes with quinacrine in hindering the growth of human glioblastoma multiforme cells. *J. Exp. Clin. Cancer Res.* **38**, 1–13 (2019).

68. Von Wowern, F. *et al.* Genetic variance of SGK-1 is associated with blood pressure, blood pressure change over time and strength of the insulin-diastolic blood pressure relationship. *Kidney Int.* **68**, 2164–2172 (2005).

69. Schwab, M. *et al.* Association of SGK1 gene polymorphisms with type 2 diabetes. *Cell. Physiol. Biochem.* **21**, 151–160 (2008).

70. Lang, F., Yang Huang, D. Y. & Vallon, V. SGK, renal function and hypertension. *J. Nephrol.* **23**, (2010).

71. Schernthaner-Reiter, M. H. *et al.* Strong association of serum-and glucocorticoid-regulated kinase 1 with peripheral and adipose tissue inflammation in obesity. *Int. J. Obes.* **39**, 1143–1150 (2015).

72. Johnson, A. M. F. & Olefsky, J. M. The origins and drivers of insulin resistance. *Cell* **152**, 673–684 (2013).

73. Li, P. *et al.* SGK1 is regulated by metabolic-related factors in 3T3-L1 adipocytes and overexpressed in the adipose tissue of subjects with obesity and diabetes. *Diabetes Res. Clin. Pract.* **102**, 35–42 (2013).

74. Ingley, E. Src family kinases: Regulation of their activities, levels and identification of new pathways. *Biochim. Biophys. Acta - Proteins Proteomics* **1784**, 56–65 (2008).

75. Magić, Z. The nobel prize in physiology or medicine 2009. *Vojnosanitetski Pregled* **66**, 861 (2009).

76. Roskoski, R. Src protein-tyrosine kinase structure and regulation. *Biochem. Biophys. Res. Commun.* **324**, 1155–1164 (2004).

77. Espada, J. & Martín-Pérez, J. An Update on Src Family of Nonreceptor Tyrosine Kinases Biology. *Int. Rev. Cell Mol. Biol.* **331**, 83–122 (2017).

78. Resh, M. D. Fatty acylation of proteins: New insights into membrane targeting of myristoylated and palmitoylated proteins. *Biochim. Biophys. Acta - Mol. Cell Res.* **1451**, 1–16 (1999).

79. Guarino, M. Src signaling in cancer invasion. *J. Cell. Physiol.* **223**, 14–26 (2010).

80. Grant, S. & Dent, P. Kinase Inhibitors and Cytotoxic Drug Resistance. *Clin. Cancer Res.* **10**, 2205–2207 (2004).

81. Irby, R. B. & Yeatman, T. J. Role of Src expression and activation in human cancer. *Oncogene* **19**, 5636–5642 (2000).

82. Couto, M. *et al.* Discovery of Potent EGFR Inhibitors through the Incorporation of a 3D-Aromatic-Boron-Rich-Cluster into the 4-Anilinoquinazoline Scaffold: Potential Drugs for Glioma Treatment. *Chem. - A Eur. J.* **24**, 3122–3126 (2018).

83. Du, J. *et al.* Bead-based profiling of tyrosine kinase phosphorylation identifies SRC as a potential target for glioblastoma therapy. *Nat. Biotechnol.* **27**, 77–83 (2009).

84. Vignaroli, G. *et al.* Prodrugs of Pyrazolo[3,4- *d*]pyrimidines: From Library Synthesis to Evaluation as Potential Anticancer Agents in an Orthotopic Glioblastoma Model. *J. Med. Chem.* **60**, 6305–6320 (2017).

85. Yamaguchi, K., Kugimiya, T. & Miyazaki, T. Substance P receptor in U373 MG human astrocytoma cells activates mitogen-activated protein kinases ERK1/2 through Src. *Brain Tumor Pathol.* **22**, 1–8 (2005).

86. Calgani, A. *et al.* Suppression of SRC signaling is effective in reducing synergy between glioblastoma and stromal cells. *Mol. Cancer Ther.* **15**, 1535–1544 (2016).

87. Fallacara, A. L. *et al.* A New Strategy for Glioblastoma Treatment: In Vitro and In Vivo Preclinical Characterization of Si306, a Pyrazolo[3,4-d]Pyrimidine Dual Src/P-Glycoprotein Inhibitor. *Cancers (Basel).* **11**, 848 (2019).

88. Bolen, J. B., Rosen, N. & Israel, M. A. Increased pp60(c-src) tyrosyl kinase activity in human neuroblastomas is associated with amino-terminal tyrosine phosphorylation of the src gene product. *Proc. Natl. Acad. Sci. U. S. A.* **82**, 7275–7279 (1985).

89. Kratimenos, P. *et al.* FAK-Src-paxillin system expression and disease outcome in human neuroblastoma. *Pediatr. Hematol. Oncol.* **34**, 221–230 (2017).

90. Kratimenos, P. *et al.* Multi-targeted molecular therapeutic approach in aggressive neuroblastoma: The effect of Focal Adhesion Kinase-Src-Paxillin system. *Expert Opin. Ther. Targets* **18**, 1395–1406 (2014).

91. Molinari, A. *et al.* Efficient optimization of pyrazolo[3,4-d]pyrimidines derivatives as c-Src kinase inhibitors in neuroblastoma treatment. *Bioorg. Med. Chem. Lett.* **28**, 3454–3457 (2018).

92. Tintori, C. *et al.* Combining X-ray crystallography and molecular modeling toward the optimization of pyrazolo[3,4-d]pyrimidines as potent c-Src inhibitors active in vivo against neuroblastoma. *J. Med. Chem.* **58**, 347–361 (2015).

93. Rossi, A. *et al.* New pyrazolo-[3,4-d]-pyrimidine derivative Src kinase inhibitors lead to cell cycle arrest and tumor growth reduction of human medulloblastoma cells. *FASEB J.* **24**, 2881–2892 (2010).

94. Forget, A. *et al.* Aberrant ERBB4-SRC Signaling as a Hallmark of Group 4 Medulloblastoma Revealed by Integrative Phosphoproteomic Profiling. *Cancer Cell* **34**, 379-395.e7 (2018).

95. Semba, K. *et al.* yes-related protooncogene, syn, belongs to the protein-tyrosine kinase family. *Proc. Natl. Acad. Sci. U. S. A.* **83**, 5459–63 (1986).

96. Alland, L., Peseckis, S. M., Atherton, R. E., Berthiaume, L. & Resh, M. D. Dual myristylation and palmitylation of Src family member p59(fyn) affects subcellular

localization. *J. Biol. Chem.* (1994).

97. Goldsmith, J. F., Hall, C. G. & Atkinson, T. P. Identification of an alternatively spliced isoform of the fyn tyrosine kinase. *Biochem. Biophys. Res. Commun.* **298**, 501–504 (2002).

98. Elias, D. & Ditzel, H. J. Fyn is an important molecule in cancer pathogenesis and drug resistance. *Pharmacol. Res.* **100**, 250–254 (2015).

99. Jelić, D. *et al.* Homology modeling of human Fyn kinase structure: Discovery of rosmarinic acid as a new Fyn kinase inhibitor and in Silico study of its possible binding modes. *J. Med. Chem.* **50**, 1090–1100 (2007).

100. Saito, Y. D., Jensen, A. R., Salgia, R. & Posadas, E. M. Fyn: A novel molecular target in cancer. *Cancer* **116**, 1629–1637 (2010).

101. Schenone, S. *et al.* Fyn Kinase in Brain Diseases and Cancer: The Search for Inhibitors. *Curr. Med. Chem.* **18**, 2921–2942 (2011).

102. Lim, S. H. *et al.* Synapse formation regulated by protein tyrosine phosphatase receptor T through interaction with cell adhesion molecules and Fyn. *EMBO J.* **28**, 3564–3578 (2009).

103. Palacios, E. H. & Weiss, A. Function of the Src-family kinases, Lck and Fyn, in T-cell development and activation. *Oncogene* **23**, 7990–8000 (2004).

104. Kawakami, T., Kawakami, Y., Aaronson, S. A. & Robbins, K. C. Acquisition of transforming properties by FYN, a normal SRC-related human gene. *Proc. Natl. Acad. Sci. U. S. A.* **85**, 3870–3874 (1988).

105. Paszek, M. J. *et al.* Tensional homeostasis and the malignant phenotype. *Cancer Cell* **8**, 241–254 (2005).

106. Zhang, S. *et al.* Suppression of protein tyrosine phosphatase N23 predisposes to breast tumorigenesis via activation of FYN kinase. *Genes Dev.* **31**, 1939–1957 (2017).

107. Elias, D. *et al.* Gene expression profiling identifies FYN as an important molecule in tamoxifen resistance and a predictor of early recurrence in patients treated with endocrine therapy. *Oncogene* **34**, 1919–1927 (2014).

108. Irwin, M. E., Johnson, B. P., Manshouri, R., Amin, H. M. & Chandra, J. A NOX2/Egr-1/Fyn pathway delineates new targets for TKI-resistant malignancies. *Oncotarget* **6**, 23631–23646 (2015).

109. Fenouille, N. *et al.* Persistent activation of the Fyn/ERK kinase signaling axis mediates imatinib resistance in chronic myelogenous leukemia cells through upregulation of intracellular SPARC. *Cancer Res.* **70**, 9659–9670 (2010).

110. Singh, M. M. *et al.* Expression and Activity of Fyn Mediate Proliferation and Blastic Features of Chronic Myelogenous Leukemia. *PLoS One* **7**, e51611 (2012).

111. Garcia, S. *et al.* Overexpression of c-Met and of the transducers PI3K, FAK and JAK in breast carcinomas correlates with shorter survival and neoangiogenesis. *Int. J. Oncol.* **31**, 49–58 (2007).

112. Lee, G.-H. *et al.* FYN promotes mesenchymal phenotypes of basal type breast cancer cells through STAT5/NOTCH2 signaling node. *Oncogene* **37**, 1857–1868 (2018).

113. Mi, H. *et al.* miR-381 induces sensitivity of breast cancer cells to doxorubicin by inactivation of MAPK signaling via FYN. *Eur. J. Pharmacol.* **839**, 66–75 (2018).

114. Posadas, E. M. *et al.* FYN is overexpressed in human prostate cancer. *BJU Int.* **103**, 171–177 (2009).

115. Gururajan, M. *et al.* SRC family kinase FYN promotes the neuroendocrine phenotype and visceral metastasis in advanced prostate cancer. *Oncotarget* **6**, 44072–44083 (2015).

116. Jensen, A. R. *et al.* Fyn Is Downstream of the HGF/MET Signaling Axis and Affects Cellular Shape and Tropism in PC3 Cells. *Clin. Cancer Res.* **17**, 3112–3122 (2011).

117. Huang, J., Asawa, T., Takato, T. & Sakai, R. Cooperative Roles of Fyn and Cortactin in Cell Migration of Metastatic Murine Melanoma. *J. Biol. Chem.* **278**, 48367–48376 (2003).

118. Huang, C., Sheng, Y., Jia, J. & Chen, L. Identification of melanoma biomarkers based on network modules by integrating the human signaling network with microarrays. *J. Cancer Res. Ther.* **10**, C114–C124 (2014).

119. Lu, K. V. *et al.* Fyn and Src are effectors of oncogenic epidermal growth factor receptor signaling in glioblastoma patients. *Cancer Res.* **69**, 6889–6898 (2009).

120. Lewis-Tuffin, L. J. *et al.* Src family kinases differentially influence glioma growth and motility. *Mol. Oncol.* **9**, 1783–1798 (2015).

121. Zhang, S. *et al.* Fyn-phosphorylated PIKE-A binds and inhibits AMPK signaling, blocking its tumor suppressive activity. *Cell Death Differ.* **23**, 52–63 (2016).

122. Comba, A. *et al.* CSIG-39. Fyn, AN ONCOGENE THAT REDUCES GLIOBLASTOMA SURVIVAL YET SENSITIZES TO CHEMO-RADIOTHERAPY. *Neuro. Oncol.* **19**, vi58–vi58 (2017).

123. Barragán Martínez, D., García Soldevilla, M. A., Parra Santiago, A. & Tejeiro Martínez, J. Alzheimer's disease. *Med.* **12**, 4338–4346 (2019).

124. Tintori, C. *et al.* Studies on the ATP Binding Site of Fyn Kinase for the Identification of New Inhibitors and Their Evaluation as Potential Agents against Tauopathies and Tumors. *J. Med. Chem.* **58**, 4590–4609 (2015).

125. Nygaard, H. B. Targeting Fyn Kinase in Alzheimer's Disease. *Biol. Psychiatry* **83**, 369–376 (2018).

126. Panicker, N. *et al.* Fyn kinase regulates misfolded α-synuclein uptake and NLRP3 inflammasome activation in microglia. *J. Exp. Med.* **216**, 1411–1430 (2019).

127. Ellis, C. E., Schwartzberg, P. L., Grider, T. L., Fink, D. W. & Nussbaum, R. L. α-Synuclein Is Phosphorylated by Members of the Src Family of Protein-tyrosine Kinases. *J. Biol. Chem.* **276**, 3879–3884 (2001).

128. Nakamura, T., Yamashita, H., Takahashi, T. & Nakamura, S. Activated Fyn phosphorylates α-synuclein at tyrosine residue 125. *Biochem. Biophys. Res. Commun.*

280, 1085–1092 (2001).

129. Panicker, N. *et al.* Fyn kinase regulates microglial neuroinflammatory responses in cell culture and animal models of parkinson's disease. *J. Neurosci.* **35**, 10058–10077 (2015).

130. Sanz-Blasco, S. *et al.* The Kinase Fyn As a Novel Intermediate in l-DOPA-Induced Dyskinesia in Parkinson's Disease. *Mol. Neurobiol.* **55**, 5125–5136 (2018).

131. Cohen, M. H. *et al.* Approval summary for imatinib mesylate capsules in the treatment of chronic Myelogenous Leukemia. *Clin. Cancer Res.* (2002).

132. Zuccotto, F., Ardini, E., Casale, E. & Angiolini, M. Through the "Gatekeeper Door": Exploiting the Active Kinase Conformation. *J. Med. Chem.* **53**, 2681–2694 (2010).

133. Lamba, V. & Ghosh, I. New Directions in Targeting Protein Kinases: Focusing Upon True Allosteric and Bivalent Inhibitors. *Curr. Pharm. Des.* **18**, 2936–2945 (2012).

134. Yaish, P., Gazit, A., Gilon, C. & Levitzki, A. Blocking of EGF-dependent cell proliferation by EGF receptor kinase inhibitors. *Science (80-.).* **242**, 933–935 (1988).

135. Berdel, H. O. *et al.* Targeting serum glucocorticoid-regulated kinase-1 in squamous cell carcinoma of the head and neck: A novel modality of local control. *PLoS One* **9**, (2014).

136. Ackermann, T. F. *et al.* EMD638683, a novel SGK inhibitor with antihypertensive potency. *Cell. Physiol. Biochem.* **28**, 137–146 (2011).

137. Towhid, S. T. *et al.* Inhibition of colonic tumor growth by the selective SGK inhibitor EMD638683. *Cell. Physiol. Biochem.* **32**, 838–848 (2013).

138. Schmid, E. *et al.* Serum and Glucocorticoid Inducible Kinase 1-Sensitive Survival, Proliferation and Migration of Rhabdomyosarcoma Cells. *Cell. Physiol. Biochem.* **43**, 1301–1308 (2017).

139. Nazarè, M. et al. N-[a-(1H-pyrazolo[3,4-b]pyrazin-6-yl)-Phenyl]-Sulfonamides and Their Use as Pharmaceuticals. WO2013041119. (2013).

140. Bezzerides, V. J. *et al.* Inhibition of serum and glucocorticoid regulated kinase-1 as novel therapy for cardiac arrhythmia disorders. *Sci. Rep.* **7**, 346 (2017).

141. Ortuso, F. *et al.* In silico identification and biological evaluation of novel selective serum/glucocorticoid-inducible kinase 1 inhibitors based on the pyrazolo-pyrimidine scaffold. *J. Chem. Inf. Model.* **54**, 1828–1832 (2014).

142. Abbruzzese, C. *et al.* The small molecule SI113 synergizes with mitotic spindle poisons in arresting the growth of human glioblastoma multiforme. *Oncotarget* **8**, 110743–110755 (2017).

143. Abbruzzese, C. *et al.* The small molecule SI113 hinders epithelial-to-mesenchymal transition and subverts cytoskeletal organization in human cancer cells. *J. Cell. Physiol.* **234**, 22529–22542 (2019).

144. Catalogna, G. *et al.* Review about the multi-target profile of resveratrol and its implication in the SGK1 inhibition. *Eur. J. Med. Chem.* **183**, 111675 (2019).

145. Hanke, J. H. *et al.* Discovery of a novel, potent, and Src family-selective tyrosine kinase

inhibitor: Study of Lck- and FynT-dependent T cell activation. *J. Biol. Chem.* **271**, 695–701 (1996).

146. Tatton, L., Morley, G. M., Chopra, R. & Khwaja, A. The Src-selective kinase inhibitor PP1 also inhibits kit and Bcr-Abl tyrosine kinases. *J. Biol. Chem.* **278**, 4847–4853 (2003).

147. Kong, L., Deng, Z., Shen, H. & Zhang, Y. Src family kinase inhibitor PP2 efficiently inhibits cervical cancer cell proliferation through down-regulating phospho-Src-Y416 and phospho-EGFR-Y1173. *Mol. Cell. Biochem.* **348**, 11–19 (2011).

148. Lindauer, M. & Hochhaus, A. Dasatinib. in *Recent results in cancer research. Fortschritte der Krebsforschung. Progres dans les recherches sur le cancer* **201**, 27–65 (2014).

149. Shah, N. P. *et al.* Overriding imatinib resistance with a novel ABL kinase inhibitor. *Science (80-.).* **305**, 399–401 (2004).

150. Li, J. *et al.* A chemical and phosphoproteomic characterization of dasatinib action in lung cancer. *Nat. Chem. Biol.* **6**, 291–299 (2010).

151. Green, T. P. *et al.* Preclinical anticancer activity of the potent, oral Src inhibitor AZD0530. *Mol. Oncol.* **3**, 248–261 (2009).

152. Nam, H. J. *et al.* Antitumor activity of saracatinib (AZD0530), a c-Src/Abl kinase inhibitor, alone or in combination with chemotherapeutic agents in gastric cancer. *Mol. Cancer Ther.* **12**, 16–26 (2013).

153. Boschelli, D. H. *et al.* Optimization of 4-phenylamino-3-quinolinecarbonitriles as potent inhibitors of Src kinase activity. *J. Med. Chem.* **44**, 3965–3977 (2001).

154. Puttini, M. *et al.* In vitro and in vivo activity of SKI-606, a novel Src-Abl inhibitor, against imatinib-resistant Bcr-Abl+ neoplastic cells. *Cancer Res.* **66**, 11314–11322 (2006).

155. Lou, J., McGinnis, L. K. & Kinsey, W. H. FYn Kinase Activity Is Required for Normal Organization and Functional Polarity of the Mouse Oocyte Cortex. *Mol. Reprod. Dev.* **76**, 819–831 (2009).

156. Ma, J. *et al.* PH006, a novel and selective Src kinase inhibitor, suppresses human breast cancer growth and metastasis in vitro and in vivo. *Breast Cancer Res. Treat.* **130**, 85–96 (2011).

157. Huang, H. *et al.* Discovery of novel purine derivatives with potent and selective inhibitory activity against c-Src tyrosine kinase. *Bioorganic Med. Chem.* **18**, 4615–4624 (2010).

158. Fallah-Tafti, A. *et al.* Thiazolyl N-benzyl-substituted acetamide derivatives: Synthesis, Src kinase inhibitory and anticancer activities. *Eur. J. Med. Chem.* **46**, 4853–4858 (2011).

159. Smolinski, M. P. *et al.* Discovery of Novel Dual Mechanism of Action Src Signaling and Tubulin Polymerization Inhibitors (KX2-391 and KX2-361). *J. Med. Chem.* **61**, 4704–4719 (2018).

160. Naing, A. *et al.* A phase i trial of KX2-391, a novel non-ATP competitive substrate-pocket- directed SRC inhibitor, in patients with advanced malignancies. *Invest. New Drugs* **31**, 967–973 (2013).

161. Niu, L. *et al.* Reversible binding of the anticancer drug KXO1 (tirbanibulin) to the colchicine-binding site of β-tubulin explains KXO1's low clinical toxicity. *J. Biol. Chem.* jbc.RA119.010732 (2019). doi:10.1074/jbc.ra119.010732

162. Moroco, J. A. *et al.* A Discovery Strategy for Selective Inhibitors of c-Src in Complex with the Focal Adhesion Kinase SH3/SH2-binding Region. *Chem. Biol. Drug Des.* **86**, 144–155 (2015).

163. Lavogina, D., Enkvist, E. & Uri, A. Bisubstrate inhibitors of protein kinases: From principle to practical applications. *ChemMedChem* **5**, 23–34 (2010).

164. Brandvold, K. R. *et al.* Exquisitely Specific Bisubstrate Inhibitors of c-Src Kinase. *ACS Chem. Biol.* **10**, 1387–1391 (2015).

165. Dalgarno, D. *et al.* Structural basis of Src tyrosine kinase inhibition with a new class of potent and selective trisubstituted purine-based compounds. *Chem. Biol. Drug Des.* **67**, 46–57 (2006).

166. Moy, F. J. *et al.* Novel synthesis and structural characterization of a high-affinity paramagnetic kinase probe for the identification of non-ATP site binders by nuclear magnetic resonance. *J. Med. Chem.* **53**, 1238–1249 (2010).

167. Bamborough, P., Drewry, D., Harper, G., Smith, G. K. & Schneider, K. Assessment of chemical coverage of kinome space and its implications for kinase drug discovery. *J. Med. Chem.* **51**, 7898–7914 (2008).

168. Nathan Tumey, L., Boschelli, D. H., Lee, J. & Chaudhary, D. 2-Alkenylthieno[2,3-b]pyridine-5-carbonitriles: Potent and selective inhibitors of PKCθ. *Bioorg. Med. Chem. Lett.* **18**, 4420–4423 (2008).

169. Chen, P. *et al.* Discovery of novel 2-(aminoheteroaryl)-thiazole-5-carboxamides as potent and orally active Src-family kinase p56 Lck inhibitors. *Bioorganic Med. Chem. Lett.* **14**, 6061–6066 (2004).

170. Parker, L. J. *et al.* Kinase crystal identification and ATP-competitive inhibitor screening using the fluorescent ligand SKF86002. *Acta Crystallogr. Sect. D Biol. Crystallogr.* **70**, 392–404 (2014).

171. Rong, H., Liang, Y. & Niu, Y. Rosmarinic acid attenuates β-amyloid-induced oxidative stress via Akt/GSK-3β/Fyn-mediated Nrf2 activation in PC12 cells. *Free Radic. Biol. Med.* **120**, 114–123 (2018).

172. Fallacara, A. L. *et al.* Identification of a new family of pyrazolo[3,4-d]pyrimidine derivatives as multitarget Fyn-Blk-Lyn inhibitors active on B- and T-lymphoma cell lines. *Eur. J. Med. Chem.* **181**, 111545 (2019).

173. Schenone, S., Radi, M., Musumeci, F., Brullo, C. & Botta, M. Biologically Driven Synthesis of Pyrazolo[3,4- *d*]pyrimidines As Protein Kinase Inhibitors: An Old Scaffold As a New Tool for Medicinal Chemistry and Chemical Biology Studies. *Chem. Rev.* **114**, 7189–7238 (2014).

174. El-Moghazy, S. M. *et al.* Novel pyrazolo[3,4-d]pyrimidines as dual Src-Abl inhibitors active against mutant form of Abl and the leukemia K-562 cell line. *Eur. J. Med. Chem.* **123**, 1–13 (2016).

175. Agholme, L., Lindström, T., Kgedal, K., Marcusson, J. & Hallbeck, M. An in vitro model for neuroscience: Differentiation of SH-SY5Y cells into cells with morphological and biochemical characteristics of mature neurons. *J. Alzheimer's Dis.* **20**, 1069–1082 (2010).

176. Wong, J., Higgins, M., Halliday, G. & Garner, B. Amyloid beta selectively modulates neuronal TrkB alternative transcript expression with implications for Alzheimer's disease. *Neuroscience* **210**, 363–374 (2012).

177. Sanna, M. *et al.* Water Solubility Enhancement of Pyrazolo[3,4- d] pyrimidine Derivatives via Miniaturized Polymer-Drug Microarrays. *ACS Med. Chem. Lett.* **9**, 193–197 (2018).

178. Christison-Lagay, E. R. & Langer, J. C. Lymphatic malformations. *Newborn Surgery, Fourth Ed.* 882–893 (2017). doi:10.4324/9781315113968

179. Huang, M. & Weiss, W. A. Neuroblastoma and MYCN. *Cold Spring Harb. Perspect. Med.* **3**, (2013).

180. Pearson, A. D. *et al.* High-dose rapid and standard induction chemotherapy for patients aged over 1 year with stage 4 neuroblastoma: a randomised trial. *Lancet Oncol.* **9**, 247–256 (2008).

181. Park, J. R., Eggert, A. & Caron, H. Neuroblastoma: Biology, Prognosis, and Treatment. *Hematol. Oncol. Clin. North Am.* **24**, 65–86 (2010).

182. Wheeler, D. L., Iida, M. & Dunn, E. F. The Role of Src in Solid Tumors. *Oncologist* **14**, 667–678 (2009).

183. Batash, R., Asna, N., Schaffer, P., Francis, N. & Schaffer, M. Glioblastoma Multiforme, Diagnosis and Treatment; Recent Literature Review. *Curr. Med. Chem.* **24**, (2017).

184. Alifieris, C. & Trafalis, D. T. Glioblastoma multiforme: Pathogenesis and treatment. *Pharmacol. Ther.* **152**, 63–82 (2015).

185. Perrin, S. L. *et al.* Glioblastoma heterogeneity and the tumour microenvironment: Implications for preclinical research and development of new treatments. *Biochem. Soc. Trans.* **47**, 625–638 (2019).

186. LemCrossed D Sign©e, J. M., Clavreul, A. & Menei, P. Intratumoral heterogeneity in glioblastoma: Don't forget the peritumoral brain zone. *Neuro. Oncol.* **17**, 1322–1332 (2015).

187. Petrecca, K., Guiot, M. C., Panet-Raymond, V. & Souhami, L. Failure pattern following complete resection plus radiotherapy and temozolomide is at the resection margin in patients with glioblastoma. *J. Neurooncol.* **111**, 19–23 (2013).

188. Carrasco-García, E., Saceda, M. & Martínez-Lacaci, I. Role of Receptor Tyrosine Kinases and Their Ligands in Glioblastoma. *Cells* **3**, 199–235 (2014).

189. Li, X. *et al.* PI3K/Akt/mTOR signaling pathway and targeted therapy for glioblastoma. *Oncotarget* **7**, 33440–33450 (2016).

190. Arora, A. & Scholar, E. M. Role of tyrosine kinase inhibitors in cancer therapy. *J. Pharmacol. Exp. Ther.* **315**, 971–979 (2005).

191. Liu, W. M. *et al.* Lyn Facilitates Glioblastoma Cell Survival under Conditions of Nutrient Deprivation by Promoting Autophagy. *PLoS One* **8**, (2013).

192. Huveldt, D. *et al.* Targeting Src Family Kinases Inhibits Bevacizumab-Induced Glioma Cell Invasion. *PLoS One* **8**, (2013).

193. Lund, C. V. *et al.* Reduced glioma infiltration in Src-deficient mice. *J. Neurooncol.* **78**, 19–29 (2006).

194. Ahluwalia, M. S., Groot, J. de, Liu, W. M. & Gladson, C. L. Targeting SRC in glioblastoma tumors and brain metastases: Rationale and preclinical studies. *Cancer Lett.* **298**, 139–149 (2010).

195. Lassman, A. B. *et al.* Phase 2 trial of dasatinib in target-selected patients with recurrent glioblastoma (RTOG 0627). *Neuro. Oncol.* **17**, 992–998 (2015).

196. Galanis, E. *et al.* A phase 1 and randomized, placebo-controlled phase 2 trial of bevacizumab plus dasatinib in patients with recurrent glioblastoma: Alliance/North Central Cancer Treatment Group N0872. *Cancer* **125**, 3790–3800 (2019).

197. Agarwal, S. *et al.* Active efflux of dasatinib from the brain limits efficacy against murine glioblastoma: Broad implications for the clinical use of molecularly targeted agents. *Mol. Cancer Ther.* **11**, 2183–2192 (2012).

198. Dreassi, E. *et al.* 2-Hydroxypropyl-β-cyclodextrin strongly improves water solubility and anti-proliferative activity of pyrazolo[3,4-d]pyrimidines Src-Abl dual inhibitors. *Eur. J. Med. Chem.* **45**, 5958–5964 (2010).

199. Vignaroli, G. *et al.* Improvement of pyrazolo[3,4-d]pyrimidines pharmacokinetic properties: Nanosystem approaches for drug delivery. *Sci. Rep.* **6**, (2016).

200. Fallacara, A. L. *et al.* Pyrazolo[3,4-d]pyrimidines-loaded human serum albumin (HSA) nanoparticles: Preparation, characterization and cytotoxicity evaluation against neuroblastoma cell line. *Bioorganic Med. Chem. Lett.* **27**, 3196–3200 (2017).

201. Vignaroli, G. *et al.* Pyrazolo[3,4-d]pyrimidine prodrugs: Strategic optimization of the aqueous solubility of dual Src/Abl inhibitors. *ACS Med. Chem. Lett.* **4**, 622–626 (2013).

202. Baghel, S., Cathcart, H. & O'Reilly, N. J. Polymeric Amorphous Solid Dispersions: A Review of Amorphization, Crystallization, Stabilization, Solid-State Characterization, and Aqueous Solubilization of Biopharmaceutical Classification System Class II Drugs. *J. Pharm. Sci.* **105**, 2527–2544 (2016).

203. Van Eerdenbrugh, B. & Taylor, L. S. Small scale screening to determine the ability of different polymers to inhibit drug crystallization upon rapid solvent evaporation. *Mol. Pharm.* **7**, 1328–1337 (2010).

204. Lennernäs, H. & Abrahamsson, B. The biopharmaceutics classification system. *Compr.*

Med. Chem. II **5**, 971–988 (2006).

205. Radi, M. *et al.* Design, synthesis, biological activity, and ADME properties of pyrazolo[3,4- d]pyrimidines active in hypoxic human leukemia Cells: A lead optimization study. *J. Med. Chem.* **54**, 2610–2626 (2011).

206. Porter, A. G. & Jänicke, R. U. Emerging roles of caspase-3 in apoptosis. *Cell Death and Differentiation* **6**, 99–104 (1999).

207. Belmokhtar, C. A., Hillion, J. & Ségal-Bendirdjian, E. Staurosporine induces apoptosis through both caspase-dependent and caspase-independent mechanisms. *Oncogene* **20**, 3354–3362 (2001).

208. Hoek, J. B., Cahill, A. & Pastorino, J. G. Alcohol and mitochondria: A dysfunctional relationship. *Gastroenterology* **122**, 2049–2063 (2002).

209. Rao, R. D. *et al.* Disruption of parallel and converging signaling pathways contributes to the synergistic antitumor effects of simultaneous mTOR and EGFR inhibition in GBM cells. *Neoplasia* **7**, 921–929 (2005).

210. Garuti, L., Roberti, M. & Bottegoni, G. Multi-Kinase Inhibitors. *Curr. Med. Chem.* **22**, 695–712 (2015).

211. Chou, T. C. Drug combination studies and their synergy quantification using the chou-talalay method. *Cancer Res.* **70**, 440–446 (2010).

212. Taresco, V. *et al.* Rapid Nanogram Scale Screening Method of Microarrays to Evaluate Drug-Polymer Blends Using High-Throughput Printing Technology. *Mol. Pharm.* **14**, 2079–2087 (2017).

213. Styliari, I. D. *et al.* High-Throughput Miniaturized Screening of Nanoparticle Formation via Inkjet Printing. *Macromol. Mater. Eng.* **303**, 1800146 (2018).

214. Chou, T. C. Theoretical basis, experimental design, and computerized simulation of synergism and antagonism in drug combination studies. *Pharmacol. Rev.* **58**, 621–681 (2006).

215. Frieden, T. Antibiotic resistance threats in the United States. *Centers Dis. Control Prev.* **114**, (2013).

216. Wohlleben, W., Mast, Y., Stegmann, E. & Ziemert, N. Antibiotic drug discovery. *Microb. Biotechnol.* **9**, 541–548 (2016).

217. Levitzki, A. Protein kinase inhibitors. in *Handbook of Cell Signaling, 2/e* **2**, 481–490 (2010).

218. Muñoz-Dorado, J., Inouye, S. & Inouye, M. A gene encoding a protein serine/threonine kinase is required for normal development of M. xanthus, a gram-negative bacterium. *Cell* **67**, 995–1006 (1991).

219. Shi, L., Potts, M. & Kennelly, P. J. The serine, threonine, and/or tyrosine-specific protein kinases and protein phosphatases of prokaryotic organisms: A family portrait. *FEMS Microbiol. Rev.* **22**, 229–253 (1998).

220. Pensinger, D. A. *et al.* Selective pharmacologic inhibition of a PASTA kinase increases

Listeria monocytogenes susceptibility to β-lactam antibiotics. *Antimicrob. Agents Chemother.* **58**, 4486–4494 (2014).

221. Vornhagen, J. *et al.* Kinase inhibitors that increase the sensitivity of methicillin resistant Staphylococcus aureus to β-lactam antibiotics. *Pathogens* **4**, 708–721 (2015).

222. Chapman, T. M. *et al.* Substituted aminopyrimidine protein kinase B (PknB) inhibitors show activity against Mycobacterium tuberculosis. *Bioorganic Med. Chem. Lett.* **22**, 3349–3353 (2012).

223. Rhodes, N. *et al.* Characterization of an Akt kinase inhibitor with potent pharmacodynamic and antitumor activity. *Cancer Res.* **68**, 2366–2374 (2008).

224. Schaenzer, A. J. *et al.* A screen for kinase inhibitors identifies antimicrobial imidazopyridine aminofurazans as specific inhibitors of the Listeria monocytogenes PASTA kinase PrkA. *J. Biol. Chem.* **292**, 17037–17045 (2017).

225. Bakavoli, M. *et al.* Molecular iodine promoted synthesis of new pyrazolo[3,4-d]pyrimidine derivatives as potential antibacterial agents. *Eur. J. Med. Chem.* **45**, 647–650 (2010).

226. El-Sayed Ali, T. Synthesis of some novel pyrazolo[3,4-b]pyridine and pyrazolo[3,4-d]pyrimidine derivatives bearing 5,6-diphenyl-1,2,4-triazine moiety as potential antimicrobial agents. *Eur. J. Med. Chem.* **44**, 4385–4392 (2009).

227. Holla, B. S., Mahalinga, M., Karthikeyan, M. S., Akberali, P. M. & Shetty, N. S. Synthesis of some novel pyrazolo[3,4-d]pyrimidine derivatives as potential antimicrobial agents. *Bioorganic Med. Chem.* **14**, 2040–2047 (2006).

228. Ali, A. *et al.* Novel pyrazolo[3,4-d]pyrimidine-based inhibitors of Staphlococcus aureus DNA polymerase III: Design, synthesis, and biological evaluation. *J. Med. Chem.* **46**, 1824–1830 (2003).

229. Abunada, N. M., Hassaneen, H. M., Kandile, N. G. & Miqdad, O. A. Synthesis and antimicrobial activity of some new pyrazole, fused pyrazolo[3,4-d]-pyrimidine and pyrazolo[4,3-e][1,2,4]-triazolo[1,5-c]pyrimidine derivatives. *Molecules* **13**, 1501–1517 (2008).

230. Harrington, G. *et al.* Reduction in Hospitalwide Incidence of Infection or Colonization with Methicillin-Resistant Staphylococcus aureus With Use of Antimicrobial Hand-Hygiene Gel and Statistical Process Control Charts. *Infect. Control Hosp. Epidemiol.* **28**, 837–844 (2007).

Acknowledgments

First of all, I would like to express my sincere gratitude to my supervisor Prof. Silvia Schenone whose guidance, support and encouragement have been invaluable throughout my PhD experience. Thanks to her I was able to develop my chemistry knowledge and experience different research environments.

A special thanks to Francesca for her precious advice and feedback which led to a consistent improvement in my career. Thank you for always being so patient and helpful!

Then, I must acknowledge Prof. Mazzei for his contagious enthusiasm in science and for including me in new and exciting projects.
Thanks also to everyone in DIFAR for providing me with any assistance I requested and the pleasant work environment I experienced. Thanks to my PhD colleagues: Monica, Ilaria, Helena, Fede, Valeria, Lorenzo, Marta, Giada, Alessandra e Federica.
I am also very grateful to Prof. Domenicotti and Doctor Marengo from DIMI with whom I had the enormous pleasure to collaborate with.
My research group actively collaborate with many other teams which I want to thank, with a particular reference to Prof. Maurizio Botta and the big affiliation he created.

I would like to express my deepest appreciation to Prof. Cameron Alexander for warmly hosting me in his lab at the University of Nottingham. This rewarding experience has been essential for my professional and personal growth. I will never forget all the amazing people I met in Boots and in Nottingham, in particular I owe a big debt to Vincenzo, Rosa and Amanda who were an important reference point for my work during my stay there. Many many thanks to Rob whom besides being an excellent teacher and the funniest lab mate, has demonstrated to be a precious friend. Thanks also for providing me with English support!

I cannot forget to mention my dearest friends: Fede, Mars, Giulia, Ida, Klea, Giorgia and all my countless flat mates I lived with, in Genova and in Nottingham. Thank you for all the funny moments and the affection you give me. A particular thanks to my new roommate Lorenzo for the wonderful holidays and the great moments we experienced, with the wish to share a lot more time and adventures together.

Lastly, the biggest acknowledgement is reserved to my family: Papà and Luca for being always preset in my life beyond the distance and the differences. Thank you for your endless support and helpful advice. I hope to make you proud of me.

I would like to dedicate this thesis to my Maman whose dreams for me have resulted in this high achievement. I am grateful for all the unconditional love and the strong courage you gave me. I will keep alive these feelings and your memory forever with me.